Imaging-based Biotyping of Prevalent Focal Epilepsy Syndromes

Hyo Min Lee

Departments of Neurology and Neurosurgery

McGill University

Montreal, Quebec, Canada

August 2023

A thesis submitted to McGill University in partial fulfillment of the requirements of the degree of Doctor of Philosophy

To

Young-Ja Hong, Aram Cho and Abigail Hae-In Lee

Acknowledgements

I thank the patients and healthy controls who participated in this research by undergoing multiple MRI sessions, neuropsychological testing and/or follow-up evaluations. The research experiments in this thesis would not have been possible without their invaluable contributions.

My thesis supervisors, Dr. Andrea Bernasconi and Dr. Neda Ladbon-Bernasconi, have my admiration for their dedicated mentorship and intellectual guidance. They have trained me to become an independent thinker and to attain deeper understandings. Their integrity, patience and generosity made all the years of my PhD study one of the best chapters of my life.

I am grateful for my mentor and friend, Dr. Seok-Jun Hong, who has been instrumental in my introduction into the field of epilepsy neuroimaging. He has helped me to learn and apply the current best practices of research in this thesis. My gratitude also goes to Dr. Benoit Caldairou, who has trained me with the essential technical skills and support needed to carry out the projects. I am indebted to Dr. Ravnoor Gill, the senior then-PhD student, for his intellectual and technical guidance on my application of machine learning techniques, which were crucial in all projects. I thank Fatemeh Fadaie, my fellow PhD student, and for her friendship, kindness and generosity as well as many productive discussions we had as colleagues. I am very fortunate to have met, worked together and shared quality time with my colleagues at the Neuroimaging of Epilepsy Laboratory.

My advisory committee has substantially contributed to the projects in this thesis. Especially, Dr. Boris Bernhardt offered numerous brilliant ideas that strengthened and

enriched the analyses in the projects. I am also grateful for Dr. David Rudko for his several constructive feedback that led to substantial improvements in the thesis.

Deep appreciation goes to the Integrated Program in Neuroscience team, namely Dr. Joe Rochford, Dr. David Ragsdale, Dr. Edward Ruthazer, Dhabisha Kohilanathan and Alexander DeGuise, not only for their administrative support, but also for creating intellectually stimulating, vibrant, diverse and inclusive community for the neuroscience graduate students at McGill University. I particularly appreciate their generous support for student-led public outreach initiatives, which I had the pleasure to lead throughout all years of my PhD study. This priceless experience has shaped my perspective that scientists have the ethical responsibility to make science accessible for the public.

I dedicate this thesis to Young-Ja Hong, Aram Cho and Abigail Hae-In Lee, for their love and inspiration.

Contributions of Authors

All manuscripts in this thesis are the products of a close collaboration between my supervisors **(Andrea Bernasconi, MD and Dr. Neda Bernasconi, MD PhD**) and I. Together, we designed the study ideas and experiments, planned the analyses, interpreted the results and wrote the manuscripts. I performed all the image processing, quality control, analyses and data visualization. Moreover, I drafted the first version of all manuscripts and made subsequent revisions based on the feedback from my supervisors.

The summary of contributions of the co-authors in the Montreal Neurological Institute and Hospital are as follows.

1. **Ravnoor Gill, PhD**. Advised on the application of machine learning techniques in all projects.
2. **Fatemeh Fadaie, PhD**. Provided pre-processed cognitive profiling data and assisted in interpreting results related to cognition in Projects 3-4.
3. **Benoit Caldairou, PhD**. Assisted in image processing and quality control in all projects.
4. **Seok-Jun Hong, PhD**. Assisted in study design and analyses in Projects 1-3.
5. **Boris Bernhardt, PhD**. Advised on study design and analyses in all projects.

Publications

Peer-reviewed Articles

1. **Lee HM**, Hong SJ, Gill R, Caldairou B, Wang I, Zhang J, Deleo F, Schrader D, Bartolomei F, Guye M, Cho KH, Barba C, Sisodiya S, Jackson G, Hogan RE, Wong-Kisiel L, Cascino GD, Schulze-Bonhage A, Lopes-Cendes I, Cendes F, Guerrini R, Bernhardt B, Bernasconi N, Bernasconi A. Multimodal mapping of regional brain vulnerability to focal cortical dysplasia. ***Brain*** **(in press).**
2. **Lee HM**, Fadaie F, Gill RS, Caldairou B, Sziklas V, Crane J, Hong SJ, Bernhardt BC, Bernasconi A, Bernasconi N. Decomposing MRI phenotypic heterogeneity in epilepsy: a step towards personalized classification. ***Brain***, 2022:145:897-908. ***Editor's Choice***.
3. Foit NA, Yung S, **Lee HM**, Bernasconi A, Bernasconi N, Hong SJ. A whole-brain 3D myeloarchitectonic atlas: Mapping the Vogt-Vogt legacy to the cortical surface. ***NeuroImage***, 2022:263:119617.
4. Gill RS, **Lee HM**, Caldairou B, Hong SJ, Barba C, Deleo F, D'Incerti L, Coelho VCM, Lenge M, Semmelroch M, Schrader DV, Bartolomei F, Guye M, Schulze-Bonhage A, Urbach H, Cho KH, Cendes F, Guerrini R, Jackson G, Hogan RE, Bernasconi N, Bernasconi A. Multicenter validated detection of focal cortical dysplasia using deep learning. ***Neurology***, 2021:97(16):e1571-1582
5. Caldairou B, Foit NA, Mutti, Fadaie F, Gill RS, **Lee HM**, Demerath T, Urbach H, Schulze-Bonhage A, Bernasconi A, Bernasconi N. MRI-based machine learning prediction framework to lateralize hippocampal sclerosis in patients with temporal lobe epilepsy, ***Neurology***, 2021:97(16):e1583-e1593

6. Fadaie F, **Lee HM**, Caldairou B,Gill RS, Sziklas V, Crane J, Bernhardt BC, Hong SJ, Bernasconi A, Bernasconi N. Atypical functional connectome hierarchy impacts cognition in temporal lobe epilepsy. ***Epilepsia***, 2021:00:0-15
7. Girardi-Schappo M, Fadaie F, **Lee HM**, Caldairou B, Sziklas V, Crane J, Bernhardt BC, Bernasconi A, Bernasconi N. Altered communication dynamics reflect cognitive deficits in temporal lobe epilepsy. ***Epilepsia***, 2021;62(4):1022-1033
8. **Lee HM**, Gill R, Fadaie F, Cho K, Guyot MC, Hong SJ, Bernasconi N, Bernasconi A. Unsupervised machine learning reveals lesional variability in focal cortical dysplasia at mesoscopic scale, ***NeuroImage Clinical***, 2020;28:102438
9. **Lee HM**, Weiger M, Giehr C, Froidevaux R, Brunner DO, Rösler MB, Prüssmann KP. Long-T_2-suppressed ZTE imaging with weighted echo subtraction and gradient error correction. ***Magn Reson Med***, 2020;83:412-426
10. Hong SJ, **Lee HM**, Gill R, Bernhardt B, Bernasconi N, Bernasconi A. A connectome-based mechanistic model of epileptogenic focal cortical developmental malformations. ***Brain***, 2019;142(3):688-699
11. Theken KN, Hersh EV, Lahens NF, **Lee HM**, Granquist EJ, Giannakopoulos H, Levin LM, Secreto-Dankanich SA, Grant GR, Detre JA, FitzGerald GA, Grosser T, Farrar JT. Variability in the analgesic response to Ibuprofen following third molar extraction is associated with differences in activation of the cyclooxygenase pathway. ***Clinical Pharmacology & Therapeutics***, 2019;106:632-341
12. Kim D, **Lee HM**, Oh SH, Lee J. Probing signal phase in direct visualization of short transverse relaxation time component. ***Magn Reson Med***, 2015;74(2):499-505

Manuscripts in Progress

1. **Lee HM**, Fadaie F, Gill RS, Caldairou B, Sziklas V, Crane J, Hong SJ, Bernhardt BC, Bernasconi A, Bernasconi N. Staging and subtyping the evolution of temporal lobe epilepsy.

Meeting Presentations

1. **Lee HM**, Fadaie F, Gill RS, Caldairou B, Sziklas V, Crane J, Hong SJ, Bernhardt BC, Bernasconi A, Bernasconi N. Staging and subtyping disease evolution in temporal lobe epilepsy. ***American Epilepsy Society***, Nashville, USA, 2022
2. **Lee HM**, Fadaie F, Gill RS, Caldairou B, Sziklas V, Crane J, Hong SJ, Bernhardt BC, Bernasconi A, Bernasconi N. Staging and subtyping disease evolution in temporal lobe epilepsy. ***NeuroSymposium***, Montreal, Canada, 2022
3. **Lee HM**, Fadaie F, Gill RS, Caldairou B, Sziklas V, Crane J, Hong SJ, Bernhardt BC, Bernasconi A, Bernasconi N. Decomposing MRI phenotypic heterogeneity in epilepsy has clinical relevance. ***American Epilepsy Society***, Chicago, USA, 2021
4. **Lee HM**, Fadaie F, Gill RS, Caldairou B, Sziklas V, Crane J, Hong SJ, Bernhardt BC, Bernasconi A, Bernasconi N. Decomposing the complex imaging signature of temporal lobe epilepsy using latent phenotypes. ***International Epilepsy Congress of the International League Against Epilepsy***, virtual, 2021
5. **Lee HM**, Fadaie F, Gill RS, Caldairou B, Sziklas V, Crane J, Hong SJ, Bernhardt BC, Bernasconi A, Bernasconi N. Decomposing the complex imaging signature of temporal lobe epilepsy using latent phenotypes. ***Asian and Oceanic Epilepsy Congress of the International League Against Epilepsy***, virtual, 2021
6. Fadaie F, **Lee HM**, Caldairou B, Gill R, Sziklas V, Crane J, Bernhardt B, Hong SJ, Bernasconi A, Bernasconi N. Cognitive deficits in temporal lobe epilepsy reflect

atypical functional connectome hierarchy. ***International Epilepsy Congress of the International League Against Epilepsy***, virtual, 2021

7. **Lee HM**, Fadaie F, Gill R, Foit NA, Caldairou B, Hong SJ, Bernasconi A, Bernasconi N. Latent whole-brain disease factors in temporal lobe epilepsy. ***American Epilepsy Society***, Seattle (virtual), USA, 2020
8. **Lee HM**, Gill R, Fadaie F, Hong SJ, Bernasconi N, Bernasconi A. MRI structural heterogeneity within and across focal cortical dysplasia. ***NeuroSymposium***, Montreal (virtual), Canada, 2020
9. **Lee HM**, Fadaie F, Gill R, Hong SJ, Bernasconi N, Bernasconi A. Temporal lobe epilepsy: MRI-based individualized prediction of medication response and surgical outcome. ***American Epilepsy Society***, Baltimore, USA, 2019
10. **Lee HM**, Gill R, Fadaie F, Hong SJ, Bernasconi N, Bernasconi A. MRI structural heterogeneity within and across focal cortical dysplasia: a data-driven approach based on consensus clustering. ***American Epilepsy Society***, Baltimore, USA, 2019
11. Fadaie F, **Lee HM**, Caldairou B, Gill R, Sziklas V, Crane J, Bernhardt B, Hong SJ, Bernasconi A, Bernasconi N. Connectome-based mapping of altered functional hierarchy in temporal lobe epilepsy. ***American Epilepsy Society***, Baltimore, USA, 2019
12. Gill R, Hong SJ, Fadaie F, Caldairou B, **Lee HM** et al. Detection of MRI-negative focal cortical dysplasia using uncertainty-informed Bayesian deep learning: a multicentre validation study. ***American Epilepsy Society***, Baltimore, USA, 2019
13. Caldairou B, Mutti C, Fadaie F, Gill R, **Lee HM**, Bernasconi A, Bernasconi N. Automated seizure focus lateralization in temporal lobe epilepsy using multicontrast MRI. ***American Epilepsy Society***, Baltimore, USA, 2019
14. **Lee HM**, Gill R, Fadaie F, Hong SJ, Bernasconi N, Bernasconi A. Data-driven MRI biotyping of epileptogenic malformations of cortical development. ***Organization for Human Brain Mapping***, Rome, Italy, 2019

15. Hong SJ, Yung S, **Lee HM**, Fadaie F, Gill R, Bernasconi N, Bernasconi A. The MNI-NOEL 3D myeloarchitectonic atlas of the human cerebral cortex. ***Organization for Human Brain Mapping***, Rome, Italy, 2019
16. Fadaie F, **Lee HM**, Caldairou B, Gill R, Bernhardt B, Hong SJ, Bernasconi A, Bernasconi N. Hierarchical organization of the cerebral cortex is disrupted in temporal lobe epilepsy. ***Organization for Human Brain Mapping***, Rome, Italy, 2019
17. **Lee HM**, Gill R, Fadaie F, Hong SJ, Bernasconi N, Bernasconi A. Data-driven MRI biotyping of epileptogenic malformations of cortical development. ***Quebec Bio-Imaging Network***, Montreal, Canada, 2019
18. Hong SJ, **Lee HM**, Gill R, Bernhardt B, Bernasconi N, Bernasconi A. Connectome-based functional biotyping of focal cortical dysplasia. ***Organization for Human Brain Mapping***, Singapore, 2018
19. Hong SJ, **Lee HM**, Gill R, Bernhardt B, Bernasconi N, Bernasconi A. Focal cortical dysplasia: relation between lesion topography and sulcal pits. ***Organization for Human Brain Mapping***, Singapore, 2018
20. Gill RS, Hong SJ, Fadaie F, Caldairou B, **Lee HM** et al. Automatic detection of focal cortical dysplasia using deep learning: a multicenter validation study. ***American Epilepsy Society***, New Orleans, USA, 2018
21. Hong SJ, **Lee HM**, Gill R, Bernhardt B, Bernasconi N, Bernasconi A. Connectome-based functional biotyping of focal cortical dysplasia. ***American Epilepsy Society***, New Orleans, USA, 2018
22. Hong SJ, **Lee HM**, Gill R, Bernhardt B, Bernasconi N, Bernasconi A. Focal cortical dysplasia: relation between lesion topography and sulcal pits. ***American Epilepsy Society***, New Orleans, USA, 2018

23. **Lee HM**, Weiger M, Pruessmann KP. Exploring various radial trajectories for optimal relative phase correction in dual-echo subtraction ZTE MRI. ***International Society for Magnetic Resonance in Medicine***, Hawaii, USA, 2017
24. **Lee HM**, Weiger M, Pruessmann KP. High resolution dual-echo subtraction ZTE imaging at 7T with TE estimation based on multiple scaled trajectories. ***International Society for Magnetic Resonance in Medicine***, Hawaii, USA, 2017
25. **Lee HM**, Vidorreta M, Chang Y, Detre JA. A perfusion phantom for arterial spin labeled MRI. ***International Society for Magnetic Resonance in Medicine***, Singapore, 2016
26. Lau KC, **Lee HM**, Singh T, Maidment ADA. Segmentation methods for breast vasculature in dual-energy contrast-enhanced digital breast tomosynthesis. ***Proc SPIE Medical Imaging***, Orlando, USA, 2015
27. **Lee HM**, Kim D, Oh SS, Choi JY, Oh SH, Lee J. The phase and magnetization transfer characteristics of a novel myelin water imaging method (ViSTa). ***International Society for Magnetic Resonance in Medicine***, Milan, Italy, 2014
28. **Lee HM**, Martin R, Merritt MH. Rapid magnetic resonance spectroscopic imaging with one dimensional flyback echo-planar trajectory. ***University of Texas Southwestern Medical Center***, Dallas, USA, 2013

Abstract

Background. Epilepsy is a prevalent condition affecting about 50 million people worldwide. A third of patients suffer from seizures unresponsive to medication. Drug response cannot be predicted and is typically ascertained after 20 years until multiple trials have failed. During these decades of delay, uncontrolled seizures damage the brain and lead to socioeconomic consequences, cognitive decline and mortality. The most common forms of focal epilepsy are neocortical epilepsy due to focal cortical dysplasia (FCD) and temporal lobe epilepsy (TLE) due to hippocampal sclerosis. Currently, surgical resection of the lesion is the only potentially curative treatment. Detecting epileptogenic lesion on magnetic resonance imaging (MRI) strongly predicts favorable surgical outcome. However, challenges remain. Many FCD patients have subtle lesions that are undetected on routine MRI but found on histology. These patients, labeled as MRI-negative, represent an utmost clinical challenge. In TLE, the inability to predict drug response and surgical outcome often leads to decades of ineffective drug trials and unfavorable seizure outcome in up to 50% of operated patients. An overarching explanation for these limitations is the "one-size-fits-all" approach to clinical care. Although current clinical practice is driven by reliable group-level studies, it is constrained by incomplete understanding of disease heterogeneity.

Objective. To investigate the heterogeneity of focal epilepsy syndromes by combining multi-modal MRI and machine learning to disentangle disease phenotypes in each syndrome based on structural pathology of the lesional tissues, cortical gray matter (GM) and superficial white matter (WM).

Methods. We first combined multi-contrast MRI and unsupervised machine learning to model the structural variability of FCD lesions at a mesoscopic scale (Project 1). We then

performed cortex-wide mapping of the regional vulnerability to FCD across multiple spatial scales, including gene expression, cytoarchitecture and large-scale organization (Project 2). In parallel, we combined multi-modal MRI and machine learning to model the inter-individual phenotypic variability based on hippocampal and whole-brain structural alterations in TLE (Project 3). Subsequently, we simultaneously characterized the phenotypic and temporal variability of TLE based on hippocampal and whole-brain structural alterations in TLE (Project 4). In all projects, we applied resampling techniques to assess the within-sample stability of the results and tested the clinical utility of structural variability for predicting drug response, postsurgical seizure outcome, histopathology and cognitive outcomes.

Results. *Project 1.* Unsupervised clustering applied to 46 patients with histologically verified FCD Type II identified four classes of lesional tissues with distinct structural profiles that aggregated to form a given FCD lesion. These classes were replicated in two independent datasets, supporting generalizability. Classes with GM anomalies impacted local function, while those with WM anomalies affected large-scale connectivity. The classes had distinct histopathological embeddings, with classes with GM anomalies linked to severe GM features and those with WM anomalies linked to severe WM features. A detection algorithm trained on class-informed data outperformed a class-naïve paradigm (77% vs 73% lesions detected), supporting added clinical utility. *Project 2.* The cortex-wide distribution of 337 FCDs collected from 13 sites worldwide showed preferential occurrence in prefrontal and fronto-limbic cortices typified by low neuron density, large soma and thick GM. Transcriptomic associations with FCD distribution uncovered a prenatal component related to neuroglial proliferation and differentiation, likely accounting for the dysplastic makeup, and a postnatal component related to synaptogenesis and circuit organization, possibly contributing to circuit-level hyperexcitability. FCD distribution showed a strong association with the anterior region

of the antero-posterior axis derived from heritability analysis of inter-regional structural covariance of cortical thickness, but not with structural and functional hierarchical axes. The reliability of all results was confirmed through resampling techniques. *Project 3.* We identified four latent disease factors representing hippocampal and whole-brain patterns of structural pathology in 82 TLE patients with histologically verified hippocampal pathology. Bootstrap analysis and parameter variations supported high stability and robustness of these factors. Moreover, they were not expressed in healthy controls and only negligibly in disease controls, supporting specificity. Supervised classifiers trained on latent disease factors could predict patient-specific drug response in 76% and postsurgical seizure outcome in 88%, outperforming classifiers that did not operate on latent factor information. Latent factor models predicted inter-patient variability in cognitive dysfunction (verbal IQ: $r = 0.40$; memory: $r = 0.35$; sequential motor tapping: $r = 0.36$), again outperforming baseline learners. *Project 4.* We identified three disease trajectory subtypes. Patients showed high assignability to their subtypes and stages. These subtypes had distinct clinical parameters, including age of epilepsy onset, history of febrile convulsion, drug response, MRI visibility and postsurgical seizure outcome, as well as cognitive profiles, including verbal IQ, digit span and sequential motor tapping. Supervised classifiers trained on subtype and stage memberships could predict drug response in 73% of patients and Engel outcomes in 76%, outperforming subtype- and stage-only models.

Significance. This thesis combined multi-modal MRI with machine learning to model the inter-individual variability based on the key aspects of structural pathology in lesional tissues, cortical GM and superficial WM in common focal epilepsy syndromes. The presented approach informed on the phenotypic and temporal variability beyond histological and electro-clinical categories. It also offered a novel basis to understand aberrant developmental and degenerative mechanisms that drive the lesional and whole-

brain structural alterations across lifespan. The presented approach may offer biomarkers that may reduce ineffective drug trails and accelerate referrals for pre-surgical evaluation, improve the detection of subtle lesions for surgical removal and enable inference on the genotypes for individual patients.

Résumé

Contexte. L'épilepsie est une maladie répandue qui touche environ 50 millions de personnes dans le monde. Un tiers des patients souffrent de crises qui ne répondent pas aux médicaments. La réponse aux médicaments ne peut être prédite et n'est généralement confirmée qu'après 20 ans d'essais et erreurs. Pendant cette période, les crises non contrôlées ont pour conséquences d'endommager le cerveau, et entraînent des problèmes socio-économiques et un déclin cognitif, voir la mort dans les cas plus graves. Les formes les plus courantes d'épilepsie focale sont l'épilepsie néocorticale due à une dysplasie corticale focale (DCF) et l'épilepsie du lobe temporal (ELT) due à une sclérose hippocampique. Actuellement, la résection chirurgicale de la lésion est le seul traitement potentiellement curatif. La détection d'une lésion épileptogène à l'imagerie par résonance magnétique (IRM) permet de prédire avec beaucoup de certitudes un résultat chirurgical favorable. Cependant, des difficultés subsistent. De nombreux patients atteints de DCF présentent des lésions subtiles qui ne sont pas détectées lors d'une IRM de routine, mais qui sont découvertes à lors de l'analyse histologique. Ces patients, qualifiés de négatifs à l'IRM, représentent un défi clinique majeur. Dans le cas des ETL, l'incapacité à prédire la réponse aux médicaments et le résultat de la chirurgie conduit souvent à des décennies d'essais de médicaments inefficaces et à une récurrence des crises chez jusqu'à 50 % des patients opérés. Une explication générale de ces limitations est l'approche thérapeutique uniformisée des soins cliniques. Bien que la pratique clinique actuelle s'appuie sur des études fiables ayant observé des divergences au sein de groupes dits homogènes, elle est limitée par une compréhension incomplète de la maladie, qui est en fait plutôt hétérogène.

Objectif. Étudier l'hétérogénéité des syndromes d'épilepsie focale en combinant l'IRM multimodale et l'apprentissage automatique pour distinguer les phénotypes de la

maladie dans chaque syndrome (DCF et ELT) sur la base de la pathologie structurelle des tissus lésionnels, de la matière grise corticale (MG) et de la matière blanche superficielle (MB).

Méthodes. Nous avons d'abord combiné l'IRM multi-contraste et l'apprentissage automatique non supervisé pour modéliser la variabilité structurelle des lésions de la DCF à une échelle mésoscopique (projet 1). Nous avons ensuite cartographié à l'échelle du cortex la vulnérabilité régionale à la DCF sur plusieurs échelles spatiales, y compris l'expression génétique, la cytoarchitecture et l'organisation à grande échelle (projet 2). Parallèlement, nous avons combiné l'IRM multimodale et l'apprentissage automatique pour modéliser la variabilité phénotypique interindividuelle basée sur les altérations structurelles de l'hippocampe et du cerveau entier dans l'ELT (projet 3). Par la suite, nous avons caractérisé simultanément la variabilité phénotypique et temporelle de l'ELT en nous basant sur les altérations structurelles de l'hippocampe et du cerveau entier (projet 4). Dans tous les projets, nous avons appliqué des techniques de rééchantillonnage pour évaluer la stabilité des résultats à l'intérieur de l'échantillon et nous avons testé l'utilité clinique de la variabilité structurelle pour prédire la réponse aux médicaments, la récurrence des crises post-chirurgicales, l'histopathologie et l'évolution des marqueurs cognitifs.

Résultats. *Projet 1*. Le partitionnement des données non supervisé appliqué à 46 patients atteints de DCF de type II vérifiée histologiquement a permis d'identifier quatre classes de tissus lésionnels avec des profils structurels distincts qui se sont agrégés pour former une lésion DCF donnée. Ces classes ont été reproduites dans deux ensembles de données indépendants, ce qui prouve qu'elles peuvent être généralisées. Les classes présentant des anomalies au niveau de la matière grise ont eu un impact sur la fonction locale, tandis que celles présentant des anomalies au niveau de la matière blanche superficielle ont eu un impact sur la connectivité à grande échelle. Les classes avaient des ancrages

histopathologiques distincts, les classes liées à la matière grise présentant des anomalies importantes de cette matière, et les classes liées à la matière blanche présentant des anomalies importantes de ce tissu. Un algorithme de détection entraîné sur des données informées par classe a surpassé un paradigme naïf de classe (77% contre 73% de lésions détectées), ce qui soutient l'utilité clinique ajoutée. *Projet 2*. La distribution à l'échelle du cortex de 337 DCFs collectés sur 13 sites dans le monde a démontré une occurrence préférentielle dans les cortex préfrontal et fronto-limbique, caractérisés par une faible densité de neurones, un grand soma et une MG épaisse. Les associations transcriptomiques avec la distribution des DCF ont mis en évidence une composante prénatale liée à la prolifération et à la différenciation neurogliales, qui explique probablement la composition dysplasique, et une composante postnatale liée à la synaptogenèse et à l'organisation des circuits neuronaux, qui contribue peut-être à leurs hyperexcitabilités. La distribution de la DCF a démontré une forte association avec la région antérieure de l'axe antéro-postérieur dérivé de l'analyse de l'héritabilité de la covariance structurelle interrégionale de l'épaisseur corticale, mais pas avec les axes hiérarchiques structurels et fonctionnels. La fiabilité de tous les résultats a été confirmée par des techniques de rééchantillonnage. *Projet 3*. Nous avons identifié quatre facteurs latents de la maladie représentant des modèles de pathologie structurelle de l'hippocampe et du cerveau entier chez 82 patients atteints de ELT avec une pathologie hippocampique vérifiée histologiquement. Une analyse par technique de bootstrap et les variations de paramètres ont confirmé la grande stabilité et la robustesse de ces facteurs. En outre, les facteurs n'étaient pas exprimés chez les témoins sains et ne l'étaient que de façon négligeable chez les témoins malades, ce qui confirme leur spécificité. Les classifieurs supervisés entraînés sur les facteurs latents de la maladie pouvaient prédire la réponse médicamenteuse spécifique au patient dans 76 % des cas et prédire les crises post-chirurgicales dans 88 % des cas, surpassant les classifieurs qui n'utilisaient pas l'information sur les facteurs latents. Les modèles de facteurs latents ont prédit la

variabilité inter-patients dans le dysfonctionnement cognitif (QI verbal : r = 0,40 ; mémoire : r = 0,35 ; séquence motrice : r = 0,36), surpassant à nouveau les classifieurs de base. *Projet 4*. Nous avons identifié trois sous-types de trajectoire de la maladie. Les patients ont montré une grande relation d'appartenance à leurs sous-types et à leurs stades. Ces sous-types présentaient des paramètres cliniques distincts, notamment l'âge d'apparition de l'épilepsie, les antécédents de convulsions fébriles, la réponse aux médicaments, la visibilité de l'IRM et la récurrence des crises post-chirurgicales, ainsi que des profils cognitifs, notamment le QI verbal, le test de l'empan numérique, et le tapotement moteur séquentiel. Des classifieurs supervisés, entrainés à partir de l'appartenance à un sous-type et à un stade, ont pu prédire la réponse aux médicaments chez 73 % des patients et les classification d'Engel chez 76 % d'entre eux, surpassant les performances de classifieurs n'ayant que le sous-type ou le stade comme connaissance préalable.

Importance. Cette thèse combine l'IRM multimodale avec l'apprentissage automatique pour modéliser la variabilité interindividuelle basée sur les aspects clés de la pathologie structurelle dans les tissus lésionnels, la MG corticale et la MB superficielle dans les syndromes d'épilepsie focale communs. L'approche présentée a permis de mieux comprendre la variabilité phénotypique et temporelle au-delà des catégories histologiques et électro-cliniques. Elle offre également une nouvelle base pour comprendre les mécanismes aberrants de développement et de dégénérescence qui entraînent des altérations structurelles au niveau des lésions et du cerveau entier tout au long de la vie. L'approche présentée peut offrir des biomarqueurs susceptibles de réduire les essais de médicaments inefficaces et d'accélérer l'orientation vers une évaluation pré-chirurgicale, d'améliorer la détection des lésions subtiles en vue d'une ablation chirurgicale et de permettre l'inférence des génotypes pour chaque individu.

Original Contributions

Project 1. Characterizing Structural Heterogeneity in Focal Cortical Dysplasia

We combined multi-contrast MRI and unsupervised clustering on 46 histologically verified FCD Type II to capture structural variability at a mesoscopic scale. We identified four classes of lesional tissues with distinct structural profiles that aggregated to form a given FCD lesion. These classes were replicated in two independent datasets, supporting generalizability. Classes with GM anomalies impacted local function, while those with WM anomalies affected large-scale connectivity. The classes had distinct histopathological embeddings, with classes with GM anomalies linked to severe GM features and those with WM anomalies linked to severe WM features. A detection algorithm trained on class-informed data outperformed a class-naïve paradigm (77% vs 73% lesions detected), supporting added clinical utility. FCD classes may offer a novel basis to improve automated lesion detection and genotype-phenotype associations.

Project 2. Uncovering Neurodevelopmental Vulnerability for Focal Cortical Dysplasia

We mapped the cortex-wide distribution of 337 FCDs collected from 13 sites worldwide across multiple scales of neurobiology. The FCD distribution showed preferential occurrence in prefrontal and fronto-limbic cortices typified by low neuron density, large soma and thick GM. Transcriptomic associations with FCD distribution uncovered a prenatal component related to neuroglial proliferation and differentiation, likely accounting for the dysplastic makeup, and a postnatal component related to synaptogenesis and circuit organization, possibly contributing to circuit-level hyperexcitability. FCD distribution showed a strong association with the anterior region

of the antero-posterior axis derived from heritability analysis of inter-regional structural covariance of cortical thickness, but not with structural and functional hierarchical axes. The reliability of all results was confirmed through resampling techniques. This project offers evidence that therapies targeting aberrant postnatal synaptogenesis, either combined with or in isolation with mTOR inhibitors, may potentially improve seizure control in FCD patients.

Project 3. Modeling Heterogeneity of Whole-Brain Alterations in Temporal Lobe Epilepsy

We identified four latent disease factors representing hippocampal and whole-brain patterns of structural pathology in 82 TLE patients. Bootstrap analysis and parameter variations supported high stability and robustness of these factors. Moreover, they were not expressed in healthy controls and only negligibly in disease controls, supporting specificity. Supervised classifiers trained on latent disease factors could predict patient-specific drug response in 76% and postsurgical seizure outcome in 88%, outperforming classifiers that did not operate on latent factor information. Latent factor models predicted inter-patient variability in cognitive dysfunction (verbal IQ: $r = 0.40$; memory: $r = 0.35$; sequential motor tapping: $r = 0.36$), again outperforming baseline learners. Modeling inter-individual variability provides a novel appraisal of the phenotypic continuum of TLE determined by multiple interacting pathological processes. Incorporating inter-individual variability is likely to improve clinical prognostics.

Project 4. Staging and Subtyping the Evolution of Temporal Lobe Epilepsy

We identified three disease trajectory subtypes. Patients showed high assignability to their subtypes and stages. These subtypes had distinct clinical parameters, including age of epilepsy onset, history of febrile convulsion, drug response, MRI visibility and

postsurgical seizure outcome, as well as cognitive profiles, including verbal IQ, digit span and sequential motor tapping. Supervised classifiers trained on subtype and stage memberships could predict drug response in 73% of patients and Engel outcomes in 76%, outperforming subtype- and stage-only models. Capturing the progression of subtype-specific MRI biomarkers enables an objective, fine-grained patient stratification, which may identify individuals at risk and help monitor the effectiveness of potential preventative therapies.

Table of Contents

List of Figures

List of Tables

Abbreviations

AD	Alzheimer's disease
BOLD	Blood oxygenation level dependent
CA	Cornu Ammonis
CLASP	Constrained Laplacian anatomic segmentation using proximity
CP	Cortical plate
CSF	Cerebrospinal fluid
DPARSF	Data Processing Assistant for Resting-State fMRI
DG	Dentate gyrus
EEG	Electroencephalography
ENIGMA	Enhancing NeuroImaging Genetics through Meta-Analysis
FA	Fractional anisotropy
FBTCS	Frontal to bilateral tonic-clonic seizure
FCD	Focal cortical dysplasia
FLAIR	Fluid-attenuated inversion recovery
FLE	Frontal lobe epilepsy
fMRI	Functional magnetic resonance imaging
FOV	Field of view
GABA	Gamma-aminobutyric acid
GM	Gray matter

GTCS	Generalized tonic-clonic seizure
GW	Gestational week
HARNESS	Harmonized Neuroimaging of Epilepsy Structural Sequences
HS	Hippocampal sclerosis
ICBM	International Consortium for Brain Mapping
IPSC	Intermediate progenitor cells
IQ	Intelligence quotient
ISVZ	Inner subventricular zone
LDA	Latent Dirichlet allocation
LI-VI	Cortical layers I-VI
MAP-2	Microtubule-associated protein-2
MCD	Malformation of cortical development
MD	Mean diffusivity
MNI	Montreal Neurological Institute
MPRAGE	Magnetization prepared rapid gradient echo
MRI	Magnetic resonance imaging
mTOR	Mammalian target of rapamycin
NE	Neuroepithelial cells
NeuN	Neuronal specific nuclear protein
ORG	Outer radial glia

RI	Relative intensity
RG	Radial glia
ROI	Regions of interest
SD	Standard deviation
SEEG	Stereoencephalography
SUB	Subiculum
SVZ	Subventricular zone
TE	Echo time
TI	Inversion time
TLE	Temporal lobe epilepsy
TR	Repetition time
TRG	Truncated radial glia
VRG	Ventricular radial glia
VZ	Ventricular zone
WM	White matter

PART I

INTRODUCTION

1. OVERVIEW

Epilepsy is a prevalent chronic condition affecting about 50 million people worldwide. Seizures are defined as transient debilitating symptoms due to excessive neuronal activity, based on which they are classified as focal or generalized. A third of patients suffer from seizures unresponsive to medication [1]. Drug response cannot be predicted and is typically ascertained after 20 years until multiple trials have failed [2, 3]. During these decades of delay, uncontrolled seizures damage the brain [4] and lead to socioeconomic consequences, cognitive decline and mortality [5]. The most common forms of drug-resistant focal epilepsy are neocortical epilepsy due to focal cortical dysplasia (FCD), a structural brain developmental malformation, and temporal lobe epilepsy (TLE) due to mesiotemporal sclerosis (MTS), a histopathological lesion that combines various degrees of neuronal loss and gliosis in the hippocampus and adjacent cortices. Currently, the surgical resection of these structural lesions is the only potentially curative treatment. In this context, magnetic resonance imaging (MRI) has been instrumental in the pre-surgical evaluation, owing to its unmatched spatial resolution and whole-brain coverage. Importantly, detecting these structural lesions on MRI is the strongest predictor favorable surgical outcome [6-8].

Yet, clinical challenges remain. Many patients have subtle lesions that are undetected on routine MRI but found on histology. In these patients, labeled as "MRI-negative," the surgical outcome is poorer compared to those in whom a structural lesion is identified [9]. In addition, the inability to predict drug response and surgical outcome often leads to decades of ineffective drug trials and unfavorable seizure outcome in up to 50% of operated patients. A likely explanation of these limitations may lie in the "one-size-fits-all" approach to clinical care, which does not fully consider variability within and across

individuals. Alternatively, analytic techniques that model data heterogeneity may foster the discovery of effective diagnostic and prognostic biomarkers.

The overall purpose of this thesis is to investigate inter-individual disease variability by combining MRI-derived features of pathology and machine learning in the two most prevalent drug-resistant syndromes, namely neocortical epilepsy related to FCD and temporal lobe epilepsy related to MTS.

Specific aims:

Aim 1. Assessing lesional variability in focal cortical dysplasia at mesoscopic scale

Over the past decades, FCD characterization has been driven by discrete histological subtypes. However, emerging evidence has shown substantial cellular variability across lesions and co-occurrence of multiple subtypes within the same lesion. We tested the hypothesis that machine learning applied to MRI features of FCD captures lesional variability at a mesoscopic scale.

Aim 2. Multimodal mapping of regional brain vulnerability to focal cortical dysplasia

Although FCD may occur across the entire cortex, clinical observations favor the frontal lobe; yet, mechanisms underpinning such vulnerability remain unexplored. Here, we hypothesized that regionally varying programs of cortical development contribute to preferential vulnerability. To that end, we conducted multivariate statistical analyses in a large cohort of patients relating the cortex-wide distribution of FCD lesions on MRI with cortical cytoarchitecture, whole-brain and spatiotemporal gene expression and macroscale organization.

Aim 3. Decomposing MRI phenotypic heterogeneity in temporal lobe epilepsy

In TLE, precise clinical predictions of drug response, surgical outcome and cognitive dysfunction at an individual level remain challenging. A possible explanation may lie in the dominant group-level analytical approaches that do not allow parsing inter-individual variations along the disease spectrum. Conversely, analyzing inter-patient heterogeneity is increasingly recognized as a step towards person-centered care. Here, we utilized unsupervised machine learning to estimate latent relations. We used unsupervised machine learning to estimate latent relations (or disease factors) from 3T multimodal MRI features representing hippocampal and whole-brain patterns of structural pathology in TLE.

Aim 4. Staging and subtyping the evolution of temporal lobe epilepsy

Evidence suggests that TLE follows a progressive course impacting brain structure and cognitive function. However, previous studies have assumed that disease progression is steady and that all patients follow the same trajectory. Our purpose was to parse phenotypic and temporal diversities of TLE evolution. To this end, we applied Subtype and Stage Inference, a computational technique that extends event-based models for simultaneous staging and subtyping.

This thesis is organized as follows. Chapter 2 is a review of relevant background literature. Chapters 3, 4, 5 and 6 are manuscripts on the specific aims. Chapter 7 summarizes the key findings and significances.

2. BACKGROUND

Neocortical epilepsy due to focal cortical dysplasia (FCD) and temporal lobe epilepsy (TLE) due to mesiotemporal sclerosis (MTS) are the most common forms of drug-resistant epilepsies that are amenable to surgery. In this chapter, I will discuss the etiologies and pathological features of FCD and TLE and review the current MRI literature.

2.1 Focal cortical dysplasia

Any molecular disturbance during embryonic corticogenesis may result in a malformation of cortical development. The developmental timetable in which the perturbation occurs largely determines the morphological features in the matured cortex [10]. FCD is the most common form of MCDs accounting for up to 50% of cases [11]. This early malformation is associated with atypical neuroglial proliferation and growth [12], impairing mitotic cycles and cell growth [13, 14]. Abnormalities in neurogenesis that typically lead to FCD Type II are characterized by cortical dyslamination, cytomegaly and cortical thickening [15, 16]. Advancing our understanding of the neurogenic mechanisms that underpin FCD and characterizing its diverse phenotypic manifestation may facilitate fine-grained patient stratification and optimized therapeutic approaches.

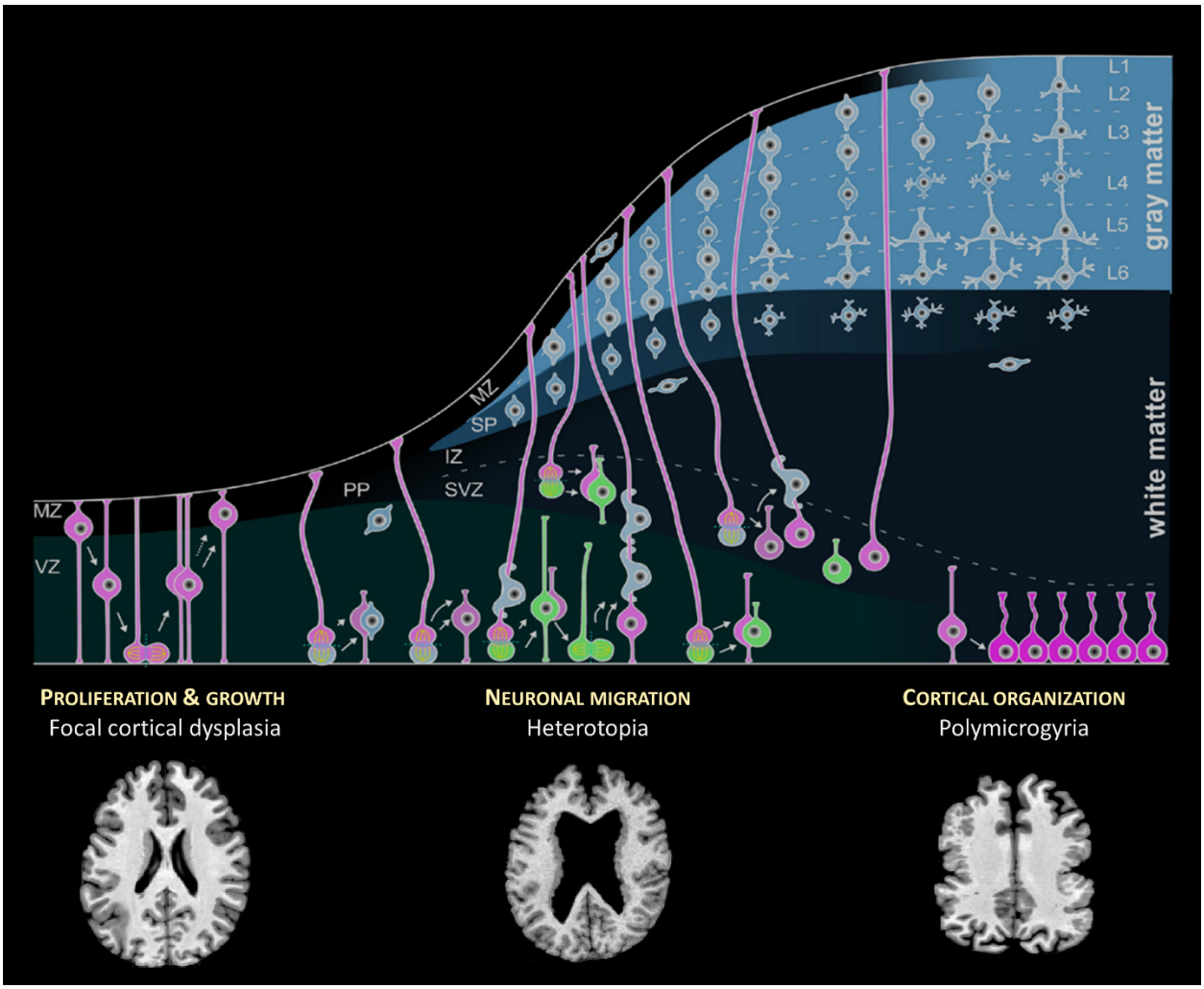

Figure 1. An overview of malformations of cortical development. Developmental timeline including neuroglial proliferation and growth, neuronal migration and cortical organization are shown. Molecular insult in these processes is associated with distinct manifestations of malformations: focal cortical dysplasia, heterotopia and polymicrogyria, respectively. Adapted from *[17]* with permission.

2.1.1 Normal cortical development

To better understand the neurobiology of FCD, this section provides an overview of the normal cortical development. Cortical development involves intricately coordinated molecular events consisting of successive and partly overlapping steps. During pre-natal development, these steps include neuroglial proliferation, differentiation and migration

[17]. During the post-migratory pre- and post-natal stages, the cortex undergoes cortical organization driven by neural circuit development [18]. The genetic regulation of these processes is area-specific, giving rise to large-scale areal variations in cytoarchitecture and function [19].

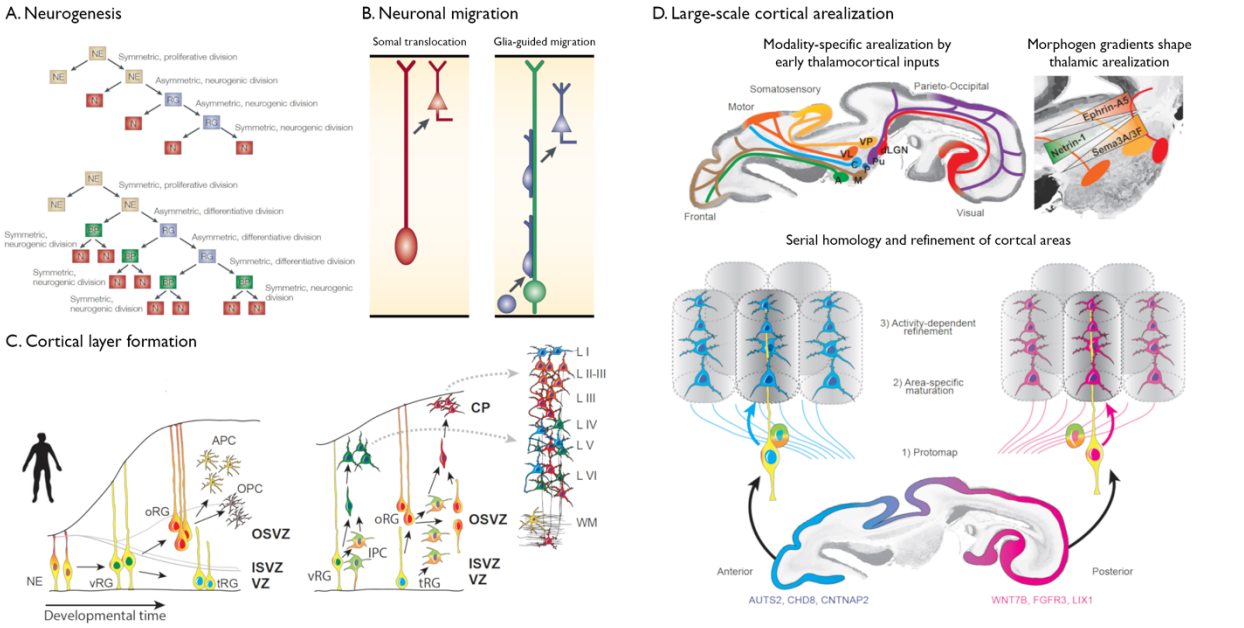

Figure 2. An overview of normal cortical development. Key developmental processes are illustrated. **A. Neurogenesis.** The lineage of neurons involves symmetric and asymmetric divisions of neuroepithelial cells (yellow box), radial glial cells (blue) and neurons (red) without (top tree) or with (bottom tree) basal progenitors (BP; green). **B. Neuronal migration.** Two main models of neuronal migration are somal translocation during the early stages of corticogenesis and glia-guided migration during the later stages. **C. Cortical layer formation.** Cortical layers forms with an expanded diversity of radial glial cells. Neurons formed in the ventricular zone in early development migrate in inside-out direction towards the outer subventricular zone. **D. Large-scale cortical arealization.** Thalamocortical inputs during early stages establish anatomical basis for modality-specific cortical regions. Morphogen gradients contribute to shaping the thalamic areal specification. Serial homology and refinement model is an integrated model for arealization positing that area-specific gene expression establish an initial protomap, which is then refined by thalamic area-specific maturation and activity-dependent processes to yield the matured cortex. IPSc (intermediate progenitor cells); ISVZ (inner subventricular zone); L1-V1 (cortical layers I-VI); NE (neuroepithelial cells); oRG (outer radial glia); OSVZ (outer ventricular zone); RG (radial glia); SVZ

(subventricular zone); tRG (truncated radial glia; vRG (ventricular radial glia); VZ (ventricular zone); WM (white matter). Adapted from [19-21] with permissions.

Neurogenesis

Neurogenesis begins with formation of the neocortex at the rostral end of the neural tube between 4th and 5th gestational weeks (GW) (**Figure 2A**). This period of early development is characterized by symmetric division of neuroepithelial cells at the ventricular zone (VZ), exponentially increasing the number of progenitor cells [22]. At approximately 5th GW, these progenitor cells, which are called radial glial cells, start to undergo asymmetric divisions, resulting in a daughter radial glial cell that remains in the VZ and the other becoming an intermediate progenitor cell or a postmitotic neuron [23]. The intermediate glial cells eventually undergo terminal symmetric division into pairs of postmitotic neurons [24]. The radial glial cells and intermediate progenitor cells form two subpopulations at the apical and basal surfaces of the VZ [25, 26]. Apical radial glial cells and intermediate progenitor cells reside in the VZ, while basal counterparts create a new distinct compartment above the VZ, called the subventricular zone (SVZ) [27]. Asymmetric divisions in the SVZ create additional intermediate progenitor cells (which contribute to larger brain size and longer migration paths) [28] and radial glial cells (which underpin cortical growth and folding) [29]. Prior to the formation of SVZ, various cells in the basal surface of VZ form a preplate that tangentially migrate to become inhibitory interneurons in the cortex or subcortex [30].

Neuronal migration and cortical layer formation

Around 7th GW, the VZ and SVZ undergo active proliferations to create pyramidal neurons that radially migrate outward to form the cortical plate (**Figure 2B**) [31]. In brief, cortical plate is the primitive form of neocortical gray matter (GM) that begins to develop as newborn neurons initiate the migration of cells from VZ and SVZ to their target layers within the cortical plate, thereby forming the six-layered cortex around 18th GW [32]. Initially, the cortical plate consists of the marginal zone and subplate (**Figure 2C**). The marginal zone contains cells that had tangentially migrated and arrest the radial migration of pyramidal neurons to help shape the inside-out transient formation of the cortex [33]. Meanwhile, neurons accumulate in the marginal zone in an inside-out sequence such that earliest and latest neurons eventually reside in the innermost layer 6 and outer layer 2. Two main models of neuronal migration are somal translocation during the early stages of corticogenesis and glia-guided migration during the later stages [21]. Approximately 80% of radially migrating neurons become excitatory glutamatergic neurons, whereas tangentially migrating neurons develop into GABAergic inhibitory interneurons [34]. Laminar organization commences during and after neuronal migration until later corticogenesis. Layer positioning of the neurons are thought to be driven by layer-specific genes, such as Cux1-2 or Foxp2, and an extracellular gradient of proteins, such as Reelin [35-37]. In addition to neuronal positioning, cell differentiation, development, selective apoptosis and extensive axonal and dendritic arborization underpin the development of cortical cytoarchitecture [17]. During 24th-34th GW, axons in the intermediate zone undergo extensive myelination, transforming the zone into white matter (WM) tissue [38].

Large-scale cortical arealization

The genetic regulation of corticogenesis is area-specific, giving rise to diverse regional variations in cytoarchitecture [19]. Indeed, different cortical areas are characterized by distinct neuronal types, density, size and connectivity, which underpin their functional specialization [39, 40]. Areal identity is defined by intrinsic and extrinsic mechanisms (**Figure 2D**). Intrinsic mechanisms involve the differential gene expression across cortical areas and the secretion of morphogen gradients along the cardinal axes of the cortex during embryonic development [41-44]. These molecular mechanisms establish large-scale organizational gradients, namely along the rostral-caudal (or anterior-posterior), dorsal-ventral and medial-lateral axes [45, 46], the confluence of which recapitulate the inter-areal cytoarchitectural and functional variations [19]. For example, the anterior-posterior axis reflects the timetable of neurogenesis and cell growth, where the anterior regions undergo earlier termination of neurogenesis and initiation of cell growth. This leads to lower density of neurons with larger soma size and denser dendritic arborization in the anterior regions relative to the posterior regions [47, 48]. In addition to intrinsic molecular mechanisms, areal identity is shaped by extrinsic activity-dependent mechanisms, including signaling molecules from the thalamocortical inputs that refine the gene regulatory networks to give rise to individual cell types and functional circuits [49-53]. These processes drive progressive refinement of boundaries between functional areas during late prenatal and early postnatal stages [54] and are thought to give rise to the sensory-association axis that reflect hierarchical neural function in the matured brain [55, 56].

2.1.2 Abnormal development leading to focal cortical dysplasia

Histopathology

FCD is characterized by a broad range of histopathological features, including cortical dyslamination, cytomegaly and gliosis. According to the current consensus classification, which has been recently updated (**Table 1**) [15, 57] FCD can be divided in various subtypes. FCD Type I is characterized by an isolated malformation with abnormal cortical layering, either showing persistence of vertical developmental microcolumns (IA), loss of the horizontal hexalaminar structure (IB) or both (IC); Type II presents with completely disorganized cortical layering and specific cytopathology including dysmorphic neurons, either isolated (IIA) or together with balloon cells (IIB); Type III comprises architectural abnormalities associated with either hippocampal sclerosis (IIIA), tumors (IIIB), vascular malformations (IIIC) or other lesions acquired during early life (IIID). FCD IIA and IIB are the most common subtypes, for which the histological diagnosis is highly reproducible within and across observers, while there is little intra- and inter-observer agreements for Type I subtypes [58].

FCD Type I	Dysplasia with abnormal radial lamination (IA)	Dysplasia with abnormal tangential lamination (IB)	Dysplasia with abnormal radial and tangential lamination (IC)	
FCD Type II	Dysplasia with dysmorphic neurons (IIA)		Dysplasia with dysmorphic neurons and balloon cells (IIB)	
FCD Type III	Lamination abnormalities in temporal lobe with hippocampal sclerosis (IIIA)	Lamination abnormalities adjacent to glial/glioneuronal tumor (IIIB)	Lamination abnormalities adjacent to vascular malformation (IIIC)	Lamination abnormalities adjacent to any other lesion (IIID)

Table 1. International League Against Epilepsy three-tiered classification system for FCD. Adapted from [15].

Causal molecular mechanisms

To date, a large number of molecular studies in resected FCD tissues have established a causal role of somatic mutations in genes implicated in the mechanistic target of the rapamycin (mTOR) pathway [59-65]. The mTOR cascade is a pivotal regulator of cell proliferation, growth and migration by monitoring growth factor cues and nutritional availability [66]. Constitutive activation of mTOR pathway via activating or dis-inhibiting mutations has shown to account for many of the histological features of FCD, namely cytomegaly [12] and dyslamination [67]. Given that mTOR hyperactivity is observed in only a subset of cell types, it is thought that somatic mutations occur in a small subset of neuroglial progenitor cells in the VZ during embryogenesis [68], which result in a focal lesion with putatively normal cortex beyond the lesion. Nevertheless, the knowledge on

FCD molecular mechanisms is incomplete, given the difficulty that the variant expressions are typically too low to be detected even with a large sample [69].

Imaging characteristics of FCD Type II

On MRI, Type II lesions appear as increased cortical thickness, best seen on T_1-weighted MRI and increased GM and WM signal intensity and blurred GM-WM boundary (**Figure 3**) [9] [11, 70], best visualized on T_2-weighted fluid-attenuated inversion recovery (FLAIR) images. A large number of lesions, particularly FCD Type IIB present with the transmantle sign in the WM, a funnel-shaped hyperintensity extending from the ventricle to the lesion, which is thought to be a footprint of disrupted neuronal radial migration [70-72]. The visibility on MRI generally corresponds to the histopathological severity [11]. Nevertheless, this spectrum of GM and WM changes can challenge visual identification in routine radiological examination. Indeed, recent series indicate that up to 33% of FCD II present with "unremarkable" routine MRI, even though typical features are ultimately identified in the histopathology of the resected tissue [70, 72, 73]. These so-called "MRI-negative" FCDs represent a major diagnostic challenge. To define the epileptogenic area, patients undergo long and costly hospitalizations for EEG monitoring with intracerebral electrodes, a procedure that carries risks similar to surgery itself [74, 75]. Moreover, patients without MRI evidence for FCD are less likely to undergo surgery and consistently show worse seizure control compared to those with visible lesions [6, 76, 77].

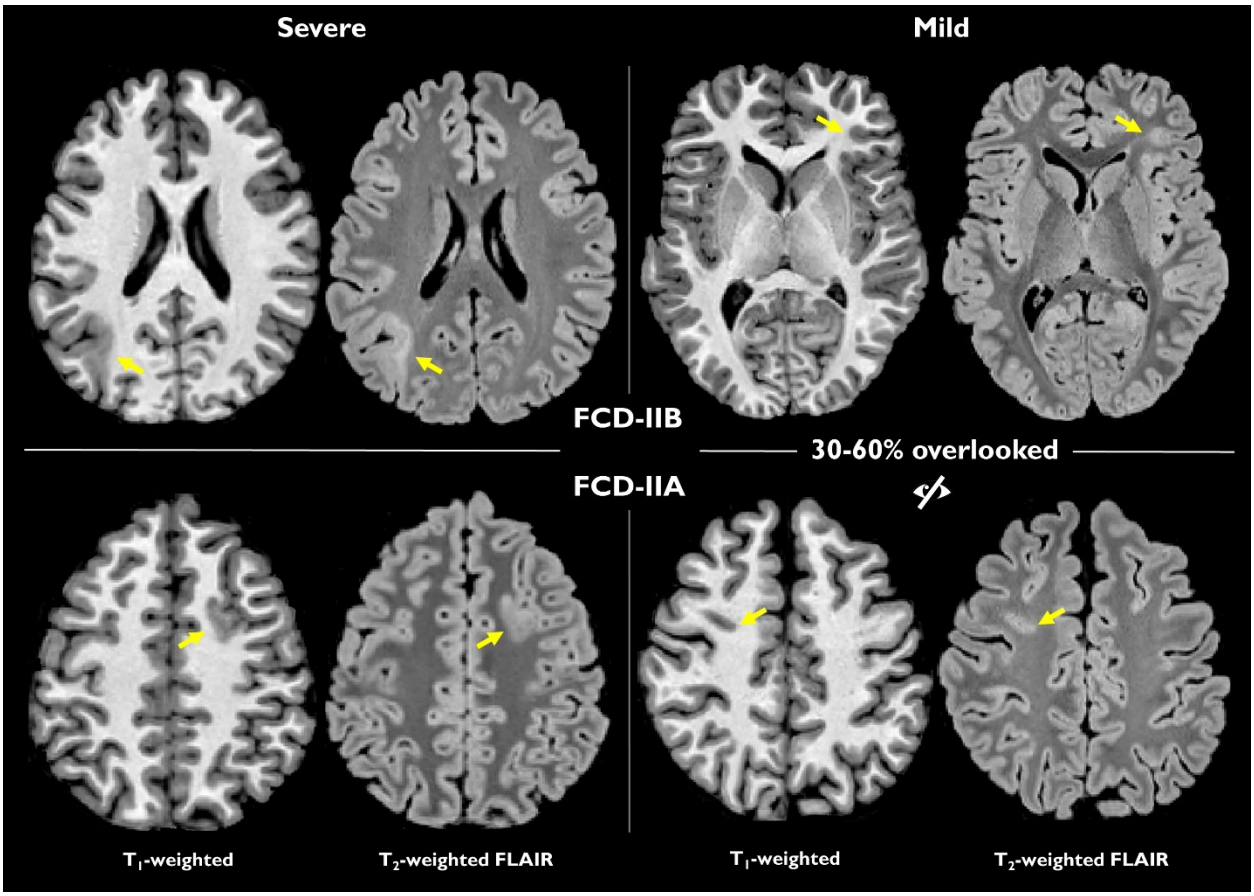

Figure 3. Visibility of FCD Type II. T_1-weighted and T_2-weighted FLAIR images of two representative cases are shown for Type IIB (top) and IIA (bottom). The cases on the left and right sides correspond to MRI-positive and MRI-negative cases. Yellow arrows indicate the lesion.

Computer-aided methods for FCD detection

This clinical difficulty of MRI-negative epilepsy has long been the motivation for the development of computer-aided methods aimed at assisting detection *in vivo* [78]. Such techniques provide distinct information through quantitative assessment without the cost of additional scanning time. Early methods opted for voxel-based methods to quantify group-level structural abnormalities related to MRI-visible FCD. For example, a previous work introduced an original approach to integrate key voxel-wise textures and morphological modeling (*i.e.*, cortical thickening, blurring of the GM-WM junction and

intensity alterations) derived from T_1-weighted images into a composite map [78, 79]. The clinical value of this computer-aided visual identification was supported by its 88% sensitivity and 95% specificity, vastly outperforming conventional MRI. In contrast to voxel-based methods, surface-based morphometry offers an anatomically plausible quantification of structural integrity that preserves cortical topology. Surface-based modeling of cortical thickness, folding complexity and sulcal depth, together with intra- and subcortical mapping of MRI intensities and textures, allow for a more sensitive description of FCD pathology. Over the last decade, several such algorithms have been developed, with detection rates up to 83% [80-86]. The addition of FLAIR has contributed to further increase in sensitivity, particularly for the detection of smaller lesions [81].

In vivo lesional biotyping, a step beyond discrete classification

Over the past decades, FCD characterization has been driven by histology, with the primary objective to establish subtype-specific imaging signatures [71]. Although histological grading is a well-defined framework, the current approach is based on descriptive criteria that do not consider the severity of each feature, thereby limiting neurobiological understanding. Indeed, a recently developed deep neural networks relying on clinically available T_1- and T_2-weighted FLAIR MRI have shown the highest sensitivity of 93% at detection with a specificity of 89% both in healthy and disease controls [87]. One advantage of these methods is that they learn abstract concepts from high-dimensional data alleviating the challenging task of hand-crafting features [88].

The ability to perform *in vivo* patient stratification is gaining relevance due to the emergence of minimally invasive surgical procedures that do not provide specimens for histological examination [89]. From a neurobiological standpoint, whether FCD IIA and IIB subtypes represent etiologically distinct entities, or a spectrum is a matter of debate.

Recent studies have shown significant cellular variability, with anomalies that may vary across lesions within the same subtype [90]. Moreover, multiple subtypes may co-exist within the same FCD, with the most severe phenotype determining the final diagnosis [12]. As such, broad ranges of somatic mutations and histological abnormalities associated with FCD are not sufficiently captured by discrete FCD subtypes [65]. Hence, MRI-based approaches to characterize the structural variability of FCD at mesoscopic scale may offer a novel basis to advance genotype-phenotype associations and automated lesion detection.

2.2 Temporal lobe epilepsy

TLE is the most common focal epilepsy syndrome in adults and make up the majority of cases referred to epilepsy surgery [91, 92]. In terms of seizure semiology, many TLE patients an *aura*, which may include flashing or flickering lights, feeling of déjà vu or detachment, memory distortions and olfactory or gustatory hallucinations [93, 94]. These symptoms are linked to temporo-limbic epileptiform activity, while motor symptoms and automatisms are linked to the spread of epileptiform activity to frontal and suprasylvian areas [95-97]. In some patients, secondary generalized seizures may occur [98-100]. A third of patients suffer from seizures unresponsive to medication [1]. Drug response cannot be predicted and is typically ascertained after 20 years until multiple trials have failed [2, 3]. During these decades of delay, uncontrolled seizures damage the brain [4] and lead to socioeconomic consequences, cognitive decline and mortality [5].

2.2.1 Histopathology of drug-resistant temporal lobe epilepsy

Hippocampal sclerosis (HS) is the histopathological hallmark of drug-resistant TLE [101-104] and combines varying degrees of neuronal loss and gliosis in sectors of the Cornu

Ammonis (CA), dentate gyrus (DG), subiculum (SUB) and adjacent cortices. International League Against Epilepsy (ILAE) had proposed a classification system that allow recognition of three HS subtypes based on slide microscopy of resected *en bloc* surgical specimens (**Table 2**) [105, 106]. HS type 1 is the most common subtype found in 60-80% of all cases [103, 107, 108]; this subtype is characterized by severe (>80%) cell loss in all subfields. HS type 2 is found in approximately 5-10% of cases and presents with predominant (80%) pyramidal cell loss in CA1. HS type 3 is the most uncommon subtype found in 4-7% of cases characterized mainly by cell loss in CA4 (50%) and DG (35%). Isolated gliosis (G) without detectable neuronal loss is found in approximately 20% of patients [107].

	HS 1	**HS 2**	**HS 3**	**G**
CA1	Severe	Moderate to severe	None to moderate	None
CA2	None to severe	None to moderate	None to moderate	None
CA3	None to severe	None to moderate	None to moderate	None
CA4	Severe	None to moderate	Moderate to severe	None
DG	None to severe	None to moderate	None to severe	None to moderate

Table 2. International League Against Epilepsy consensus classification of hippocampal sclerosis. The data indicate the severity of neuronal loss and gliosis found in *en bloc* resected samples. For each HS class, the defining features are indicated with gray shades. Adapted from [105].

Despite the logistical difficulty of obtaining whole brain samples from TLE patients, ample evidence has shown pathology beyond the hippocampus. A seminal histopathological study of 55 TLE patients reported atrophy across the cerebral cortex and cerebellum and suggested that they may influence the electrophysiological features of seizures [109]. A more recent quantitative histology study has corroborated this

finding by showing loss of neurons in the neocortical GM, particularly with large neurons [110]. Increased neuron density in temporal lobe WM secondary to cortical microdysgenesis [111] as well as demyelination and axonal degeneration are also among the key features coupled to clinical and cognitive outcomes [112]. Aside from cortical atrophy, gliosis has shown to be a feature in temporal and frontal poles and orbitofrontal cortex [113].

2.2.2 In vivo mapping of hippocampal sclerosis and whole-brain pathology

On MRI, marked hippocampal sclerosis (HS) appears as atrophy and T_2-weighted signal hyperintensity, generally more severe ipsilateral to the seizure focus. Accurate identification of hippocampal atrophy as a marker of HS is crucial for deciding the side of surgery. While volumetry has been one of the first computational analyses applied to TLE [114-119], the need for accurate localization of pathology has motivated a move from whole-structure volumetry to surface-based approaches allowing a precise mapping of anomalies along the hippocampal axis. In this context, 3D surface-based shape models permit localizing regional morphological differences that may not be readily identifiable [120]. Surface modeling based on spherical harmonics [121] has been particularly performant [122]. Following this method, hippocampal labels are processed using a series of spherical harmonics with increasing degree of complexity to parametrize their surface boundary. Anatomical inter-subject correspondence is guaranteed by aligning the surfaces of each individual to the centroid and the longitudinal axis of the first-order ellipsoid of the mean surface template derived from controls and patients. Computing the Jacobian determinants of the surface displacement vectors allows quantifying localized areas of atrophy [122, 123]. Overall, surface-based methods have proven superior to their volumetric counterparts not only in terms of segmentation performance [124] but also in predicting clinical outcomes as well as mapping disease progression [125,

126]. Extending this methodology by extracting features along the medial surface of hippocampal subfields has allowed to further probe the laminar integrity of this structure [127, 128] with increased lateralization performance [129].

The evidence for distributed whole-brain pathology has motivated the conceptualization of TLE as a system-level disorder[128]. Indeed, beside hippocampal pathology, a large number of *in vivo* MRI studies based on surface-based analysis has shown widespread, non-overlapping morphological [130, 131], intensity [132, 133], and microstructural [134] anomalies of the neocortex and the subcortical WM [112, 135-137] underscoring the complexity of this system disorder. Specifically, neocortical GM atrophy [130, 131], has been suggested to represent regions of neuronal loss [109] as well as synaptic reorganization [138]. Bilateral paralimbic neocortical gliosis indexed by FLAIR hyperintensity may hint at cytoarchitectural vulnerability of paralimbic cortices to gliotic processes [110, 132, 139], and may contribute to hyperexcitability and seizures [140, 141]. Widespread microstructural alterations of superficial WM likely reflect combined effects of decreased fiber density, altered myelin sheath and reactive astrogliosis [142-144]. Moreover, GM microstructural damage in the limbic cortices have been suggested to reflect myeloarchitectural alteration that disrupts fronto-limbic functional networks [134].

2.2.3. MRI evidence for disease progression

TLE follows a progressive course impacting brain structure and function. A plethora of cross-sectional studies has shown positive correlation between duration of epilepsy with GM atrophy and WM microstructural alterations of the mesiotemporal structures and beyond [4, 125, 131, 135, 145]. Concordantly, there is progressive cognitive impairment across multiple domains with longer disease duration [146-149]. Although relatively scarce due to logistical constraints, longitudinal data that adequately control for effects

of normal aging have confirmed these findings [125, 130, 150-152]. Potential mechanisms underpinning progressive structural alterations include the century-old hypothesis, "seizures beget seizures" [153], in that the seizures from the hippocampus damage itself and other mesiotemporal structures, namely thalamus [126, 151], which serve as a hub to spread seizure-induced damages to the neocortical GM [154] and WM microstructure [135] via thalamocortical networks [155, 156]. Furthermore, emerging data suggest that neurodegenerative processes driven by amyloid [157] and tau [158] pathology underpin TLE evolution. In Alzheimer's disease, neurodegenerative processes have shown to drive hippocampal and neocortical atrophy [159] as well as widespread axonal degeneration [160], which parallel the progressive structural pathology in TLE.

One key limitation of previous imaging studies analyzing disease progression has been the use of linear models that identify regions undergoing steady alterations, which do not account for the possibly variable temporal course of the disease that would inform on the sequence in which these regions become abnormal. In addition, by fitting a single population average, they assume that all patients follow the same disease trajectory, thereby not addressing possible phenotypic variability. Indeed, the increasingly recognized inter-individual heterogeneity of structural pathology and cognitive deficits [137, 161, 162] is a strong incentive to adopt novel image-based models of disease evolution. In this context, event-based models [163] estimate distinct stages that capture dynamic patterns of disease evolution from cross-sectional data, circumventing logistical burdens of a longitudinal design. A recent ENIGMA-Epilepsy study identified progressive atrophy that begins in the hippocampus, subsequently extending to the neocortex [164]. However, in addition to limiting the analysis to GM only, the inherent assumption was that all patients follow the same disease trajectory. Inability to disentangle temporal heterogeneity from phenotypic diversity limits the biological insights into disease mechanisms and the utility for patient stratification. Conversely, a

comprehensive framework that reconciles both sources of heterogeneity may inform on how TLE evolves for different subtypes, ultimately facilitating personalized diagnostics.

2.2.4. Phenotypic variability – Key to reliable prediction of clinical outcomes

While science investigating the neurobiology of epilepsy has been growing rapidly, translating knowledge into clinical practice has been limited. Specifically, individualized predictions of drug resistance, surgical outcome and cognitive dysfunction have been attempted with limited success [165]. For example, early investigations that aimed to predict anti-seizure medication response used machine learning on genomic data (namely single nucleotide polymorphisms) showed limited generalizability with inconsistent performance across studies [166-168]. Similarly, other models trained on electro-clinical and demographic features of thousands of patients [169-172] achieved high sensitivity (>90%), but unacceptably low specificity (<25%). Importantly, no external validation was performed on independent cohorts.

The prediction of seizure outcome after surgery has been extensively explored in TLE patients. Some of the early investigations relied on clinical [173] and neuropsychological features [174], achieving high performance, but in limited samples of less than 20 patients. Given the increasing conceptualization of TLE as a system-level disorder, numerous studies have tested the hypothesis that structural and functional alterations beyond the mesial temporal lobe may contribute to negative seizure outcome [175, 176]. For instance, WM microstructural features derived from diffusion tensor imaging have shown to achieve high sensitivity (70-86%), but modest specificity (65-70%) [177, 178]. Other studies have relied on connectivity features for prediction; these include nodal hubness of the thalamus and whole-brain distance-based measures of functional connectivity, which achieve an accuracy at about 75% but modest specificity (ranging from 35 to 62%)

[179, 180]. Conversely, while topological features of structural connectome have generally shown high predictive value for favorable post-surgical outcome, with an area under the receiver operating characteristics of 0.88, specificity for prediction of seizure relapse is low (29-54%) [181, 182]. Overall, the lack of large-scale external validation and relatively low specificity of these models need to be addressed to establish their generalizability and potential clinical use.

To date, most neuroimaging studies of epilepsy have been based on "one-size-fits-all" group-level analytical approaches. While such study designs can isolate reliable and consistent average group-level differences, they merely decipher the common patterns without modelling the inter-individual variations along the disease spectrum [183]. Conversely, the conceptualization of epilepsy as a heterogeneous disorder and explicit modeling of inter-individual phenotypic variations may be exploited to predict individual-specific clinical outcomes [184].

Initial histopathological report of phenotypic variability in the distribution and severity of MTS dates back to 1966 [109]. Moving beyond this diagrammatic representation, a quantitative approach based on neuronal counts on immunohistochemistry has shown several patient subgroups with distinct patterns and severity of hippocampal sclerosis [103]. Subsequently, a data-driven unsupervised clustering technique applied to immunohistochemistry-derived neuronal counts have established five HS subtypes with varying severity of atrophy across CA sectors and DG [107]. These histological evidence of variability motivated the emergence of international consensus system for HS classification by ILAE [105].

Inspired by these findings, recent studies have exploited inter-individual variability of imaging or cognitive phenotypes to optimize predictions of clinical outcomes. The first attempts were based on categorical models, which provided subtypes of patients with a given phenotype. Clustering applied to surface-based morphometry uncovered four TLE

subtypes having distinct subregional patterns of mesiotemporal atrophy [162]. These four subtypes differed with respect to histopathology and postsurgical seizure outcome. Classifiers operating on class membership accurately predicted surgical outcome in >90% of patients, outperforming learners trained on conventional MRI volumetry. In the context of cognition, unsupervised techniques have identified phenotypes, such as language and memory impairment associated with distinct patterns of WM microstructural damage [137] and connectome disorganization [161].

PART II

PROJECTS

3. Unsupervised Machine Learning Reveals Lesional Variability in Focal Cortical Dysplasia at Mesoscopic Scale

Preface

The critical role of detecting a structural lesion, particularly small FCD, for successful surgery has motivated automated techniques. To date, however, algorithms have assumed structural homogeneity, possibly limiting sensitivity and specificity.

This study tested a hypothesis that FCD variability is measurable at a millimetric scale and may improve automated lesion detection. We applied consensus clustering on structural MRI features to identify lesional tissue classes that collectively formed a given lesion. We then evaluated the link between FCD classes and histopathology and reproduced the classes in two independent datasets. To assess clinical utility, we compared the performance of a detection algorithm trained on class-informed data to a class-naïve paradigm.

MANUSCRIPT I – Published in NeuroImage Clinical

Unsupervised machine learning reveals lesional variability in focal cortical dysplasia at mesoscopic scale

Hyo M. Lee PhDc,[1] Ravnoor Gill PhDc,[1] Fatemeh Fadaie PhDc,[1] Kyoo H. Cho MD,[2] Marie C. Guiot MD,[3] Seok-Jun Hong PhD,[1] Neda Bernasconi MD PhD,[1] Andrea Bernasconi MD[1]

1) Neuroimaging of Epilepsy Laboratory, Montreal Neurological Institute and Hospital, McGill University, Montreal, Quebec, Canada; 2) Department of Neurology, Yonsei University College of Medicine, Seoul, Korea; 3) Department of Pathology, Montreal Neurological Institute and Hospital, McGill University, Montreal, Quebec, Canada

ABSTRACT

Focal cortical dysplasia (FCD) is the most common epileptogenic developmental malformation and a prevalent cause of surgically amenable epilepsy. While cellular and molecular biology data suggest that FCD lesional characteristics lie along a spectrum, this notion has not been verified *in vivo*. We tested the hypothesis that machine learning applied to MRI captures FCD lesional variability at a mesoscopic scale. We studied 46 patients with histologically verified FCD Type II and 35 age- and sex-matched healthy controls. We applied consensus clustering, an unsupervised learning technique that identifies stable clusters based on bootstrap-aggregation, to 3T multicontrast MRI (T1-weighted MRI and FLAIR) features of FCD normalized with respect to distributions in controls. Lesions were parcellated into four classes with distinct structural profiles variably expressed within and across patients: Class-1 with isolated white matter (WM) damage; Class-2 combining grey matter (GM) and WM alterations; Class-3 with isolated GM damage; Class-4 with GM-WM interface anomalies. Class membership was replicated in two independent datasets. Classes with GM anomalies impacted local function (resting-state fMRI derived ALFF), while those with abnormal WM affected large-scale connectivity (assessed by degree centrality). Overall, MRI classes reflected typical histopathological FCD characteristics: Class-1 was associated with severe WM gliosis and interface blurring, Class-2 with severe GM dyslamination and moderate WM gliosis, Class-3 with moderate GM gliosis, Class-4 with mild interface blurring. A detection algorithm trained on class-informed data outperformed a class-naïve paradigm. Machine learning applied to widely available MRI contrasts uncovers FCD Type II variability at a mesoscopic scale characterized by tissue classes with distinct structural dimensions, functional and histopathological profiles. Integrating *in vivo* staging of FCD traits with automated lesion detection is likely to inform the development of novel personalized treatments.

3.1 Introduction

Focal cortical dysplasia (FCD) Type II is the most common epileptogenic developmental malformation and a prevalent cause of surgically amenable epilepsy. Histopathologically, FCD is typified by intracortical dyslamination and dysmorphic neurons, either in isolation (Type IIA) or together with balloon cells (Type IIB) [15]. From a neurobiological standpoint, whether FCD II subtypes represent distinct entities or a spectrum is a matter of debate. Recent studies have shown significant cellular variability, with anomalies that may vary across lesions with the same subtype [90]. Moreover, multiple subtypes may co-exist within the same FCD, with the most severe features determining the final diagnosis [12]. On MRI, FCD may appear as increased cortical thickness, abnormal signal intensity and blurred appearance [9]. The critical role of a lesion for successful surgery [6, 7] has motivated the development of automated methods aimed at detecting small FCD lesions often overlooked on routine radiological inspection [81, 82]. To date, algorithms have assumed structural homogeneity [185], possibly limiting sensitivity and specificity. In recent years, data-driven techniques applied to neuroimaging have offered novel perspectives on brain disorders. Specifically, categorical discovery of subtypes and dimensional modeling of disease traits variably expressed within individuals, have provided diagnostic and prognostic markers in several conditions, including in Alzheimer's disease [186], depression [187] and autism [188].

Assessing variability may offer a novel basis to advance our understanding of FCD neurobiology and improve lesion detection. Here, we tested the hypothesis that FCD variability is measurable at a millimetric scale within and between lesions. Specifically, we applied consensus clustering, a procedure in which clustering is repeated across 10,000 bootstraps (i.e. random subsampling of intra-FCD tissues with replacement) to estimate the stability matrix that stores the likelihood of intra-lesional tissues to belong to the same cluster (or classes); a subsequent clustering on this matrix identifies "stable"

classes that had consistently emerged across bootstraps [189]. The resulting FCD classes, which aggregate to form a given FCD, quantifies the *in vivo* expression of multiple pathological traits rather than assigning a given FCD to a single category. Hence, this approach combines dimensional modelling of individual lesions with categorical description of intra-lesional tissue classes. In addition, we evaluated the relationship of FCD classes to histopathology, as well as local function and large-scale connectivity as determined by resting-state fMRI. Reproducibility was assessed in two independent datasets. Finally, clinical utility was tested by comparing the performance of a detection algorithm trained on class-informed data to a class-naïve paradigm.

3.2 Materials and methods

Participants

From a database of patients with drug-resistant epilepsy admitted to the Montreal Neurological Institute and Hospital between 2009 and 2018, we selected 46 consecutive individuals with histologically-proven FCD (22 females, 47.8%; mean ± SD age = 27.1 ± 8.6 years) who had research-dedicated structural and functional MRI scans, henceforth named discovery dataset. The pre-surgical workup included seizure history, neurologic examination, neuroimaging, and video-EEG monitoring. EEG inter-ictal activity and ictal onset were concordant with the location of FCD lesions in 42 (91%) and 32 (70%) patients, respectively. In 25, surgery was preceded by invasive monitoring using stereotactic depth electrodes; all displayed high inter-ictal activity and focal changes at seizure onset in electrodes targeting the lesion. At a mean ± SD postoperative follow-up [190] of 8.4 ± 2.2 years, 30 patients became seizure-free (Engel-I), 11 had rare disabling seizures (Engel-II), and 5 had worthwhile improvement (Engel-III).

Serial 5µm paraffin-embedded histological sections of lesional tissue were stained with haematoxylin and eosin or Bielschowsky, and others immunostained using antibodies against GFAP, non-phosphorylated neurofilaments (SMI-32 monoclonal), microtubule-associated protein-2 (MAP-2), and neuronal specific nuclear protein (NeuN). FCD Type-II was defined as disrupted cortical lamination with dysmorphic neurons in isolation (IIA, n=21) or together with balloon cells (IIB, n=25). We evaluated severity of cortical dyslamination, blurring of cortical interface and gliosis using categorical scoring (1=mild, 2=moderate, 3=severe).

In 70% of patients, routine radiological assessment was unremarkable with equal proportions between Type IIA (16/21) and Type IIB (16/25) ($p = 0.37$); the FCD lesion was subsequently recognized through inspection of texture maps that combine intensity model of cortical thickness, gradient map of GM-WM boundary blurring and normalized intensity map [9]. There were no differences in age (27.7 ± 10.1 years *vs.* 26.6 ± 6.2 years, $p = 0.64$), sex (11 *vs.* 13 females, $p = 0.98$) and age at onset (13.6 ± 8.5 years *vs.* 11.2 ± 7.5 years, $p = 0.31$) between patients with FCD Type IIA and Type IIB.

The control group consisted of 35 age- and sex-matched healthy individuals (16 females, age = 28.8 ± 5.7 years). The Ethics Committee of the Montreal Neurological Institute and Hospital approved the study, and the written consent was obtained from all participants in accordance with the Declaration of Helsinki.

MRI acquisition

Images were acquired on a 3T Siemens TimTrio scanner using a 32-channel head coil. The protocol included the following sequences: 3D T1-weighted MPRAGE (T1w; TR = 2300 ms, TE = 2.98 ms, flip angle = 9°, voxel size = 1×1×1 mm^3), 3D fluid-attenuated inversion recovery (FLAIR; TR = 5000 ms, TE = 389 ms, flip angle = 120°, 0.9×0.9×0.9 mm^3) and echo

planar resting state fMRI (rsfMRI; TR = 2020 ms, TE = 30 ms, flip angle = 90°, 34 slices, voxel size = 4×4×4 mm^3, 150 volumes). For the latter, participants were instructed to lie still with their eyes closed while remaining awake. To reduce signal loss and distortions in orbitofrontal and mesiotemporal regions, slices were tilted in an oblique axial orientation.

MRI preprocessing and surface construction

T1w and FLAIR images underwent field non-uniformity correction, intensity normalization and linear registration to stereotaxic space based on the hemisphere-symmetric ICBM MNI152 template using MINC toolkit (https://bic-mni.github.io/). T1w images were classified into white matter (WM), grey matter (GM) and cerebrospinal fluid (CSF) [191]. FLAIR images were linearly mapped to T1w images in MNI space. The rs-fMRI was analyzed using DPARSF (rfmri.org/DPARSF); after discarding the first 5 time-points, the data underwent slice-timing and motion correction, realignment and statistical correction for nuisance effects of WM and CSF signals. To further correct for residual motion, time-points with a frame-wise displacement of >0.5 mm were included as separate covariates [192] in a linear model alongside the estimates of head motion (i.e., 3D rotations and translations, obtained from motion correction procedure) and used as final signals for the analyses. The time-points were then band-pass filtered at 0.01-0.08 Hz. Images were co-registered to the native T1w space using a boundary-based approach that maximizes alignment between intensity gradients of structural and echo-planar data [193]. The accuracy of multimodal registration was verified through visual inspection and errors corrected manually; we have shown accuracy of our registration using quantitative metrics [194].

We applied Constrained Laplacian Anatomic Segmentation using Proximity (CLASP) algorithm to generate models of GM-WM and GM-CSF surfaces with 41k surface points (or vertices) per hemisphere [191]. In short, CLASP iteratively expands a surface mesh to fit the GM-WM surface and subsequently estimates the GM-CSF surface by expanding the GM-WM surface along the Laplacian gradient between the two surfaces. Surface-based registration, which aligns individual participants based on cortical folding, was performed to enhance vertex-wise anatomical correspondence across participants [195]. Surface extraction accuracy was visually verified, and inaccuracies were manually corrected.

Surface-based feature extraction

Two experts (AB, NB) blinded to clinical information independently segmented the FCD lesions on co-registered T1w and FLAIR images; interrater Dice agreement index was 0.91 ± 0.11. Their combined volume label (the union of the two segmentations) was intersected with cortical surfaces to generate surface based FCD label, which served as input to the clustering algorithm. We calculated at each vertex belonging to the label morphological, intensity and functional features. To minimize interpolation, we mapped the surfaces to the native space of each modality using the inverse transform of the initial co-registration. To enhance the signal-to-noise of the features while retaining high spatial specificity, we applied smoothing using a 2D quadratic diffusion kernel with 2 mm full-width-half-maximum. We then computed z-scores for each feature with respect to the distribution of the analogous tissues in healthy controls. For controls, we computed z-scores using a leave-one-out scheme.

To examine intracortical GM, we positioned three surfaces between the inner GM-WM and outer GM-CSF surfaces at 25%, 50%, and 75% cortical thickness, systematically

sampling the axis perpendicular to the cortical ribbon [194]. To assess the superficial WM, we generated surfaces running 1, 2 and 3 mm below the GM-WM surface guided by a Laplacian gradient between the GM-WM surface and ventricles [135]. We then sampled the following vertex-wise features:

a) Cortical thickness. To model GM thickening, we measured cortical thickness as the Euclidean distance between corresponding vertices of GM-WM and GM-CSF surfaces [196].

b) Normalized FLAIR intensity. Gliosis is associated with increased FLAIR signal intensity [71]. We divided FLAIR intensity by the average of GM-WM interface intensity. This value was normalized with respect to the mode of the FLAIR intensity histogram [82], corrected for CSF partial volume and mapped on each intracortical/subcortical surface. Intensities were sampled at 25, 50 and 75% intracortical and 1, 2 and 3 mm subcortical surfaces.

c) Gradient. To model GM-WM interface blurring, vertical gradients were computed at the GM-WM interface as T1w and FLAIR intensity differences between corresponding vertices along the 75% intracortical and 1 mm subcortical surfaces divided by the Euclidean distance between them.

d) T1w/FLAIR ratio. Despite histopathological evidence [197], FCD-associated microstructural anomalies have not been previously assessed *in vivo*. To this purpose, we sampled T1w/FLAIR ratio as a proxy for myelin content [198]; decreases are interpreted as hypomyelination [134]. After sampling T1w/FLAIR ratio at 25, 50 and 75% intracortical and 1, 2 and 3 mm subcortical surfaces, we used a local cylindrical kernel approach to correct for outliers due to bulk blood vessels and CSF partial volumes [198].

e) Functional derivatives. To assess local function, we calculated amplitude of low frequency fluctuations (ALFF), a measure of bulk activation shown to relate to interictal spiking [199]. Moreover, we computed degree centrality (DC), a measure of connectivity to the rest of the brain [200]. These features were computed voxel-wise in volume space and then mapped to the 50% intracortical surface.

Data-driven clustering of lesional vertices

We applied consensus clustering [189], a procedure in which clustering is repeated across 10,000 bootstraps (i.e. random subsampling of intra-FCD tissues with replacement) to estimate the stability matrix that stores the likelihood of intra-lesional tissues to belong to the same cluster (or classes); a subsequent clustering on this matrix identifies "stable" classes that had consistently emerged across bootstraps (**Figure 4**). Specifically, we first generated a data matrix where columns represent FCD vertices and rows the structural features (for a total of 19,253 columns and 15 rows). We then defined six feature groups representing distinct aspects of FCD pathology [194]: 1) Intracortical FLAIR intensity (derived from 75, 50 and 25% intracortical surfaces); 2) Subcortical FLAIR intensity (1, 2 and 3 mm subcortical surfaces); 3) Intracortical T1w/FLAIR ratio (75, 50 and 25% intracortical surfaces); 4) Subcortical T1w/FLAIR ratio (1, 2 and 3 mm subcortical surfaces); 5) GM-WM interface T1w and FLAIR vertical gradients; 6) Cortical thickness. Since groups had different number of features, a stratified duplication matched numbers across categories given by the lowest common denominator, namely six; this ensured that the feature groups' contributions to the clustering solution was not driven by differences in the number of features. To ensure equal contribution of each patient regardless of FCD size, we performed 10,000 iterations of patient-stratified bootstrapping. For each bootstrap, we randomly sampled 70% of FCD vertices with replacement after setting their

sampling probability proportional to the inverse of the lesion size and computed pairwise similarity matrices using eta^2, a metric accounting for differences in scaling and offsets between features [201]. Finally, we performed spectral clustering on this similarity matrix by combining clustering solutions from the 10,000 bootstraps into a consensus matrix that stores pairwise probabilities of FCD vertices to belong to the same cluster. Spectral clustering on this consensus matrix, henceforth consensus clustering, identified classes with distinct structural profiles that consistently emerged across bootstraps.

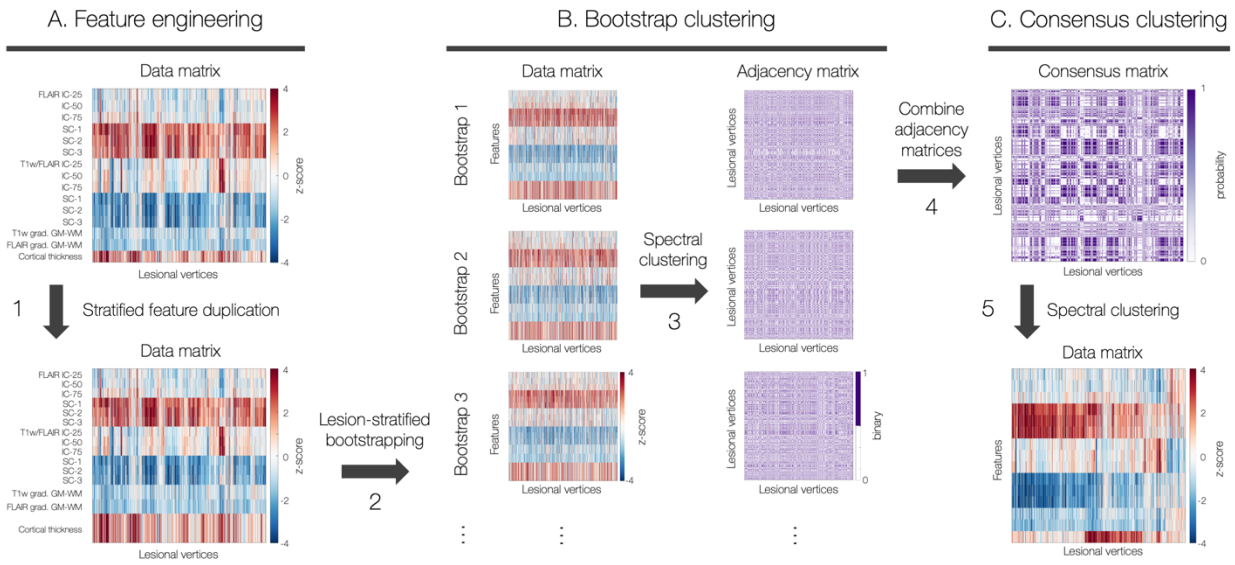

Figure 4. Clustering framework. A. Feature engineering. Data matrix shows vertex-wise lesional features at various intra-/subcortical levels, z-scored with respect to the distribution in healthy controls. To obtain balanced contributions, stratified feature duplication matched the number of member features of the feature groups (**1**). **B. Bootstrap clustering.** Lesion-stratified bootstrapping generated 10,000 data subsets based on 70% random subsampling with replacement while ensuring equal contributions from all patients regardless of FCD size (**2**). Spectral clustering was applied to each bootstrap using an eta-squared similarity matrix (**3**). **C. Consensus clustering.** Solutions from 10,000 bootstraps were combined into a consensus matrix storing probabilities of all pairs of lesional vertices to belong to the same cluster (**4**). Spectral clustering on the consensus matrix identified distinct clusters that consistently emerged across bootstraps **(5)**. B and C were repeated for K = 2 to 5. See methods for details. Abbreviations. FLAIR: fluid-attenuated inversion recovery; GM: gray matter; int: intensity; IC/SC: intra-/subcortical; WM: white matter.

Evaluation of clustering solutions

For each pair of lesional vertices, we calculated the percentage of bootstrap solutions that had the same adjacency as the one in the consensus clustering solution. The percentage averaged across all pairs defined the percent agreement for the stability of fit for each K. The goodness of fit was computed using the inverse of Davies-Bouldin index, which measures the ratio between inter-cluster distance (how far clusters are separated from each other) and intra-cluster distance (how far members of a cluster are from its centroid); a higher index indicates a better fit. Bootstrap and consensus clustering were repeated for K = 2-5. We chose the K that yielded optimal percent agreement and goodness of fit.

Statistical analysis

Student t-tests assessed vertex-wise differences in structural profiles of FCD classes with respect to analogous vertices of healthy controls. Linear mixed-effect models evaluated associations between FCD classes and function; the hemisphere harboring each patient's FCD was matched to that of a healthy control for sex and closest age (without re-using the same control hemisphere), for a total of 19,253 healthy vertices matched to 19,253 lesional vertices. For patient-wise analysis, Student t-tests compared the relative proportion of each FCD class with histopathology. Logistic regression assessed associations between proportions of classes and clinical parameters, including age at onset, generalized seizures, interictal epileptic discharges distribution and frequency and multinomial logistic regression for variables with more than two categories. Age, sex and

lesion size were included as covariates. Results were corrected for multiple comparisons using the False discovery rate (FDR) at $q_{FDR} < 0.05$ [202].

Data-driven FCD detection

We evaluated the yield of FCD class-membership for automated lesion detection using extreme gradient boosting, a scalable tree boosting system [203]. Each vertex was indexed with structural features and FCD class label. Inputs consisted of the original 15 features used for clustering in addition to their means across neighboring vertices in distance intervals of 0-2 and 2-4 mm. We implemented a two-stage classification strategy. The first was designed to maximize sensitivity and consisted of four classifiers each tuned to one of the discovered FCD classes; predictions were fed into a meta-classifier to produce the final prediction. The second was aimed at improving specificity by removing false positives from the first stage; it also consisted of the same four classifiers followed by a meta-classifier. For training, we performed random upsampling with replacement of each FCD lesion to match the number of vertices to that of the largest lesion; the same procedure was applied to the sampling of healthy vertices, thus ensuring that each patient contributed equal number of lesional and healthy vertices. In addition, to ensure that the lesional and healthy vertices contribute equal weights, we scaled the weight of the lesional class by the ratio between the total number of healthy and lesional vertices. The classifier was then trained using a 5-fold cross validation with 100 repetitions; this procedure, by which 20% of patients are classified using data from the remaining 80%, allows unbiased estimation of performance for previously unseen FCD. Finally, we compared the classification performance of the class-informed algorithm to a class-naïve classifier using two-sided McNemar's test. Student t-test assessed patient-wise sensitivity (percentage of detected FCD) and specificity (number of false-positive clusters).

Replication analysis

We assessed generalizability in two separate cohorts of patients with histologically-verified FCD examined at the Montreal Neurological Institute and Hospital (n = 14; 7 females; mean age = 24.3 ± 4.6 years) and the Severance Hospital in South Korea (n = 12, 4 females; mean age = 25.8 ± 8.0 years), with 3D T1w and FLAIR images acquired on a 3T Siemens Prisma and 3T Philips Achieva using 32-channel head coils, respectively. The MRI pre-processing and clustering procedures were identical to those applied to the discovery cohort. To mitigate effects of scanner/site difference, imaging features underwent subject-wise z-normalization prior to z-normalization with respect to healthy controls.

3.3 Results

FCD Type II lesions were parcellated into four classes with distinct structural profiles, functional impact and histopathological embedding.

Data-driven FCD clustering (**Figure 5**)

Clustering achieved optimal stability and goodness of fit parameters at K=4, dichotomizing lesional vertices across patients into four distinct classes; results were highly stable across 10,000 bootstrap instances, supporting robustness. Across classes,

GM and WM profiles were significantly different from healthy controls (Student t-tests, $q_{FDR} < 0.05$): Class-1 with severe isolated WM anomalies, characterized by increased FLAIR intensity (indexing gliosis) and decreased T1w/FLAIR intensity (indexing hypomyelination), as well as subtle decrease in vertical gradients of T1w and FLAIR at the GM-WM interface (indexing blurring), but virtually no GM changes; Class-2 with severe GM thickening combined with moderate increase in WM FLAIR, decreased T1w/FLAIR and subtle interface blurring; Class-3 with only moderate increase in intracortical FLAIR and decreased T1w/FLAIR, but no WM abnormalities; Class-4 with moderate increase in intracortical T1w/FLAIR and decrease in FLAIR intensity, as well as moderate interface blurring. FCD lesions expressed at least two classes, regardless of lesion size.

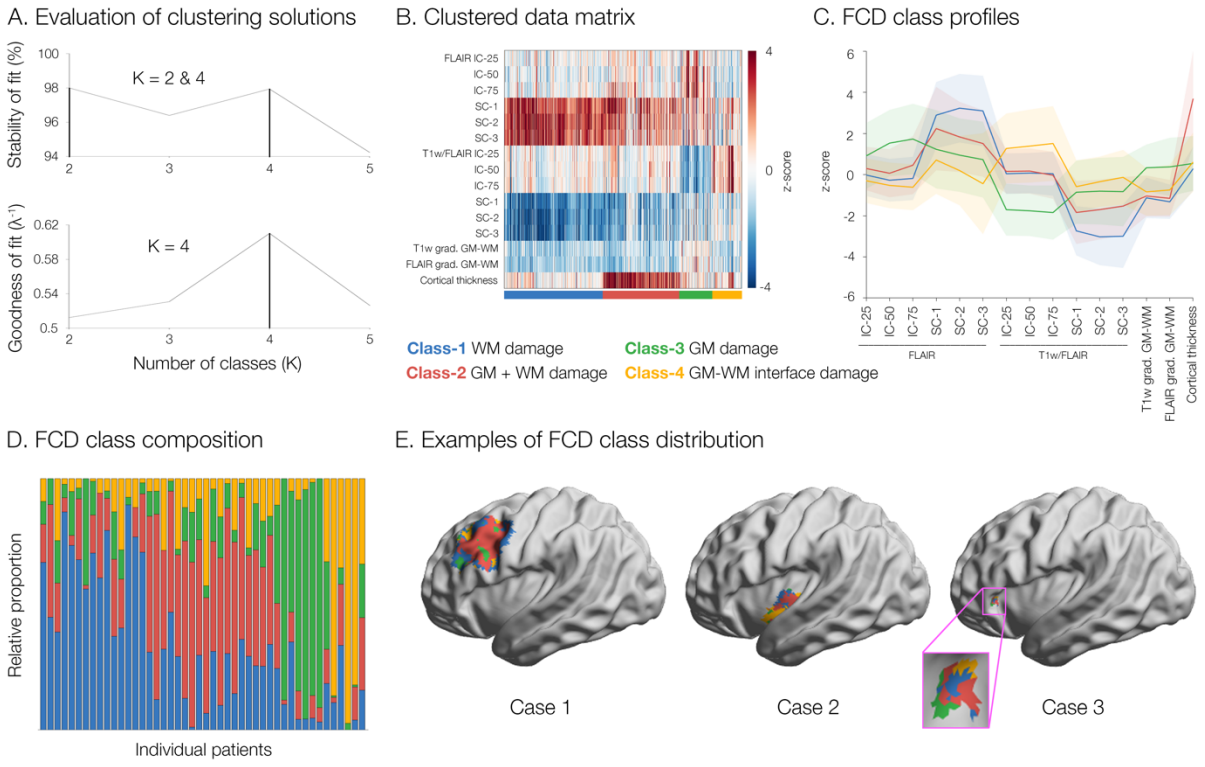

Figure 5. Class membership. A. Stability of fit (based on percent agreement of clustering solutions) and goodness of fit (based on inter-/intra-cluster scatter ratio) indicated K=4 as optimal. **B.** The data matrix shows the feature profiles of the four FCD classes color-coded with respect to class memberships. The rows

represent features, the columns represent the lesional vertices; features are z-scored with respect to the distribution in healthy controls. **C.** The line plots show the mean and standard deviations of feature profiles of the four FCD classes z-scored with respect to healthy controls. **D.** Relative proportions of FCD classes within individual patients. **E.** Representative examples of large (case 1), medium (2) and small (3) FCD lesions are shown.

Similar to the discovery dataset, K=4 showed optimal stability and goodness of fit in the two independent cohorts with the structural profiles of FCD classes closely matching (**Supplemental Figure 1**).

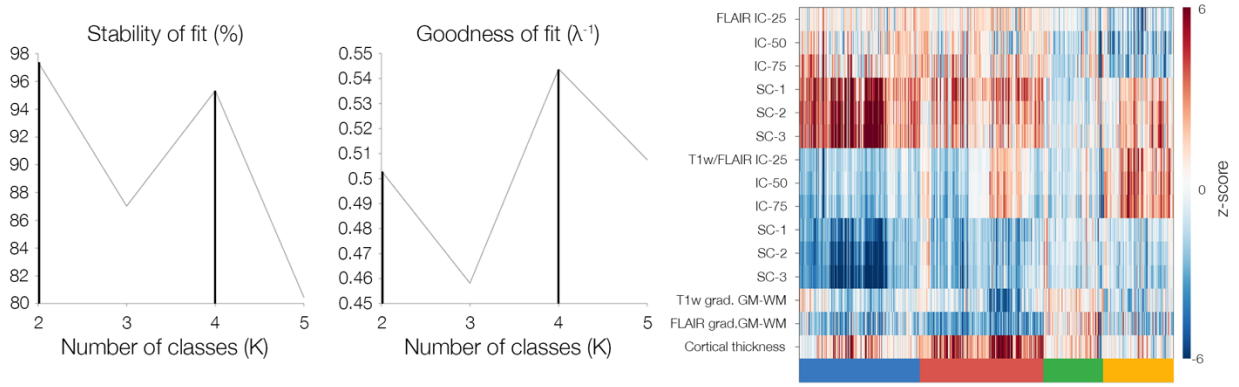

Supplemental Figure 1. Replication analysis. Consensus clustering was performed on two independent datasets, from the Montreal Neurological Institute, Canada (Dataset 1; 3T Siemens Prisma scanner) and the Severance Hospital, South Korea (Dataset 2; 3T Philips Achieva). The matrix shows feature profiles of the four classes, which closely resemble those observed in the discovery dataset.

Relationship to function (**Figure 6**)

Class-1 was mainly characterized by moderate decrease in large-scale connectivity ($q_{FDR} < 0.01$, Cohen's effect size d = -0.23), but negligible decrease in local function ($q_{FDR} < 0.001$, d = -0.05); Class-2 by severe decrease in local function ($q_{FDR} < 0.001$, d = -0.69) and moderate decrease in connectivity ($q_{FDR} < 0.01$, d = -0.46); Class-3 and Class-4 by decrease

in local function, severe in the former ($q_{FDR} < 0.001$, d = -0.77) and moderate in the latter ($q_{FDR} < 0.01$, d = -0.40), but no change in connectivity.

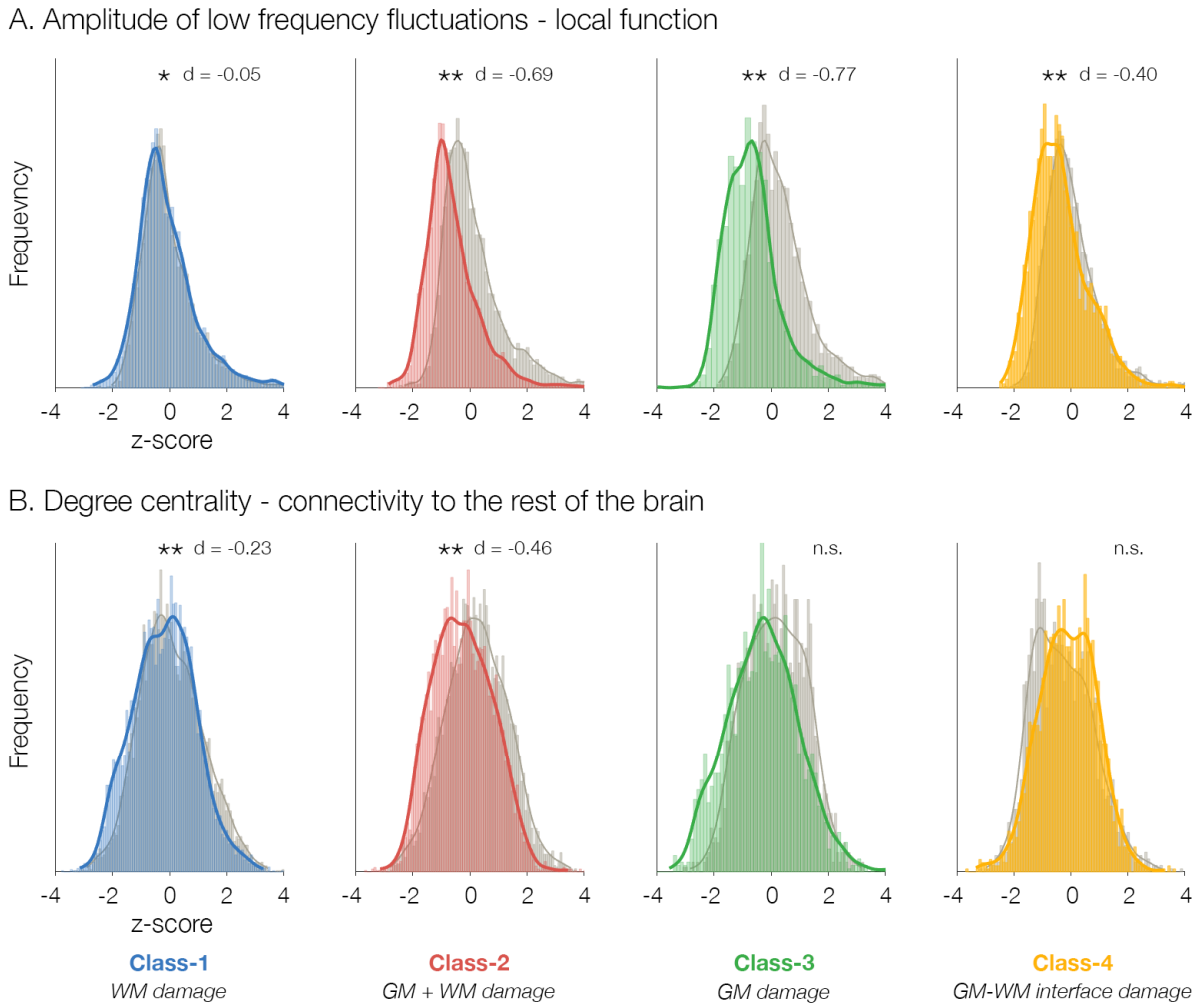

Figure 6. Relationship of FCD classes to function. Histograms show group results of amplitude of low frequency fluctuations indexing local function (**A**) and degree centrality, a measure of connectivity to the rest of the brain (**B**) for each FCD class (colored) compared to healthy controls (gray). Cohen's d effect size is indicated above each histogram; n.s./*/**: not significant/trends ($p < 0.05$)/significant after FDR correction ($q_{FDR} < 0.05$).

Relationship to histopathology (**Figure 7**)

Overall, MRI classes reflected typical histopathological FCD characteristics. The proportion of Class-1 vertices was more prevalent in lesions with severe WM gliosis and GM-WM interface blurring ($q_{FDR} < 0.05$), Class-2 in those with severe GM dyslamination and gliosis, as well as moderate interface blurring and WM gliosis ($q_{FDR} < 0.05$), Class-3 with moderate GM gliosis ($q_{FDR} < 0.05$), Class-4 with mild interface blurring ($q_{FDR} < 0.05$). While Class-2 was associated with Type IIB with balloon cells (log odds ratio: 5.02, $p < 0.01$), the proportion of Type IIB and IIA did not differ among the other Classes.

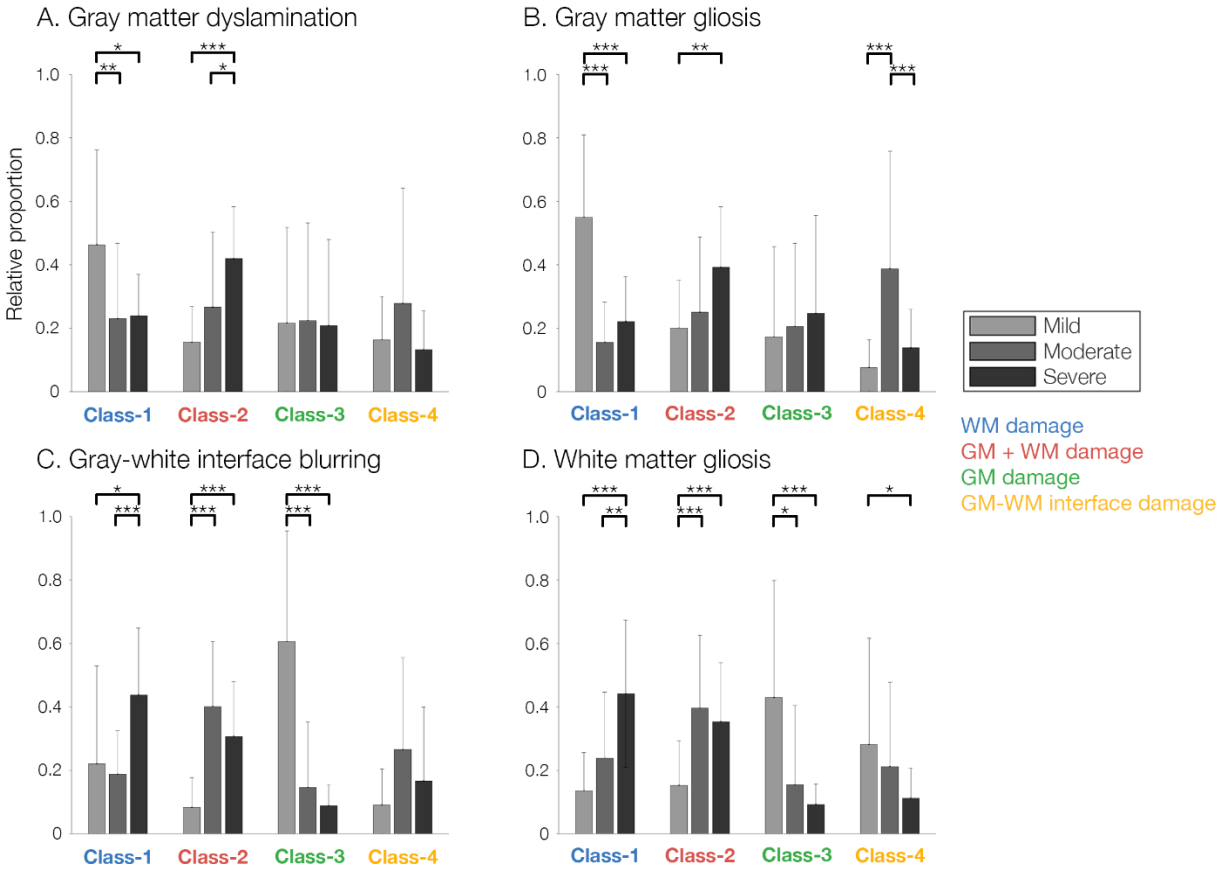

Figure 7. Histopathological embedding of FCD classes. The bar graphs indicate mean and standard deviation proportions of FCD classes in lesions with mild, moderate and severe histopathological features. Student's t-test compared class proportions between subdivisions with trends at $p < 0.1$ (*), $p < 0.05$ (**) and significant differences at $q_{FDR} < 0.05$ (***).

Relationship to clinical parameters

The relative proportions per lesion of Class-2 and Class-4 were associated with early disease onset (< 10 years; log odds ratio: 4.20 and 3.78; p=0.02 and p=0.04, respectively). With regards to epileptic activity, Class-1 and showed marginal association with rare compared to very frequent IEDs (log odds ratio=-2.81; p=0.07), and Class-3 with focal compared to bilateral IEDs (log odds ratio = -8.84; p = 0.07).

Data-driven FCD detection

The number of FCD vertices that the class-informed paradigm correctly predicted but class-naïve incorrectly predicted (mean ± SD = 4,770 ± 826) was higher than those the class-naïve correctly predicted but class-informed incorrectly predicted (n = 2,698 ± 172); disparity in performance was significant across all 100 repetitions (two-sided McNemar's test; p < 1e-5). At patient-level, the class-informed paradigm detected a higher number of lesions than the class-naïve (77 ± 3% *vs.* 73 ± 3%; p < 1e-5), while the number of false positive clusters did not differ (5 ± 0.3 *vs.* 5 ± 0.5).

3.4 Discussion

Whether FCD Type IIA and IIB represent distinct entities or a spectrum has been a matter of debate. Beside evidence for molecular variability [204], recent observations suggest co-expression of multiple histological subtypes within the same FCD lesion [12, 90]; moreover, severity and arrangement of pathological features may vary between lesions

assigned to the same subtype [205], supporting the notion of a spectrum. Harnessing the power of bootstrap-aggregated consensus clustering, we quantified the *in vivo* expression of multiple pathological traits for a given FCD rather than assigning them to a single category, thus moving beyond previous studies assuming structural homogeneity. The high stability of clustering solutions from 10,000 bootstraps, obtained using a conservative approach based on 70% random subsampling with replacement, suggests that the FCD classes may generalize beyond the discovery dataset of this study. Indeed, this was consolidated by the replication in two independent datasets. Lesions were parcellated into four classes with distinct structural profiles variably expressed within and across patients. Classes had differential histopathological features and functional embeddings. Clinical utility is supported by gain in performance of a lesion detection algorithm trained on class-informed data compared to a class-naïve paradigm; a main contributor resides in the explicit modeling of structural variability in the class-informed paradigm allowing FCD classes to equally contribute to the training.

The gradual structural compromise we observed across individual lesions is compatible with a spectrum and provides the basis for a dimensional conceptualization of FCD. Phenotypical variability is further supported by the fact that discovered classes did not show consistent associations with histological subtypes. While the absence of digitized tissue samples prevented a fully quantitative comparison between MRI and histology, our imaging markers reflecting categorical variations of main FCD features emphasize the ability of post-processing to capture histopathological variations at mesoscopic scale. Indeed, MRI-derived Classes with preferential WM damage (1 and 4) were more commonly associated with histopathological features of severe GM-WM interface blurring and WM gliosis, while those with GM damage (2 and 3) displayed intracortical dyslamination and gliosis. Notably, only Class-2 typified by severe cortical thickening was associated with Type IIB, possibly in relation to increased neuronal cell diameter and

balloon cells [206]. Notably, however, accurate histological characterization may be arduous for various reasons, including incomplete surgical sampling [73, 207], difficulty of perpendicular sectioning with respect to the pial surface [208] due to variability in size and quality of resections, as well as the logistic burden of immunohistochemistry [208, 209].

Besides optimized performance for automated detection, the clinical relevance of FCD classes is further supported by their relation to electro-clinical parameters and age of onset. From an electrophysiological perspective, Class-1 with preferential WM damage, was associated with rare IEDs, while Class-3 with selective cortical anomalies being associated with focal discharges. Classes driven by GM anomalies had an impact on local function, whereas those with WM changes affected large-scale connectivity. A likely explanation lies in the developmental origin of FCD with stage-dependent modulation of genetically-driven molecular perturbations [65]. Anomalous local function may relate to GM alterations secondary to aberrant cell proliferation during mitotic cycles, whereas WM alterations may be linked to defective later-stage neuronal migration [10]. This is consistent with our results showing early disease onset in patients with predominant GM pathology classes. Cortical development consists of three successive but partially overlapping stages of cell proliferation, neuronal migration and cortical organization [22]. Thus, co-expression of two or more classes within lesions suggests that molecular perturbations along overlapping stages of neurodevelopment may contribute to the overall pathological makeup of FCD.

3.5 Conclusions

The presented data-driven approach uncovered FCD Type II variability at a mesoscopic scale, revealing tissue classes with distinct structural dimensions, functional and

histopathological profiles. From a clinical standpoint, integrating *in vivo* staging of FCD pathology with automated algorithms relying on widely available MRI contrasts is likely to pave the way for the detection of the most subtle form of cortical dysplasia characterized by isolated intra-cortical dyslamination, an elusive entity currently representing one of the main barriers to epilepsy surgery [7, 73]. Moreover, addressing the full spectrum of FCD traits may play a key role in establishing genotype-phenotype associations and their clinical translation, opening opportunities to inform the development of novel personalized treatments [210] so far mainly hindered by the lack of phenotypes linked to FCD somatic variants [211].

BRIDGING TEXT

Project I characterized a wider diversity of FCD's MRI signatures, motivated by the diversity of its histopathological features, and demonstrated an added utility in detecting subtle lesions for surgical resection. Conversely, understanding the molecular mechanisms that give rise to a broad spectrum of FCD pathology is a pivotal milestone that may lead to novel therapeutic targets. Yet, previous molecular studies have largely focused on the regulatory genes of the mTOR pathway as the causal mechanism. In the following project, we explore the neurogenic mechanisms associated with FCD-prone cortices across multiple spatial scales, including whole-brain transcriptomics and histology.

4. MULTIMODAL MAPPING OF REGIONAL BRAIN VULNERABILITY TO FOCAL CORTICAL DYSPLASIA

PREFACE

Clinical observations suggest that FCD frequently occurs in the frontal lobe, but the mechanisms for such propensity remain unexplored. The normally developing cortex undergoes area-specific, genetically regulated neurogenesis, synaptogenesis and circuit development that give rise to variations in cytoarchitecture. Given the strong genetic influence on regional cytoarchitecture, the molecular and architectural features of the FCD-prone cortices may inform on the neurogenic mechanisms underpinning this malformation.

Here, we hypothesized that cortex-wide spatial associations of FCD distribution with cortical cytoarchitecture, gene expression and organizational axes may offer complementary insights into processes that predispose given cortical regions to harbor FCD.

MANUSCRIPT II – Accepted for publication in Brain

Multimodal Mapping of Regional Vulnerability to Focal Cortical Dysplasia

Hyo M. Lee,[1] Seok-Jun Hong,[1,2] Ravnoor Gill,[1] Benoit Caldairou,[1] Irene Wang,[3] Jian-guo Zhang,[4] Francesco Deleo.[5] Dewi Schrader,[6] Fabrice Bartolomei,[7] Maxime Guye,[8] Kyoo Ho Cho,[9] Carmen Barba,[10] Sanjay Sisodiya,[11] Graeme Jackson,[12] R. Edward Hogan,[13] Lily Wong-Kisiel,[14] Gregory D. Cascino,[14] Andreas Schulze-Bonhage,[15] Iscia Lopes-Cendes,[16] Fernando Cendes,[16] Renzo Guerrini,[17] Boris Bernhardt,[18] Neda Bernasconi[1] and Andrea Bernasconi[1]

1) Neuroimaging of Epilepsy Laboratory, Montreal Neurological Institute, McGill University, Montreal, Canada; 2) Center for Neuroscience Imaging, Research Institute for Basic Science, Department of Global Biomedical Engineering, SungKyunKwan University, Suwon, KoreaSuwon, Korea; 3) Epilepsy Center, Neurological Institute, Cleveland Clinic, Cleveland, OH, USA; 4) Department of Functional Neurosurgery, Beijing Tiantan Hospital, Capital Medical University, Beijing, China; 5) Epilepsy Unit, Fondazione IRCCS Istituto Neurologico C. Besta, Milano, Italy; 6) Department of Pediatrics, British Columbia Children's Hospital, Vancouver, Canada; 7) Aix Marseille Univ, INSERM, INS, Institut de Neurosciences des Systèmes, Marseille, 13005, France; 8) Aix Marseille University, CNRS, CRMBM UMR 7339, Marseille, France; 9) Department of Neurology, Yonsei University College of Medicine, Seoul, Korea; 10) Neuroscience Department, Children's Hospital A. Meyer-University of Florence, Italy; 11) Department of Clinical and Experimental Epilepsy, UCL Queen Square Institute of Neurology, London, UK; 12) The Florey Institute of Neuroscience and Mental Health and The University of Melbourne, Victoria, Australia; 13) Department of Neurology, Washington University School of Medicine, St Louis, Missouri, USA; 14) Mayo Clinic, Department of Neurology, Rochester, MN, USA; 15) Epilepsy Center, University Medical Center-University of Freiburg, Freiburg, Germany; 16) Department of Translational Medicine, School of Medical Sciences, University of Campinas (UNICAMP) and the Brazilian Institute of Neuroscience and

Neurotechnology (BRAINN), Campinas SP, Brazil; 17) Department of Neurology, School of Medical Sciences, University of Campinas (UNICAMP), and the Brazilian Institute of Neuroscience and Neurotechnology (BRAINN), Campinas SP, Brazil; 18) Multimodal Imaging and Connectome Analysis Lab, McConnell Brain Imaging Centre, Montreal Neurological Institute and Hospital, McGill University, Montreal, QC, Canada

ABSTRACT

Focal cortical dysplasia (FCD) type II is a highly epileptogenic developmental malformation and a common cause of surgically treated drug-resistant epilepsy. While clinical observations suggest frequent occurrence in the frontal lobe, mechanisms for such propensity remain unexplored. Here, we hypothesized that cortex-wide spatial associations of FCD distribution with cortical cytoarchitecture, gene expression and organizational axes may offer complementary insights into processes that predispose given cortical regions to harbor FCD.

We mapped the cortex-wide MRI distribution of FCDs in 337 patients collected from 13 sites worldwide. We then determined its associations with 1) cytoarchitectural features using histological atlases by Von Economo and Koskinas and BigBrain, 2) whole-brain gene expression and spatiotemporal dynamics from prenatal to adulthood stages using the Allen Human Brain Atlas and PsychENCODE BrainSpan and 3) macroscale developmental axes of cortical organization.

FCD lesions were preferentially located in the prefrontal and fronto-limbic cortices typified by low neuron density, large soma and thick gray matter. Transcriptomic associations with FCD distribution uncovered a prenatal component related to neuroglial proliferation and differentiation, likely accounting for the dysplastic makeup, and a postnatal component related to synaptogenesis and circuit organization, possibly contributing to circuit-level hyperexcitability. FCD distribution showed a strong association with the anterior region of the antero-posterior axis derived from heritability analysis of inter-regional structural covariance of cortical thickness, but not with structural and functional hierarchical axes. Reliability of all results was confirmed through resampling techniques.

Multimodal associations with cytoarchitecture, gene expression and axes of cortical organization indicate that prenatal neurogenesis and postnatal synaptogenesis may be key points of developmental vulnerability of the frontal lobe to FCD. Concordant with a causal role of atypical neuroglial proliferation and growth, our results indicate that FCD-vulnerable cortices display properties indicative of earlier termination of neurogenesis and initiation of cell growth. They also suggest a potential contribution of aberrant postnatal synaptogenesis and circuit development to FCD epileptogenicity.

4.1 Introduction

Focal cortical dysplasia (FCD) type II is the most prevalent epileptogenic developmental brain malformation and a common cause of surgically amenable epilepsy [212]. This lesion is characterized by cortical dyslamination, cytomegaly and cortical thickening [15], likely due to atypical neuroglial proliferation, growth and migration [12]. At a molecular scale, studies in resected FCD tissue have established a causal role of somatic mutations in genes implicated in the mechanistic target of the rapamycin (mTOR) pathway [59, 67, 213, 214]; mTOR hyperactivity disrupts neuronal migration and cortical lamination [67]. A recent multiomic study of somatic mutations in hemimegalencephaly and FCD also implicated genes related to calcium dynamics and synaptic function as potential contributors to epileptogenesis.[215]

Although FCD type II lesions may occur across the entire cortex, histopathological reports of surgically resected tissues in large cohorts [87, 212, 216] as well as a recent atlas of lesion location [217], suggest a propensity for frontal lobe involvement. However, mechanisms underpinning this regional vulnerability remain unexplored. Notably, the developing cortex undergoes area-specific, genetically regulated neurogenesis, synaptogenesis and circuit development that give rise to variations in cytoarchitecture [19]. Given the strong genetic influence on regional cytoarchitecture [218], it is conceivable that architectural features of the putative FCD-prone cortices may inform on the morphopathogenic characteristics of this malformation [219]. Likewise, given the substantial variability of gene expression profiles across the cortex [220], their relation to FCD topology may provide insights into the molecular pathways contributing to the pathogenesis of this brain malformation. Furthermore, cortical organization is thought to be governed by graded macroscale axes, emerging from gene expression [19, 221, 222], morphology and microstructure [223-226] as well as functional and structural connectivity [55, 227]. Specifically, the antero-posterior axis related to the prenatal

timetable of neuroglial proliferation and growth [47, 48, 228], results in a gradient of neuronal density, size and cortical thickness that persists throughout adulthood [218, 225, 229]. Another increasingly recognized axis marks the transition from sensory to transmodal association cortices [55, 56, 222, 226, 230]. Recapitulating classic accounts formulated in non-human primates,[231] this axis has been thought to mature during late prenatal and early postnatal stages [54] and reflect the hierarchical organization of neural function. In sum, cortex-wide spatial associations of FCD distribution with cortical cytoarchitecture, gene expression and organizational axes may offer complementary insights into the neurogenic processes that predispose given cortical regions to harbor this developmental malformation [219, 230].

Whole-brain cross-modal associations are facilitated by the availability of human brain atlases based on histological features [232-234] and spatiotemporal gene expression profiles [235, 236]. The overall purpose of this work was to investigate the intrinsic regional vulnerability of cortices harboring FCD. To this end, we mapped the cortex-wide lesional distribution of a multicentric dataset collected from epilepsy centers worldwide, determined cellular and genetic factors based on postmortem histology and transcriptomics, and examined the embedding of FCD lesions within the axes of neurogenic patterning and structure-function hierarchy. Specifically, after creating a topographic map of FCD type II lesions on MRI-derived cortical surface models, we cross-referenced it against histological taxonomies [232, 233] and a 3D high-resolution human brain histological model [234]. In parallel, we performed spatial correlation with whole-brain gene expression data from the Allen Human Brain Atlas [235] and examined spatiotemporal gene expression dynamics from prenatal to adulthood stages using the PsychENCODE BrainSpan, an independent development-targeted genetic dataset [18, 236]. Targeted gene enrichment analysis probed transcriptomic associations for previously known pathogenic FCD variants [12, 62, 65], as well as non-FCD epilepsies

[237] and other neurological disorders. Finally, we contextualized the FCD distribution within the antero-posterior axis previously associated with genetic cortical patterning and timetable of neurogenesis [47, 48, 218, 228], contrasting these findings with hierarchical cortical axes derived from myelin-sensitive MRI [56] and resting-state MRI functional connectivity [55].

4.2 Materials and methods

Study design and participants

We studied a consecutive retrospective cohort of 337 patients (153 females; mean±SD age = 22.2±12.7 years) with histologically verified FCD lesions collected from 13 tertiary epilepsy centers worldwide. All patients had been investigated for drug-resistant epilepsy with a standard presurgical workup including assessment of seizure history, routine MRI and video-EEG recordings. Histological examination of the surgical specimen [15] determined FCD type II as disrupted cortical lamination with dysmorphic neurons in isolation (IIA, n=134) or together with balloon cells (IIB, n=203). Site-specific demographics are summarized in **Table 3**. The Ethics Committees and Institutional Review Boards at all participating sites approved the study, and written informed consent was obtained from all patients.

	Sample size (n)	Age (years)	Sex (female/male)	Age at onset (years)
All	337	22.2±12.7	153/184	7.6±6.7
S1	114	24.8±10.5	56/58	9.1±7.1
S2	8	10.5±6.4	2/6	5.5±4.2
S3	10	25.3±14.2	5/5	7.2±7.4
S4	43	24.3±14.4	20/23	7.3±7.6
S5	18	6.8±5.6	8/10	5.6±4.1
S6	22	17.4±13.5	8/14	5.0±4.8
S7	11	30.8±14.0	7/4	4.1±3.1
S8	14	29.1±11.8	5/9	7.5±5.6
S9	8	31.9±15.3	3/5	8.9±4.7
S10	14	25.3±7.5	6/8	9.9±5.6
S11	11	20.8±6.8	7/4	6.8±8.2
S12	42	17.0±10.7	17/25	6.6±5.8
S13	22	20.9±15.5	9/13	7.1±8.6

Table 3. Overall and site-specific demographics. Data for age and age at onset indicate mean±SD years. SD: standard deviation

MRI acquisition and processing

All patients had high-resolution 3D T1-weighted MRI (T1w) acquired as a part of the clinical presurgical investigation, consisting of images with isotropic 1x1x1 mm voxel resolution.[238] Data underwent intensity non-uniformity correction and normalization, and linear registration to the ICBM MNI152 symmetric template. To generate cortical surface models, we applied the Constrained Laplacian Anatomic Segmentation using Proximity algorithm, yielding GM-WM and GM-CSF surfaces with 41k surface points (or vertices) per hemisphere.[191] Surface-based registration, which aligns individual

participants based on cortical folding, was performed to optimize vertex-wise anatomical correspondence across participants [239].

Cortex-wide MRI mapping of FCD lesions

Two experts (AB, NB) independently segmented each FCD lesion on the 3D MRI registered onto the ICBM MNI152 template. The consensus labels (the union of the two segmentations; inter-rate Dice index: 0.94±0.13) was intersected with the cortical surfaces to generate surface-based FCD labels. To enhance regional sensitivity while retaining specificity, labels were minimally smoothed using a surface-based 4 mm full width at half maximum Gaussian kernel to maximize local specificity [194]. We then calculated for each vertex the FCD probability, defined as the percentage of patients whose lesion label coincided with that vertex. To assess *within-sample* reliability, we calculated bootstrap certainty at each vertex, defined by mean of lesion probability from the bootstrap subsamples divided by their standard deviation. Similarly, we assessed *cross-site* reliability as defined by the mean divided by the standard deviation from leave-one-site-out subsamples. We assessed the lobar distribution by counting the number of FCD lesions located within each lobe; to account for lobar size, we divided the lesion counts by the relative surface areas of each lobe, defined based on automated anatomical labelling parcellation atlas [240].

Association analyses

Histological atlases

To assess associations of regional FCD probability with histological markers, we used the von Economo-Koskinas MRI atlas (http://dutchconnectomelab.nl) indexed with

quantitative histological information (cell size, cell density and cortical thickness) of 43 cortical regions per hemisphere [233]. For independent validation, we leveraged the BigBrain atlas, a 3D reconstruction of a stained post-mortem human brain [234]; this histological data, mapped to intracortical surface models in standard space and to the Schaefer 400 parcellations [241], were obtained from https://github.com/MICA-MNI/micaopen/tree/master/bigbrain.

Cortex-wide gene expression

To investigate the molecular properties of cortical vulnerability, we related the FCD distribution with the anatomically comprehensive gene expression data from Allen Human Brain Atlas (AHBA; six postmortem adult brains; 1 female; age = 42.5±13.4 years; https://human.brain-map.org) [235], which was mapped onto the 308 parcels of the Desikan-Killiany atlas (DKA) [242]. The microarray data of these donors were acquired using ~500 samples per hemisphere, with each sample indexed with expression levels for ~60,000 genes from at least two probes. Following an established procedure [243], the Maybrain package (https://github.com/87ittman/maybrain) matched the closest AHBA sample in each donor to the centroids of 308 parcels of equal area (500 mm^2) averaged across donors. Notably, data were averaged across probes corresponding to the same gene, excluding those not matched to gene symbols in the AHBA data. To reduce inter-donor variability, expression data for each probe were normalized through z-transformations across the 308 DKA parcels within each donor. The final output was a matrix of z-scored expression values for each of 20,737 genes mapped onto the 308 DKA parcels.

Spatiotemporal gene expression

We determined how genes associated with the FCD distribution are spatially and temporally regulated throughout the pre- and postnatal development. To this purpose, we used PsychENCODE BrainSpan (http://development.psychencode.org) [236], a dataset including tissue-level mRNA-sequencing of 607 samples across 16 anatomical brain regions of 41 postmortem human brains ranging from 8 postconceptional weeks to 40 postnatal years (18 females; postmortem interval = 12.9±10.4 hours; tissue pH = 6.5±0.3; RNA integrity number = 8.8±1). After bulk tissue mRNA-sequencing, this dataset has yielded expression levels for 60,154 genes. The final output consisted of a matrix of reads per kilobase million transcript expression level for each of 17,584 genes overlapping with the 20,737 genes from the AHBA atlas.

Developmental axes of cortical network organization

Gradient axes of cortical structural and functional network organization are shaped by gene expression and cytoarchitecture during the pre- and postnatal development. The antero-posterior axis relates to the prenatal timetable of neurogenesis and growth [47, 48, 228]; we derived this axis from a heritability analysis of structural covariance networks [218] mapped on the Schaefer 400 parcellations [241]. Structural and functional hierarchical axes are thought to mature during late prenatal and early postnatal circuit development [54]; we derived these axes from MRI-based covariance of microstructural profiles [56] and resting-state functional connectivity [55], which we mapped to the Schaefer 400 parcellations using the BrainSpace toolbox (https://github.com/MICA-MNI/BrainSpace) [244]. The FCD distribution and developmental axes were mapped to Schaefer 400 parcellations prior to correlation analysis to achieve anatomical correspondence between them.

Statistical analysis

Multivariate analysis

Cortex-wide linear models assessed associations of regional FCD probability with histological markers and neurodevelopmental axes. For the gene expression analysis, given the high dimensionality of AHBA data, we used partial least squares (PLS) regression, a multivariate linear model, to uncover weighted combinations of genes (or PLS components) that best explained the regional variance in FCD probability. The statistical significance of the variance explained by the PLS components was tested based on 10,000 spin permutations of the FCD distribution, accounting for spatial autocorrelations [245]. The regional expression profile of each PLS component was defined as the average of the spatial expression profile of 20,757 genes, adjusted by their PLS weight; weight stability was estimated by dividing the PLS weight by the bootstrap SD.

Enrichment analysis

A web-based gene set analysis toolkit (https://webgestalt.org) [246] was utilized to uncover biological processes enriched in the list of genes whose bootstrap weights (absolute value) were ranked within the top 10 percentile of 20,757 genes. In other words, this analysis quantified the significance and enrichment ratio, namely the number of PLS-derived genes overlapping with each biological process divided by the number of genes expected to overlap by random permutations.

Spatiotemporal gene expression profiles

Using the PsychENCODE BrainSpan dataset, we calculated the spatiotemporal profile for each PLS component obtained in the gene expression analysis. This profile, defined as the regional average of each gene's expression level weighted by its bootstrap weight, was obtained across 16 cortical regions and timepoints based on major neurodevelopmental milestones derived from whole-brain transcriptomic signatures [247]. Student's t-tests compared the expression levels between time windows, and between different regions within time windows.

Specificity analysis

We assessed whether known genes of the pathways causing FCD via somatic mutations were enriched in the PLS components, including the PI3K-AKT-mTOR pathway [59, 65, 214, 248, 249], PI3K-PTEN-AKT-TSC-RHEB pathway [61, 214, 248, 250, 251], TSC1-TSC2 complex [60, 69, 252, 253], GATOR1 complex [61, 69, 214, 250, 254-257] and other reported variants (IRS1, RAB6B, ZNF337, RALA and HTR6) [253]. These genes are listed in **Supplementary Table 1**. We also assessed associations with risk genes of focal epilepsy with hippocampal sclerosis, generalized epilepsy and all epilepsies as determined by a recent genome-wide association study [237], neurodevelopmental conditions, namely autism [258] and bipolar spectrum [259]. Finally, our specificity analysis included frontotemporal dementia [260] due to the preferential involvement of the frontal lobe.

A	AKT1, AKT1S1, AKT2, AKT3, ASCL1, BRAF, CAB39, CAB39L, DDIT4, DEPDC5, Delta1, EIF4B, EIF4E, EIF4E1B, EIF4E2, EIF4EBP1, FOXG1, GSk3, HIF1A, ID1-4, IGF1, IKBKB, INS, IRS1, MAPK1, MAPK3, MIOS, MLST8, MTOR, NEUROD1, NEUROG1, NEUROG2, NPRL2, NPRL3, PDPK1, PIK3C2B, PIK3C3, PIK3CA, PIK3CB, PIK3CD, PIK3CG, PIK3R1, PIK3R2, PIK3R3, PIK3R5, PRKAA1, PRKAA2, PRKCA, PRKCB, PRKCG, PTEN, RAB6B, RALA, RHEB, RICTOR, RND1-3, RPS6, RPS6KA1, RPS6KA2, RPS6KA3, RPS6KA6, RPS6KB1, RPS6KB2, RPTOR, RRAGA, RRAGB, RRAGC, RRAGD, SEC13, SEH1L, STK11, STRADA, TBR2, TNF, TSC1, TSC2, ULK1, ULK2, ULK3, VEGFA, WDR24, WDR59, ZBTB18, ZNF337
B	C3orf33, GJA1, KCNAB1, SLC33A1
C	SCN1A, SCN2A, SCN3A, TTC21B
D	ATXN1, BCL11A, FANCL, GABRA2, GRIK1, KCNN2, PCDH7, PNPO, SCN1A, SCN2A, SCN3A, STAT4, STX1B, TTC21B, ZEB2
E	FANCL, BCL11A, SCN3A, SCN2A, TTC21B, SCN1A, HEATR3, BRD7
F	C8orf74, KIZ, KMT2E, LOC102723661, MACROD2, NKX2-2, NKX2-4, PINX1, PTBP2, SOX7, SRPK2, XRN2
G	ADCY2, ADD3, ANK3, CACNA1C, CD47, FADS2, FSTL5, GRIN2A, HDAC5, ITIH1, LMAN2L, MRPS33, NCAN, PACS1, PC, PLEKHO1, POU3F2, RIMS1, RPS6KA2, SCN2A, SHANK2, SRPK2, SSBP2, STARD9, STK4, THSD7A, TRANK1, ZCCHC2, ZNF592
H	AC074212.3, ABCA7, ABI3, ADAM10, ADAM10, ADAMTS4, ALPK2, APH1B, APOE, BIN1, BZRAP1-, S1, CASS4, CD2AP, CD33, CLNK, CLU, CNTNAP2, CR1, ECHDC3, EPHA1, HESX1, HLA-DRB1, HS3ST1, INPPD5, KAT8, MS4A6A, PICALM, PTK2B, SCIMP, SLC24A4, SORL1, SUZ12P1, TREM2, ZCWPW1
I	BTNL2, C9orf72, GRN, HLA-DRA, HLA-DRB5, MAPT

Supplemental Table 1. The lists of candidate genes used for disease specificity analysis presented in Figure 3 for focal cortical dysplasia (**A**), hippocampal sclerosis (**B**), focal epilepsy (**C**), generalized epilepsy (**D**), all epilepsy (**E**), autism spectrum disorder (**F**), bipolar disorder (**G**), Alzheimer's disease (**H**) and frontotemporal dementia (**I**).

For each PLS component, we quantified the enrichment ratio (defined as the difference between the mean bootstrap weight of the candidate genes and the mean bootstrap

weight of the same number of randomly permuted genes), which was then divided by the standard deviation weight of the permutated genes. Significance was determined by percentile of the bootstrap weight of the candidate genes relative to the bootstrap weights of randomly selected genes from 10,000 permutations. Positive/negative ER of a given condition indicates that the risk genes are expressed to a higher/lower degree relative to the baseline expression level. In addition, the function of the risk genes needs to be considered when interpreting ER. For example, the FCD candidate genes are inhibitory regulators of mTOR pathway; thus, negative ER for these genes indicates activation of mTOR pathway.

Corrections for multiple comparisons

For all spatial correlation analyses, findings were corrected using spin permutation tests at p_{spin}=0.05.[245] Remaining results were corrected for multiple comparisons using false discovery rate (FDR) at 0.05 [202].

Data availability

The data supporting findings of this study are available from the corresponding author upon request. The datasets are not publicly available as they contain information that could compromise privacy of research participants.

4.3 Results

Cortex-wide MRI distribution of FCD

The vertex-wise MRI mapping of FCD lesions across the cortex (**Figure 8**) showed aggregation within the frontal lobe, particularly in prefrontal (dorsolateral, ventrolateral, dorsomedial and medial frontopolar; Brodmann areas 4, 9, 10, 44, 45, 46, 57) and cingulate (anterior-mid and pre-genual; Brodmann areas 24, 32, 33) cortices. The reliability of these areas was supported by higher within-sample and cross-site certainty as compared to the other regions. Lobar mapping also confirmed higher occurrence in the frontal lobe compared to other areas, even after normalizing for lobar surface area.

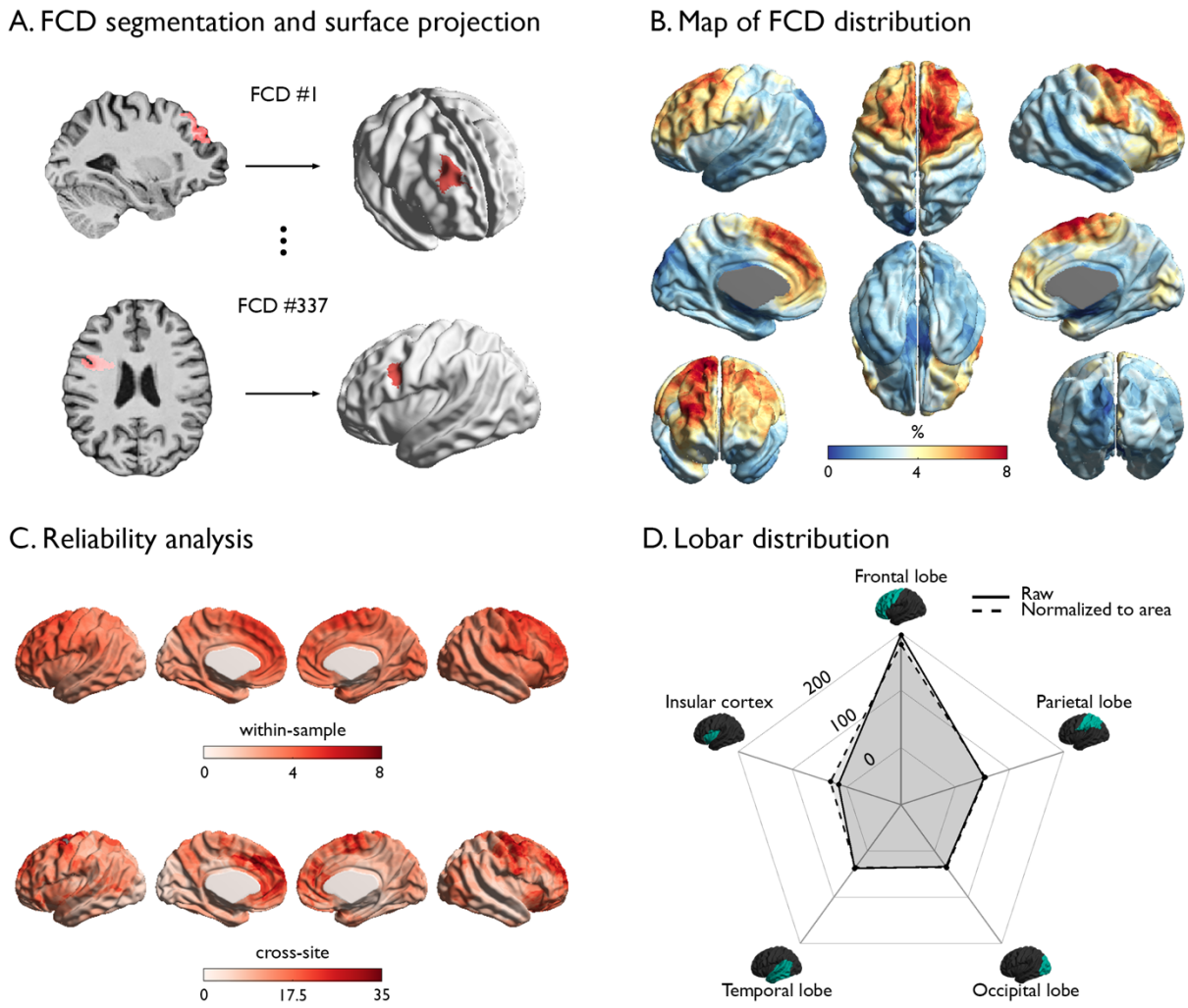

Figure 8. Cortex-wide FCD distribution. A. For each patient, the FCD lesion was manually segmented on MRI and mapped onto its cortical surface. **B.** Map of FCD distribution. **C.** Reliability analysis. Within-sample and cross-site robustness of regional FCD probability is high where the FCD probability is high. **D.** Lobar distribution. The spider plot of the FCD distribution across lobes demonstrates remarkable preference towards the frontal lobe, which holds after normalizing for the surface area of each lobe (dotted line).

Association between FCD distribution and cytoarchitecture

With respect to the von Economo and Koskinas data (**Figure 9**), mapping 43 regions per hemisphere, we found a positive correlation between FCD distribution and cortical thickness (R=0.35, p_{spin}<0.05) and cell size (R=0.46, p_{spin}<0.05) and a negative correlation with cell density (R=-0.52, p_{spin}<0.001). We also found a negative correlation with cell density obtained from the BigBrain atlas (R=-0.34, p_{spin}<0.01). In other words, frontal lobe areas with the highest probability of lesions were those displaying lower neuronal density, larger neurons, and higher cortical thickness.

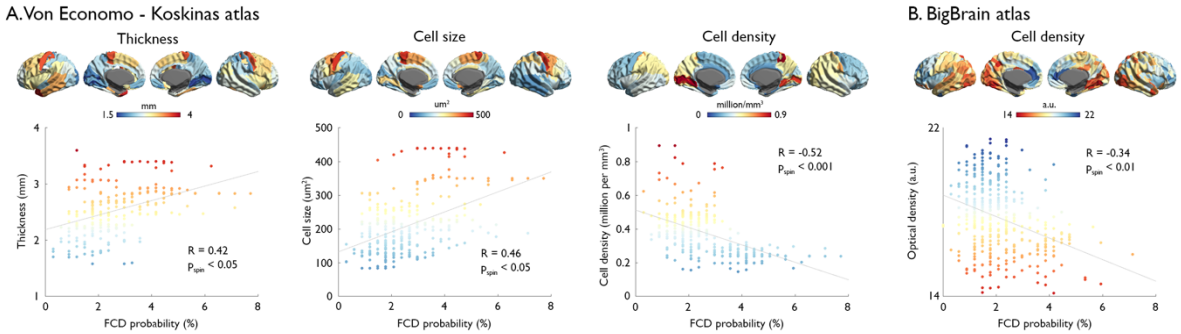

Figure 9. Associations between FCD distribution and histological measures. Plots show correlations between FCD probability and cortical thickness, cell size, and cell density derived from the Von Economo-Koskinas atlas (**A**), as well as cell density (in arbitrary units, a.u.) indexed by optical density of silver-stained cells in the BigBrain atlas (**B**). In the scatterplots, x- and y-axes represent FCD probability (in %) and histological quantities, respectively; dots indicate 308 parcels of the Desikan-Killiany atlas. Color-coding is identical for brain maps and dots; p_{spin} indicates p value after adjusting for spatial autocorrelation.

Transcriptomic associations and relation to spatiotemporal gene expression

Two PLS components explained 25% (PLS-1: p_{spin}<0.001) and 27% (PLS-2: p_{spin}=0.03) of the covariance between the FCD probability and AHBA gene expression (**Figure 10**). As shown by the gene enrichment analysis, PLS-1 reflected regulation at epigenetic, RNA and post-translational levels, as well as covalent chromatin modification and

chromosome organization (*FDR*<0.05), both critical for mitotic cell division and differentiation. Conversely, PLS-2 was mainly characterized by general synaptic organization and activity (*FDR*<0.05) and marginally by glutamate receptor signaling (*FDR*<0.1).

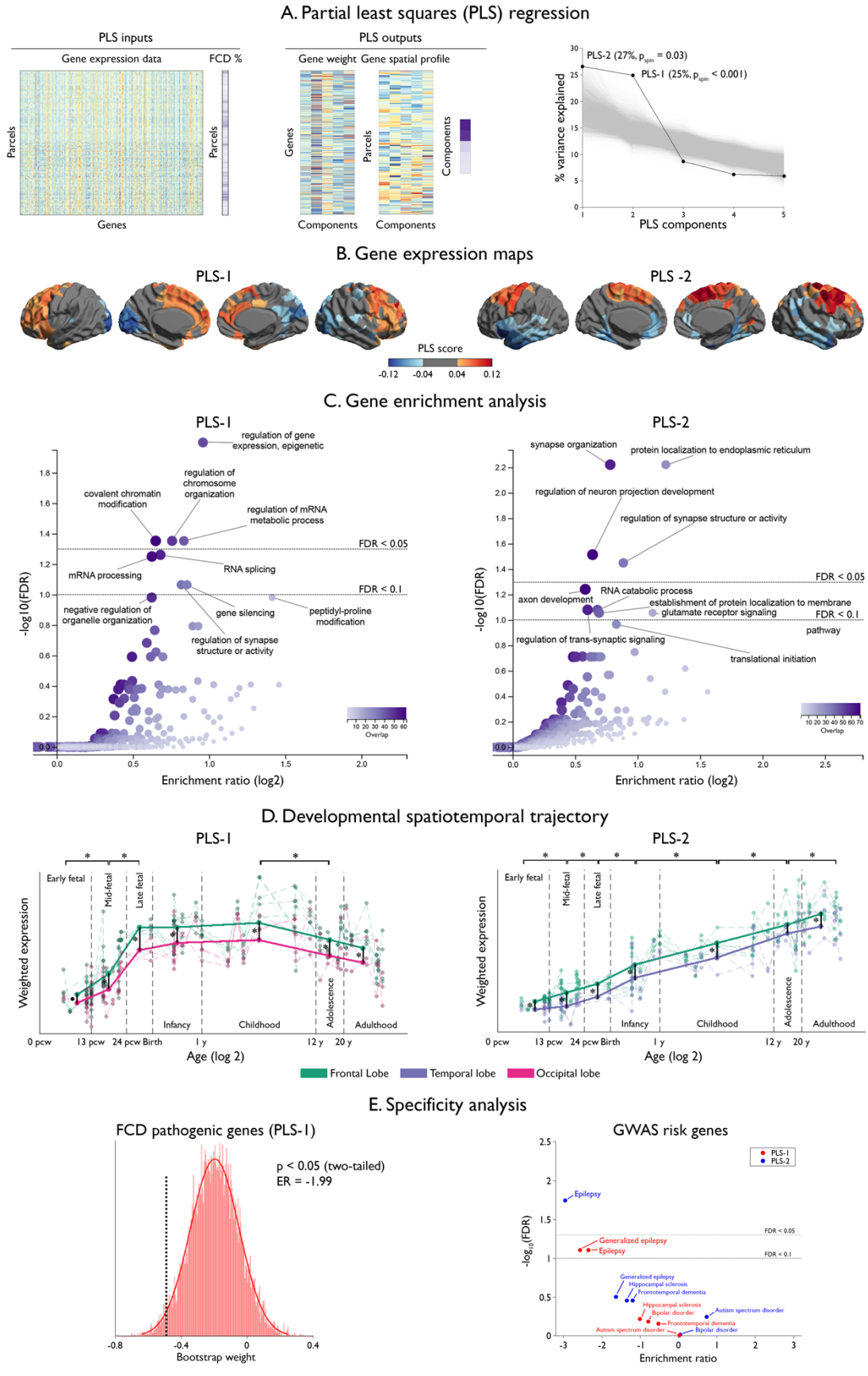
A. Partial least squares (PLS) regression
PLS inputs
Gene expression data
FCD %
Parcels
Genes
PLS outputs
Gene weight
Gene spatial profile
Components
PLS-2 (27%, p_spin = 0.03)
PLS-1 (25%, p_spin < 0.001)
% variance explained
PLS components
B. Gene expression maps
PLS-1
PLS -2
PLS score
-0.12 -0.04 0.04 0.12
C. Gene enrichment analysis
PLS-1
regulation of gene expression, epigenetic
covalent chromatin modification
regulation of chromosome organization
regulation of mRNA metabolic process
mRNA processing
RNA splicing
negative regulation of organelle organization
gene silencing
peptidyl-proline modification
regulation of synapse structure or activity
FDR < 0.05
FDR < 0.1
-log10(FDR)
Enrichment ratio (log2)
Overlap
PLS-2
synapse organization
protein localization to endoplasmic reticulum
regulation of neuron projection development
regulation of synapse structure or activity
RNA catabolic process
axon development
establishment of protein localization to membrane
glutamate receptor signaling
regulation of trans-synaptic signaling
translational initiation
pathway
D. Developmental spatiotemporal trajectory
PLS-1
PLS-2
Weighted expression
Early fetal
Mid-fetal
Late fetal
Infancy
Childhood
Adolescence
Adulthood
0 pcw
13 pcw
24 pcw
Birth
1 y
12 y
20 y
Age (log 2)
Frontal Lobe
Temporal lobe
Occipital lobe
E. Specificity analysis
FCD pathogenic genes (PLS-1)
p < 0.05 (two-tailed)
ER = -1.99
Bootstrap weight
GWAS risk genes
PLS-1
PLS-2
Epilepsy
Generalized epilepsy
Hippocampal sclerosis
Frontotemporal dementia
Bipolar disorder
Autism spectrum disorder
-log10(FDR)
Enrichment ratio

Figure 10. Cortex-wide association between FCD topography and gene expression. A. Partial least squares (PLS) regression identified weighted combinations of genes, or PLS components, and their spatial expression profiles that best explained the regional variance in FCD distribution, or percent variance explained; p_{spin} indicates p value after adjusting for spatial autocorrelation). Inputs to PLS include the whole-brain gene expression data matrix (parcels by genes) and FCD distribution across parcels (in %). Outputs include gene weights (genes by components), gene spatial profiles (parcels by components) and percent variance explained by PLS components. **B.** Maps of gene expression. The color scale indicates the score for PLS-1 and 2, namely the weighted average expression level of 20,737. **C.** Gene enrichment analysis. Genes associated with PLS-1 were enriched for epigenetic, RNA and post-translational levels as well as covalent chromatin modification and chromosome organization; and PLS-2 for general synapse organization and activity. In the volcano plots, x-axis indicates $\log_2$ of enrichment ratio and y-axis indicates $-\log_{10}$ of FDR. Color codes indicate the number of genes related to the biological processes that overlap with the input list of top 10 percentile genes; upper/lower dotted lines indicate FDR=0.05/0.1. **D**. Developmental spatiotemporal trajectory. The expression of genes associated with PLS-1 sharply increased from early to late fetal stages, plateaued during infancy and childhood, and decreased thereafter. Conversely, PLS-2 showed monotonic increase from early fetal stage to adulthood. In both instances, expressions were more marked in the frontal lobe. Dots represent cortical samples at a given timepoint color-coded by lobes; dotted lines connecting dots correspond to the same region of interest. Thick colored lines connect the average of samples within each time window, thereby showing the overall trajectory. Asterisks indicate FDR<0.05. **E.** Specificity analysis. PLS-1 was significantly enriched for FCD pathogenic genes; the histogram shows bootstrap weights of 10,000 permutations; the dotted line indicates the bootstrap weight of the candidate genes. In relation to GWAS-risk genes, PLS-2 (blue) was enriched for genes associated with all epilepsies, while PLS-1 (red) was marginally enriched for those associated with all and generalized epilepsies. Top dotted line indicates FDR = 0.05; bottom dotted line indicates FDR = 0.1.

Evaluating the developmental spatiotemporal trajectories, the expression of genes associated with PLS-1 sharply increased from early to late fetal stages (*FDR*<0.05), plateaued during infancy and childhood and decreased thereafter (*FDR*<0.05). Conversely, the expression of genes associated with PLS-2 showed a monotonic increase from early fetal stage to adulthood (*FDR*<0.05). Expressions were more marked in the

frontal lobe, with a fronto-occipital gradient for PLS-1 and a fronto-temporal gradient for PLS-2. We did not find differential associations between early and late onset lesional distribution and the PLS components.

Appendices – Supplemental Table 1 lists the risk genes used for each condition. Specificity analysis revealed that PLS-1 and PLS-2 were enriched for the risk genes of all epilepsies (PLS-1: *FDR*=0.08; enrichment ratio, *ER*=-2.60; PLS-2: *FDR*<0.001, *ER*=-3.01), with PLS-1 additionally enriched for genes causing FCD via somatic mutations (p<0.05, *ER*=-1.99) and risk genes of generalized epilepsy (*FDR*=0.08, *ER*=-2.6). Neither PLS showed associations to genes for focal epilepsy with hippocampal sclerosis, frontotemporal dementia, bipolar or autism spectrum disorders. **Supplemental Table 2** provides uncorrected p values for the enrichment of the GWAS risk genes.

	Epilepsy	**Generalized epilepsy**	**Hippocampal sclerosis**	**Autism spectrum disorder**	**Bipolar disorder**	**Frontotemporal dementia**
PLS-1	-2.954 (0.003)	-1.629 (0.105)	-1.345 (0.185)	0.041 (0.961)	0.734 (0.473)	-1.197 (0.234)
PLS-2	-2.560 (0.014)	-2.348 (0.026)	-1.009 (0.303)	0.028 (0.988)	-0.786 (0.434)	-0.523 (0.579)

Supplemental Table 2. Enrichment ratio (uncorrected p value) of risk genes used for disease specificity analysis presented in Figure 3.

Relation to developmental axes of cortical organization (**Figure 11**)

The multisite-derived FCD distribution showed a strong positive association with the anterior region of the antero-posterior axis derived from heritability analysis of inter-regional structural covariance of cortical thickness (*R*=0.51, p_{spin}<0.001), but not with structural (*R*= 0.12, p=0.37) and functional (*R*=-0.07, p=0.92) hierarchical axes.

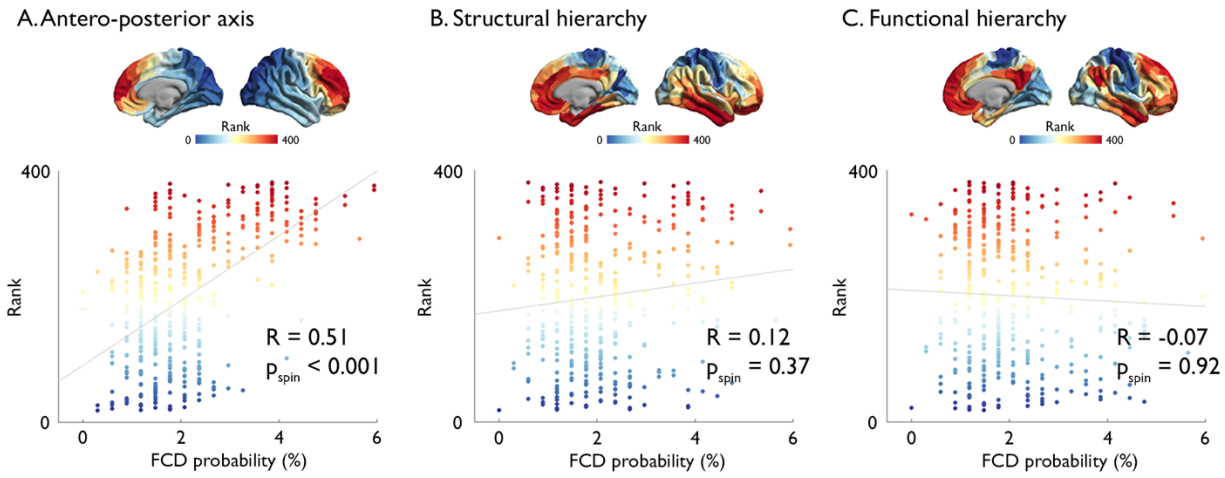

Figure 11. Relation to developmental axes of cortical organization. FCD distribution showed a strong association with the anterior region of the antero-posterior axis derived from heritability analysis of inter-regional structural covariance of cortical thickness (**A**), but not with structural (**B**) and functional (**C**) hierarchical axes. X and y- axes represent the FCD probability (in %) and the rank along the gradient axes, also represented as maps. The color scale represents the percentage of patients in whom the FCD is located at a given vertex.

4.4 Discussion

We systematically investigated the cellular, genetic and organizational features of cortices harboring FCD. Mapping the cortex-wide MRI distribution of 337 histologically verified lesions collected from 13 sites worldwide, we found a propensity for the frontal lobe. Associations with histological markers derived from Von Economo and Koskinas and BigBrain atlases showed that in the healthy brain these areas display lower neuronal density, larger neurons and thicker cortices. Using whole-brain and spatiotemporal gene expression datasets, we identified two genetic factors related to FCD distribution: one defined by prenatal regulation of gene expression and chromosome organization and another related to postnatal synapse organization and activity driving neural circuits [261]. At macroscale, FCD distribution was associated with the antero-posterior

organizational axis reflective of the timetable of neurogenesis. Concordant with a causal role of atypical neuroglial proliferation and growth, our results indicate that FCD-vulnerable cortices display cytoarchitectural, molecular and organizational properties indicative of earlier termination of neurogenesis and initiation of cell growth. Our findings also suggest a potential contribution of postnatal synaptogenesis and circuit development to FCD epileptogenicity.

While propensity for frontal lobe involvement is in keeping with previous observations [87, 212, 216, 217], our multisite dataset refined this knowledge by demonstrating locoregional vulnerability of prefrontal and fronto-limbic cortices, the consistency of which was supported by high within-sample and cross-site reliability. Notably, normalizing for lobar surface did not modify results, attesting that such susceptibility is not merely due to the frontal lobe's larger size, but rather linked to intrinsic developmental, likely multifactorial vulnerability. With respect to cytoarchitectural markers, frontal cortices are typified by lower neuronal density, larger cell soma and thicker gray matter. Given that these are also key histopathological traits of FCD [15, 262], the association we found may hint at potential pathophysiological developmental processes linked to intrinsic anatomical characteristics of the prefrontal and fronto-limbic cortices. In this context, the timetables of neurogenesis and synaptogenesis of the prefrontal cortices are distinct from other cortices [263], as they undergo earlier initiation of proliferation, transition from symmetric (cloning) to asymmetric (differentiation) division, reduction of cell cycle rates and termination of neurogenesis, resulting in lower neuronal density. This is followed by early initiation of neuronal growth leading to larger soma and more complex dendritic arborization of frontal relative to occipital cortices [47, 48, 228]. Hence, although subtle somatic mutations can occur randomly throughout the developing cortex [264], this tighter regulation of neurogenesis in the frontal cortex may explain its heightened susceptibility to harboring FCD. This longer period of cell growth

sets the basis for the frontal neurons to undergo a longer period of synaptogenesis [263, 265-267], resulting in the overproduction of synapses and a protracted period of pruning [265, 266, 268, 269]. Similarly, limbic cortices, marked by agranular or dysgranular laminar patterns, develop earlier and undergo longer period of synaptic plasticity through adulthood relative to the isocortex [270, 271]. Fronto-limbic cortices have shown vulnerability for other developmental disorders, such as schizophrenia [272, 273] and autism [274-277], while temporo-limbic cortices preferentially harbor neurodegenerative disorders, namely Alzheimer's and Parkinson's diseases [278-281]. Interestingly, tau pathology has been suggested to mediate premature neurodegeneration and cell injury in FCD [282, 283]. The frontal and limbic regions have been shown to become central hubs in the mature cortical network architecture, which also render themselves vulnerable to structural pathology in numerous lesional and degenerative conditions [284, 285].

Contextualizing lesional distribution within axes of developmental cortical organization revealed that FCD preferentially occurs in the rostral portion of the anterior-posterior axis defined by genetically determined inter-regional synchrony of cortical development [218, 286, 287]. Given that this axis reflects the prenatal timetable of neurogenesis and cell growth, the rostral concentration of FCD supports the predisposing roles of aberrant neurogenesis and cell growth as contributors to the histopathological makeup of FCD. In contrast, FCD distribution was disassociated from the sensory-association axis established during late prenatal and postnatal neural circuit development [54], a finding consistent with the prenatal occurrence of this malformation [12]. A potential genetic underpinning of FCD distribution was also suggested assessing associations to whole-brain gene expression. Indeed, transcriptomic associations based on data-driven PLS regression uncovered a component (PLS-1) reflecting regulation of gene expression at epigenetic, RNA and post-translational levels, as well as covalent chromatin modification and chromosome organization. Chromatin architecture is tightly coupled to mitotic cell

cycle and fate. As such, its modification regulated by epigenetic, transcriptional and post-transcriptional mechanisms plays a key role in cell division [288] and differentiation [289]. Chromosome organization, which involves assembly, arrangement or disassembly of chromosomes, is the process that allows the parent cell to replicate its DNA such that each daughter cell receives a copy during mitosis [290]. Therefore, within the cortex, PLS-1 likely represents molecular mechanisms underpinning neuroglial proliferation and differentiation. On the other hand, PLS-2 was related to general synaptic organization and activity, circuit organization [18], as well as glutamate receptor signaling. Evaluating the developmental spatiotemporal trajectories, PLS-1 expression sharply increased from the early fetal stage to late fetal stage, while PLS-2 expression showed steady increase from fetal stages to adulthood. The relevance of these PLS components was supported by the disease specificity analysis. Indeed, while PLS-1 and -2 were both associated with risk genes for all epilepsies, PLS-1 was additionally associated with genes causing FCD via somatic mutations and risk genes of generalized seizures, Therefore, on one hand, it is conceivable that PLS-1 may indicate early cortical vulnerability to aberrant neurogenesis and cell growth, ultimately resulting in a dysplastic lesion. On the other hand, PLS-2 may account for the susceptibility to aberrant synaptogenesis and neurotransmitter systems that for hyperexcitable circuits during a latent period following the precipitating lesion [291], thereby promoting epileptogenesis. Although synaptic and white matter maturation have been postulated to contribute to FCD occurrence [292], the presented work is the first to provide evidence for the role of postnatal synaptogenesis and circuit development for FCD epileptogenesis.

Associations with cytoarchitecture, whole-brain and spatiotemporal gene expression, as well as macroscale organizational axes, collectively suggest a vulnerability continuum spanning from prenatal neurogenesis and cell growth to postnatal synaptogenesis. Although age at epilepsy onset has been postulated to account at least partly to variability

in FCD histological features [293], the link to molecular or cellular pathogenic processes remains still unclear. In our study, while we did not find differential associations between early and late disease onset lesional distribution with the PLS components, our findings clearly establish developmental underpinnings of FCD occurrence. To date, a plethora of molecular studies of resected FCD tissues have established a causal role of somatic variants that lead to hyperactivity of the mTOR pathway [59, 61-65, 69, 253, 294]. A recent large-scale multiomic study of somatic mutations suggested genes implicated in calcium dynamics and synaptic function as potential causes for epileptogenesis [215]. Nevertheless, given that the variant allelic frequency is typically below 5% in FCD, uncovering variants distinct from mTOR pathway may be difficult, even with a large sample of resected lesions [69]. Notably, the present study circumvents this logistical and statistical burdens by identifying the genetic fingerprints of the FCD-prone cortices based on noninvasive imaging and offers novel insights that may be difficult to obtain otherwise. It has been shown that somatic activating mutations in the mTOR pathway causes a continuum of malformations, spanning from hemimegaloencephaly to posterior quadrantic dysplasia. Although these malformations share some of the genetic determinants with FCD, the time of molecular insult, as well as additional genetic mutations, may lead to varying phenotypes, as suggested by the two-hit germline and somatic mechanisms in hemimegaloencephaly [61]. As for the posterior quadrantic dysplasia, prolonged neurogenesis in the posterior isocortex involving higher number and rate of proliferation cycles translates to a greater amplification of abnormal founder cells lesion [295]. Subtle structural, possibly neurodevelopmental anomalies have been reported in generalized genetic epilepsy (GGE) and have been described as microdysgenesis in neuropathological studies [57, 296] that share histological similarity with FCD Type IA [297]. However, such reports have been sparse, as GGE patients generally do not undergo surgery. Furthermore, the replicability of identifying microdysgenesis in GGE has been limited, thereby not establishing it as a common

feature of this condition [298]. In terms of genotype-phenotype associations, while the cellular mechanisms that drive the histopathological features of dysplasia are being elucidated [67], those underlying circuit-level alterations that drive recurrent seizures in this condition remain elusive. Conceivably, mitigating the circuit-level alterations precipitated by FCD may reduce seizures [291]. Hence, future work should elucidate the molecular and cellular mechanisms of aberrant postnatal synaptogenesis that drive circuit hyperexcitability and identify novel therapeutic targets, possibly combined with mTOR inhibitors, for improved seizure control.

BRIDGING TEXT

Previous projects have investigated the individual variability and pathogenic mechanisms of FCD, the most common form epileptogenic brain malformation. Conversely, TLE is the most common form of drug-resistant epilepsy in adults. The following projects have characterized the inter-individual variability in the disease processes and progression.

5. Decomposing MRI Phenotypic Heterogeneity in Epilepsy: A Step Towards Personalized Classification

Preface

In TLE, reliable prediction of drug response, surgical outcome and cognitive dysfunction at an individual level remain challenging. This shortcoming is owing to the dominant "one-size-fits-all" group-level analytical approaches that do not allow parsing inter-individual variations along the disease spectrum. In this context, explicit modeling of inter-patient variability is increasingly recognized as a step towards person-centered care.

Here, we applied unsupervised machine learning to uncover latent disease factors from 3T multimodal MRI features that represent whole-brain patterns of structural pathology in TLE. We assessed the specificity of the uncovered disease factors against age- and sex-matched healthy individuals and a cohort of frontal lobe epilepsy patients with histologically verified focal cortical dysplasia. We then assessed the clinical utility of the disease factors by comparing the performance of predictions of drug response, surgical outcome and cognitive dysfunction between the classifier trained on disease factors and the one trained on conventional group-level features.

MANUSCRIPT III – Published in Brain. Editor's Choice.

Hyo Min Lee PhDc,[1] Fatemeh Fadaie PhDc,[1] Ravnoor Gill PhDc,[1] Benoit Caldairou PhD,[1] Viviane Sziklas PhD,[2] Joelle Crane PhD,[2] Seok-Jun Hong PhD,[1] Boris C. Bernhardt PhD,[3] Andrea Bernasconi MD,[1] Neda Bernasconi MD PhD,[1]

1) Neuroimaging of Epilepsy Laboratory, McConnell Brain Imaging Centre, Montreal Neurological Institute and Hospital, McGill University, Montreal, QC, Canada; 2) Department of Neurology and Neurosurgery, Montreal Neurological Institute and Hospital, McGill University, Montreal, QC, Canada; 3) Multimodal Imaging and Connectome Analysis Lab, McConnell Brain Imaging Centre, Montreal Neurological Institute and Hospital, McGill University, Montreal, QC, Canada

ABSTRACT

In drug-resistant temporal lobe epilepsy (TLE), precise predictions of drug response, surgical outcome, and cognitive dysfunction at an individual level remain challenging. A possible explanation may lie in the dominant *"one-size-fits-all"* group-level analytical approaches that do not allow parsing inter-individual variations along the disease spectrum. Conversely, analyzing inter-patient heterogeneity is increasingly recognized as a step towards person-centered care. Here, we utilized unsupervised machine learning to estimate latent relations (or disease factors) from 3T multimodal MRI features (cortical thickness, hippocampal volume, FLAIR, T1/FLAIR, diffusion parameters) representing whole-brain patterns of structural pathology in 82 TLE patients. We assessed the specificity of our approach against age- and sex-matched healthy individuals and a cohort of frontal lobe epilepsy patients with histologically verified focal cortical dysplasia. We identified four latent disease factors variably co-expressed within each patient and characterized by ipsilateral hippocampal microstructural alterations, loss of myelin and atrophy (Factor-1), bilateral paralimbic and hippocampal gliosis (Factor-2), bilateral neocortical atrophy (Factor-3), bilateral white matter microstructural alterations (Factor-4). Bootstrap analysis and parameter variations supported high stability and robustness of these factors. Moreover, they were not expressed in healthy controls and only negligibly in disease controls, supporting specificity. Supervised classifiers trained on latent disease factors could predict patient-specific drug-response in 76±3% and postsurgical seizure outcome in 88±2%, outperforming classifiers that did not operate on latent factor information. Latent factor models predicted inter-patient variability in cognitive dysfunction (verbal IQ: r=0.40±0.03; memory: r=0.35±0.03; sequential motor tapping: r=0.36±0.04), again outperforming baseline learners. Our findings underscore the potential of embracing inter-patient heterogeneity in TLE and show the utility of these approaches in predicting clinical outcomes. Data-driven analysis of disease factors

provides a novel description of the continuum of interindividual variability, which is likely determined by multiple interacting pathological processes.

5.1 Introduction

In drug-resistant temporal lobe epilepsy (TLE), besides the common finding of mesiotemporal sclerosis [299], histopathological studies have revealed neuronal loss and gliosis [109, 110] demyelination [111] and axonal degradation [112] in several regions outside the temporal lobe. Concordantly, a large body of *in vivo* MRI literature has shown widespread, non-overlapping morphological [130, 131], intensity [132, 133] and microstructural [134] anomalies of the neocortex and the subcortical white matter [112, 135-137] underscoring the complexity of this system disorder.

Science investigating TLE has been growing rapidly; yet progress towards translating knowledge into clinical practice has been limited. Precise predictions of drug-resistance, surgical outcome, and cognitive dysfunction at an individual level remain challenging. A possible explanation may lie in the dominant *"one-size-fits-all"* group-level analytical approach. Indeed, although isolation of consistent and reliable average differences is useful, such design merely highlights common patterns and does not allow parsing inter-individual variations along the disease spectrum [183]. Conversely, analyzing inter-patient heterogeneity is increasingly recognized as a step towards person-centered care [186, 300]. Inspired by histopathological reports of variability in the distribution and severity of mesiotemporal sclerosis [103, 107, 109], a handful of *in vivo* MRI studies have previously utilized machine learning to address heterogeneity. Clustering techniques have identified subtypes of TLE patients with distinct patterns of mesiotemporal atrophy [162]; similarly, patients have been stratified into different subtypes based on cognitive profiles [137, 161]. Nevertheless, these *subtype* models remain categorical, disregarding continuous inter-individual variations. Alternatively, conceptualization of heterogeneity through dimensional methods, such as factor analysis, allows assessing co-expression of patterns of observable and latent (non-observable) anomalies within each patient that may reflect co-existing pathologies. These approaches allow each individual to express

multiple disease factors to various degrees rather than assigning them to a single subtype. Such uniqueness may be exploited to predict individual-specific clinical outcomes [184].

Here, we Identified dimensions of heterogeneity in TLE based on multiple *in vivo* markers of structural pathology. Our approach utilized latent Dirichlet allocation [186, 300, 301], an unsupervised method. This technique estimates multivariate relations from MRI features representing whole-brain patterns of structural pathology or *disease factors* and quantifies their degrees of co-expression within each patient. We assessed the specificity of our approach against healthy individuals and a cohort of frontal lobe epilepsy patients with histologically verified focal cortical dysplasia. Moreover, we evaluated the potential of this novel data-driven subtyping for the individualized prediction of drug-resistance, post-surgical seizure freedom as well as degrees of cognitive dysfunction in TLE.

5.2 Methods

Study design and participants

We studied 82 consecutive TLE patients (30 males, mean±SD age = 35±9 years, range=19-61 years) referred to our hospital who had a research-dedicated 3T MRI that included structural imaging and diffusion-weighted MRI. Seventy patients were presented with drug-resistant seizures; twelve were responsive to anti-seizure medication.

Demographic and clinical data were obtained through interviews with patients and their relatives. TLE diagnosis and lateralization of the seizure focus into left TLE (LTLE; n=41) and right TLE (RTLE; n=41) were determined by a comprehensive evaluation including detailed history, neurological examination, review of medical records, video-EEG recordings, neuropsychology, and clinical MRI evaluation. Notably, no patient had a

mass lesion (e.g., malformations of cortical development, tumor, vascular malformations) or a history of traumatic brain injury or encephalitis.

Patients underwent a routine neuropsychological battery administered by clinical neuropsychologists (V.S. and J.C.); among tests, we chose those available for all. Verbal IQ was evaluated with the WAIS-III, and visuo-constructional skill was evaluated with Block design [302]. Rey Auditory Verbal Learning and Abstract word list learning [303] and their nonverbal analogs assessed memory [304]. Thurstone Word Fluency Test evaluated verbal fluency [305] and the Leonard tapping task measured sequential motor tapping [306], as a measure of motor coordination incorporating visuo-motor learning ability.

The comprehensive investigation recommended surgery for all 70 DRE patients, 57 (81%) of whom underwent a selective amygdalo-hippocampectomy so far. Histological analysis of the resected specimens [105] revealed hippocampal sclerosis characterized by neuronal cell loss and gliosis (HS) in 37 patients and isolated hippocampal gliosis in 20. At a mean follow-up time of 72 ± 24 months (range: 14-120 months), 43 (75%) patients had Engel-I outcome, 7 (12%) Engel-II, and 7 (12%) Engel-III. Among the 13 non-operated patients, 8 are currently awaiting surgery and 5 delayed it for personal reasons. Patients responsive to anti-seizure medication remained seizure-free.

The patients had mean ± SD epilepsy duration of 17.4 ± 12 years and 8 ± 12 seizures per month. Moreover, 26 (32%) patients had a history of febrile convulsion, 42 (51%) had focal-to-bilateral tonic-clonic seizures (FBTCS), 61 (74%) had frequent or very frequent inter-ictal spikes, 42 (51%) were not diagnosed with HS on MRI (MRI-negative) and 17 (21%) had SEEG.

The control groups consisted of age- and sex-matched healthy individuals (n=41, 18 males, mean±SD age=32±8years, range=20-53 years) as well as patients with drug-resistant

frontal lobe epilepsy (FLE; n=29, 15 males, mean±SD age=32±6years, range=17-48 years) with histologically verified type-II focal cortical dysplasia.

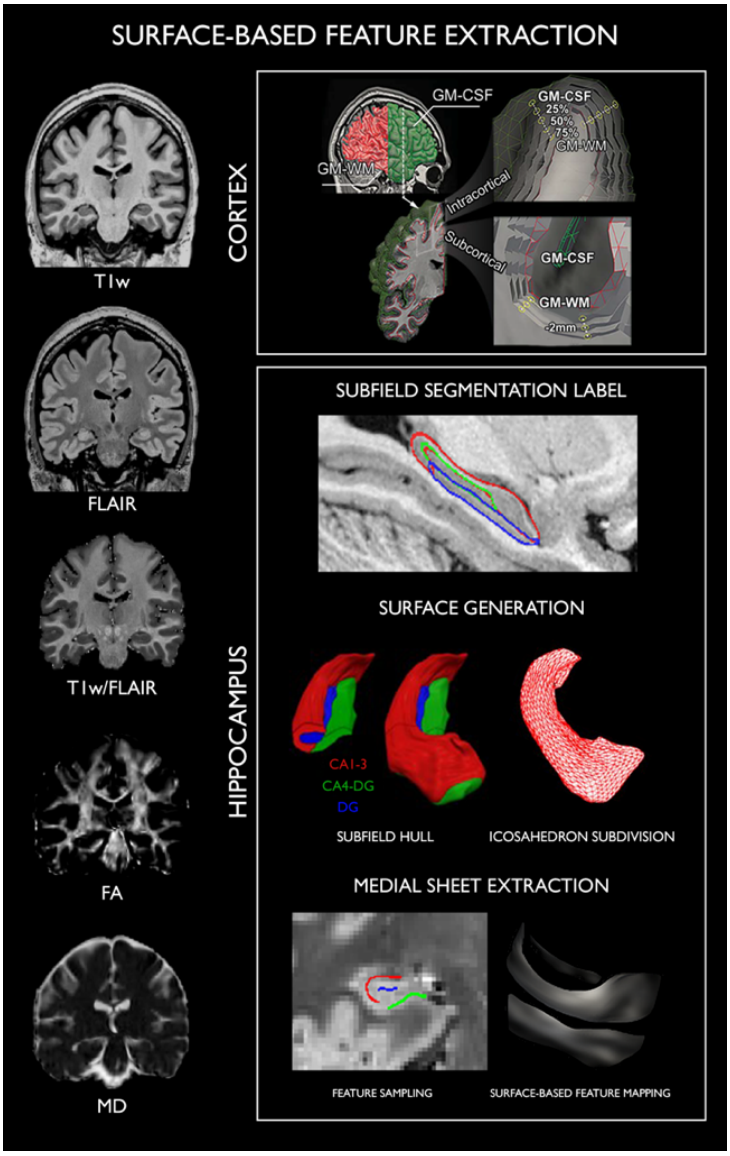

Figure 12. Surface-based feature extraction. To model prevalent features of TLE pathology (atrophy, gliosis, demyelination and microstructural damage), we carried out surface-based sampling of morphological (MOR; cortical thickness, hippocampal volume) and intensity features (FLAIR, T1-weighted/FLAIR), as well as diffusion-derived fractional anisotropy (FA) and mean diffusivity (MD), across grey and white matter (GM, WM) and hippocampal surface points (or 'vertices'). T1w = T1-weighted.

The Ethics Committee of the Montreal Neurological Institute and Hospital approved the study, and the written consent was obtained from all participants in accordance with the Declaration of Helsinki.

MRI acquisition and pre-processing

Images were acquired on a 3T Siemens Magnetom TimTrio scanner using a 32-channel head coil (**Figure 12**). The protocol included the following sequences: 3D T1-weighted (T1w) MPRAGE (TR = 2,300 ms, TE = 2.98 ms, flip angle = 9°, voxel size = 1×1×1 mm^3), 3D fluid-attenuated inversion recovery (FLAIR; TR = 5,000 ms, TE = 389 ms, flip angle = 120°, 0.9×0.9×0.9 mm^3), and twice-

refocused diffusion-weighted images with axial slices (TR = 8,400 ms, TE = 90 ms, flip angle = 90°, voxel size = 2x2x2 mm^3, 64 directions, b = 1,000 s/mm^2).

T1-weighted (T1w) and FLAIR images underwent field non-uniformity correction and intensity normalization using MINC toolkit (https://bic-mni.github.io/). T1w images were linearly registered to stereotaxic space based on the hemisphere-symmetric MNI ICBM152 template [307] and classified into white matter (WM), gray matter (GM) and cerebrospinal fluid (CSF) [196]. FLAIR images were linearly registered to T1w MRI, and subsequently to MNI ICBM152 based on the previously estimated registration. Using FSL 5.0 (http://fmrib.ox.ac.uk/fsl) [308], diffusion-weighted images underwent distortion correction, based on the gradient echo field map acquired within the same imaging session, and correction for motion and eddy currents. Fractional anisotropy (FA) and mean diffusivity (MD) maps were derived using a tensor model and mapped to the native T1w space using a boundary-based registration technique that maximizes alignment between intensity gradients of structural and echo-planar data. [193, 196]. We applied Constrained Laplacian Anatomic Segmentation using Proximity algorithm (CLASP) to generate models of GM-WM and GM-CSF surfaces with 41k surface points (henceforth *vertices*) per hemisphere [191]. In short, CLASP iteratively expands a surface mesh to fit the GM-WM surface and subsequently estimates the GM-CSF surface by expanding the GM-WM surface along the Laplacian gradient between the two surfaces. Surface-based registration aligned individual participants based on cortical folding to enhance vertex-wise anatomical correspondence [195]. Surface extraction accuracy was visually verified, and inaccuracies were manually corrected.

Surface-based feature extraction

We calculated at each vertex morphological, intensity, and diffusion features (**Figure 12**). To minimize interpolation during feature sampling, we mapped the surfaces to the native space of each modality using the inverse transform of the initial co-registration. To enhance the signal-to-noise of the cortical feature sampling, we applied smoothing using a 2D quadratic diffusion kernel with 20 mm full-width-half-maximum. To examine intracortical GM, we positioned three surfaces at 25%, 50%, and 75% cortical depths, systematically probing the axis perpendicular to the cortical ribbon [194]; for each vertex, we averaged features across these surfaces. To assess the WM immediately beneath the cortex, we generated a surface running 2 mm below the GM-WM surface guided by a Laplacian gradient between the GM-WM surface and ventricles [135]. Hippocampal subfields (CA1-4, dentate gyrus, subiculum) were segmented using a patched-based multi-template algorithm [309] trained on our open access dataset (Kulaga-Yoskovitz et al., 2015), followed by the automated generation of the medial surface sheet running along the central path of each subfield [310]. In brief, we extracted a 3D skeleton from a given subfield using Hamilton-Jacobi level-sets. To derive shape-inherent inter-subject correspondence, outer subfield surfaces were parametrized using spherical harmonics shape descriptors. The boundary was deformed along a Laplacian field gradient towards the skeleton, propagating the vertex correspondence onto the medial sheet. In prior work, we validated this approach to discriminate between histopathological grades of HS [128].

To model prevalent features of TLE pathology (atrophy, gliosis, demyelination and microstructural damage), we sampled at each vertex morphological (cortical thickness, volume) and intensity features (FLAIR, T1w/FLAIR), as well as diffusion parameters as follows. Cortical thickness was measured as the Euclidean distance between corresponding vertices on GM-WM and GM-CSF surfaces. We calculated hippocampal columnar volume by multiplying the distance between corresponding vertices on the outer and medial surfaces by the mean area of the triangles whose edges include both

vertices. To assess gliosis, we divided voxel-wise FLAIR intensity by the average GM-WM boundary intensity; this value was normalized with respect to the mode of the FLAIR intensity histogram [194] and mapped onto intracortical and hippocampal surfaces. We estimated myelin content by mapping T1w/FLAIR ratio; a local cylindrical kernel corrected for outliers due to bulk blood vessels and CSF partial volumes [198]. Diffusion-derived FA and MD were used as surrogate markers of fiber architecture and microstructural integrity [142].

Modelling latent disease factors

Latent Dirichlet allocation (LDA) [301] is an unsupervised machine learning technique. LDA estimates *latent relations* from MRI data representing distinct patterns of alterations, or *disease factors*, expressed as posterior probability (P[Vertex|Factor] or disease load) and quantifies their co-expression within each patient (P[Factor|Patient]). LDA is a dimensional model allowing each individual to express multiple latent factors instead of assigning them to a single category. This method was originally developed for text mining and later applied to neuroimaging [186], with the assumption that patients are defined by the severity of pathological features counted on MRI vertices and expressed as posterior probabilities.

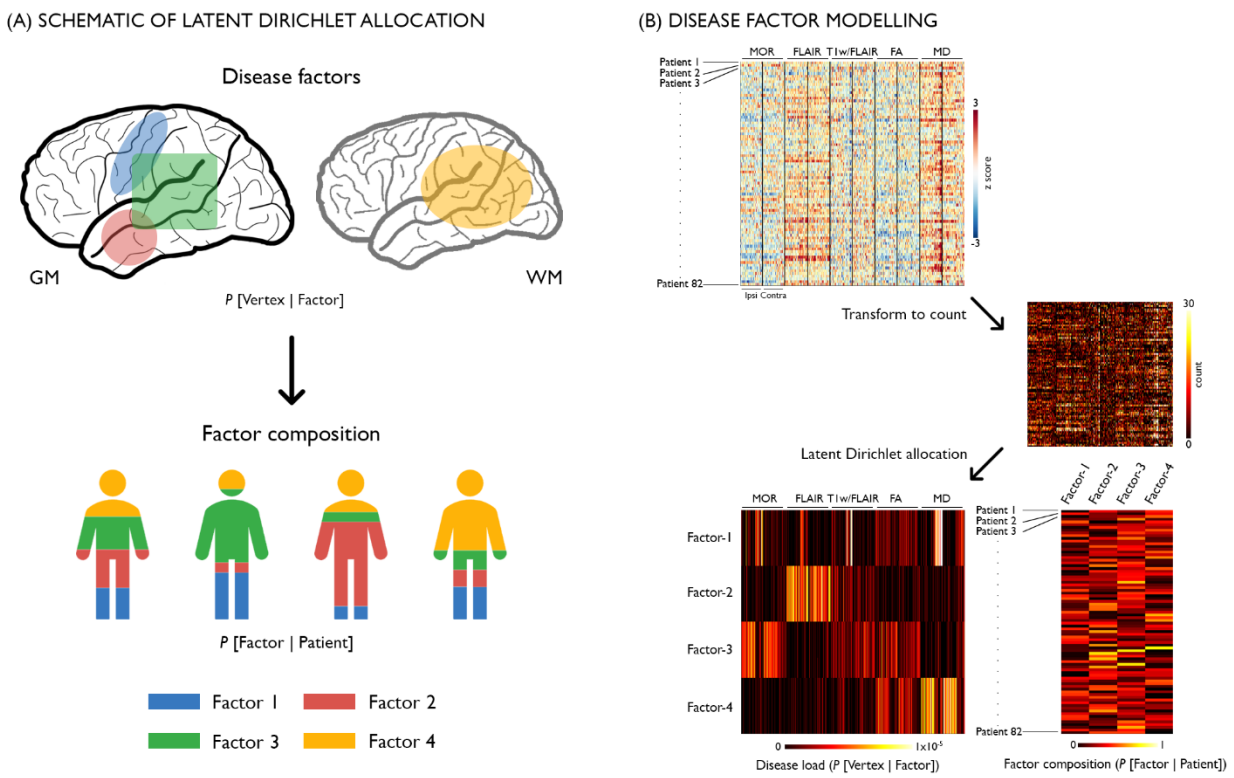

Figure 23. Analysis of latent disease factors. A. Schematic representation of the LDA. LDA uncovers latent relations from MRI data representing distinct patterns of alterations (or disease factors) and quantifies their coexpression within each patient. Factors are extracted across grey matter (GM) and white matter (WM) surface points (or vertices) and are expressed as posterior probability P(Vertex j Factor). Here, Factor 1 (blue), 2 (red) and 3 (green) are localized to the somatomotor, temporal lobe and perisylvian grey matter, respectively; Factor 4 (yellow) is localized in the white matter of the posterior quadrant. Factors may be partially overlapping (3 with 1 and 2) or non-overlapping (1 and 2). This schematic example illustrates only one pathological process. By allowing patients to express varying degrees of disease factors [P(Factor j Patient)], instead of assigning patients to a single disease subtype, LDA captures interindividual variability. **B. Factor modelling.** For each modality, features were z-normalized with respect to the analogous vertices of healthy controls ipsi- and contralateral to the seizure focus. Scores were transformed into counts, multiplied by 10/–10 and rounded to the nearest integer such that the larger counts indicated more severe pathology. We then applied Latent Dirichlet Allocation to uncover latent relations (namely, disease factors) from these features [expressed as posterior probability P(VertexjFactor), or disease load] and quantify their coexpression (namely factor composition) within each patient [P(FactorjPatient)].

Steps involved in factor modeling are shown in **Figure 13**. Prior to applying LDA, for each feature, we computed vertex-wise z-scores with respect to the corresponding vertices in controls. FLAIR intensity and MD were indexed as positive z-scores; thickness, columnar volume, T1w/FLAIR and FA were indexed as negative z-scores. Scores were multiplied by 10/-10 and rounded to the nearest integer such that the larger counts indicated more severe pathology. We evaluated a range of latent factors K from 1 to 4. Because the estimation of factors may vary depending on random initialization [301], for each K, we ran the algorithm 100 times and selected the solution closest to the remaining 99 runs [300] based on product-moment linear correlation (r) of the factors. Correlations between runs were stored into a 100x100 matrix. After averaging the rows, we selected the run with the highest correlation with the remaining 99 runs ($r>0.8$) and the final K that offered high stability across runs ($r>0.8$). To assess within-sample robustness, we estimated confidence intervals of each factor-specific pattern of structural alterations by applying a bootstrapping procedure that generated 100 samples from the patients' data. This procedure involved computing z-scores by dividing the vertex-wise pattern of structural alterations (i.e., P[Vertex|Factor]) by the bootstrap standard deviation and converting them to p-values, corrected for multiple comparisons using a false-discovery rate (FDR) of 0.05 [202].

Linear regressions assessed the relationship between disease factors and continuous variables (disease duration, cognitive scores); logistic regression was used for binary variables (history of febrile convulsion, histopathology). In all analyses, age and sex were used as covariates. Findings were corrected at FDR of 0.05. To assess the specificity of findings, we quantified the expression of factors in healthy controls and FLE disease controls. Specifically, for each individual, we calculated the average z-score across the five modalities for each disease factor weighted by its posterior probability ($P[\text{Vetex}|\text{Factor}_K]$, $K=1,2,\ldots,K_{max}$).

Individual-based predictions of clinical outcomes and cognitive scores

We assessed the performance of latent factors to predict the binary outcomes drug response (resistant *vs.* controlled) seizure outcome (Engel I *vs*. Engel II-IV). We also predicted continuous cognitive scores (verbal IQ, memory index, sequential motor tapping). In both cases, we used Gradient Boosting, an ensemble of decision trees that controls for overfitting [203]. To train the classifier, for each patient, we inputted patient-factor composition ($P[Factor_K|Patient]$, $K=1,2,\ldots,K_{max}$) and the average z-scores of each of the five modalities from cortical GM, subcortical WM and hippocampal regions falling within the 90 percentile mask of the disease factors after weighted summation into a single map ($\Sigma_{K=1}^{Kmax} P[Factor_K|Patient]*P[Vertex|Factor_K]$). For performance evaluation of binary outcome measures, we calculated balanced accuracy defined as the arithmetic mean between sensitivity and specificity, thereby removing the bias that may arise from imbalanced datasets. To evaluate performance for continuous cognitive scores, we calculated product-moment linear correlations (r) between the predicted and true scores. The classifier was cross-validated using a 10-fold scheme repeated 100 times; this procedure, by which 10% of patients are predicted using the data of the other 90%, allows an unbiased assessment for previously unseen cases. We compared the performance of classifiers trained on latent factors to those trained on features derived from the conventional group-level data. For the latter, we extracted the average z-scores of regions presenting with significant group differences compared to healthy controls ($P_{FWE}<0.05$), thus yielding two features (GM/WM and hippocampus) for each modality.

The contributions of disease factors to individualized predictions

Understanding how a predictive model uses factors to make predictions may facilitate adoption in clinical decision-making. To that end, we used Shapley additive explanation

(SHAP) analysis, which quantified the direction of each factor's impact on individual predictions [311]; summing SHAP values across patients yielded the difference between the actual and average model output over the training data. For instance, for "drug response" a predicted probability of >0.5 classifies a given patient as drug-controlled, while that of <0.5 as drug-resistant. Hence, for each factor, positive/negative correlation between the factor expression degrees and SHAP values indicate that the factor drives the prediction towards drug-controlled/drug-resistant. For numeric cognitive scores, positive/negative correlation indicates that the factor drives the prediction towards normal/low performance. We thus multiplied the sign of correlation (indicating directionality) and the absolute SHAP values (indicating magnitude).

5.3 Results

Latent disease factors and relation to clinical parameters

The algorithm identified four latent disease factors that differed with respect to hippocampal and neocortical signatures (**Figure 14**). Factor-1 was defined almost exclusively by severe ipsilateral hippocampal anomalies, yet with differential expression across subfields and MRI features. Microstructural alterations, indexed by increased MD, were the most severe finding present across all subfields and accounting for 31% of the disease load (i.e., the summation of posterior probability across vertices). Moderate hippocampal atrophy (9%) was also evenly distributed across all subfields. Intensity anomalies were observed in CA1-3 and CA4-DG, as indexed by decreased T1w/FLAIR (9%), a likely marker of abnormal myelin content, and increased FLAIR (3%) a marker of gliosis. Finally, only subtle fiber architectural alteration, as indexed by decreased FA (2%) were seen in the anterior temporal subcortical WM. Factor-2 was dominated by severe bilateral hippocampal and neocortical paralimbic FLAIR intensity increases, with marked

changes in CA4-DG, together with parahippocampal, cingulate, insula and prefrontal cortices, accounting for more than 80% of the disease load. Factor-2 also showed subtle T1w/FLAIR decreases, particularly in bilateral prefrontal and anterior temporal regions. Factor-3 was mainly characterized by bilateral neocortical thinning accounting for 20% of the disease load. Affecting regions included medial frontocentral, insular and cingulate regions. In addition, the hippocampus displayed mild architectural damage (decreased FA; 6%). Factor-4 was dominated by severe bilateral diffuse WM microstructural damage (increased MD), accounting for 44% of the disease load and moderate fiber architectural damage (decreased FA; 21% disease load), while hippocampal alterations were minimal to none.

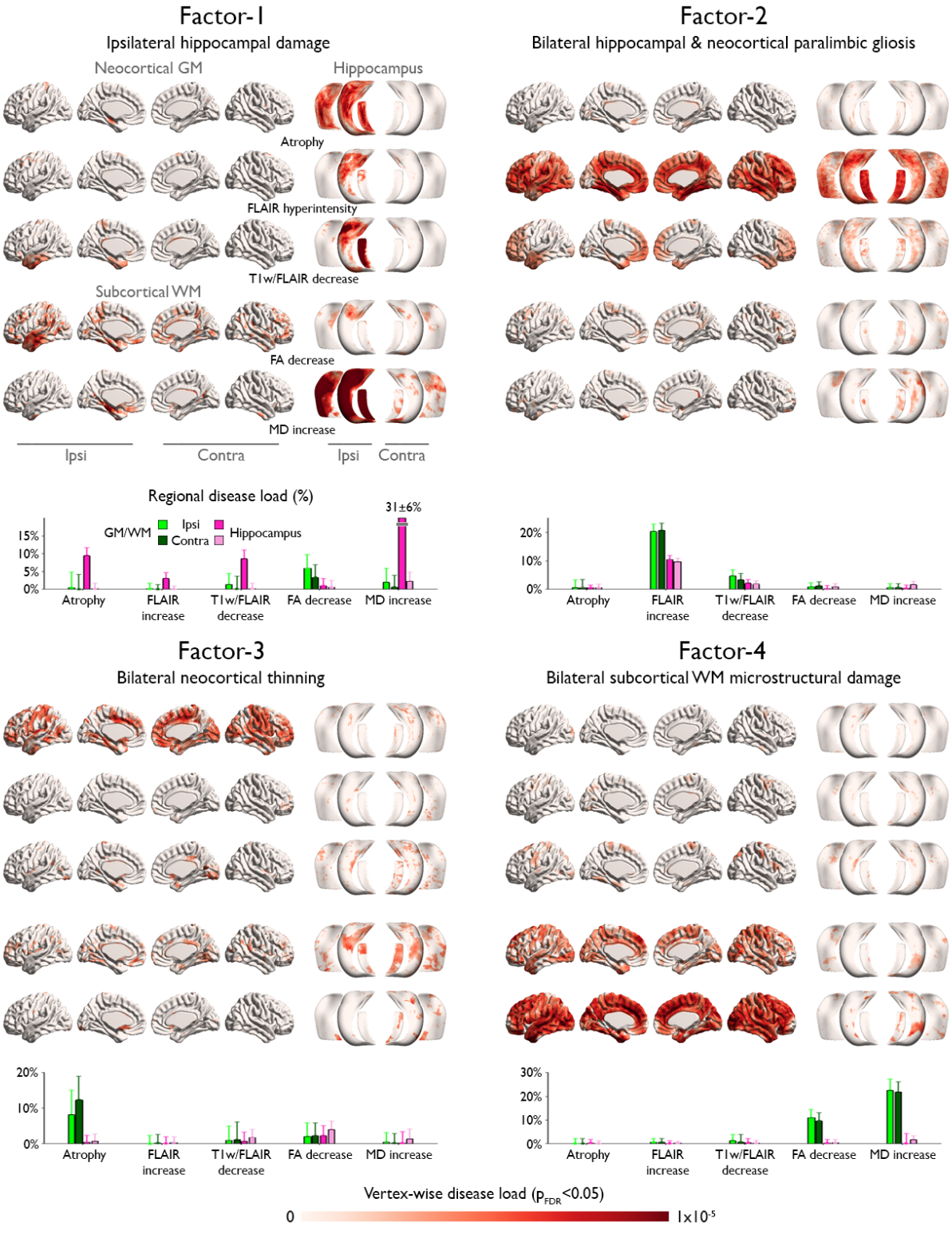

Figure 14. Mapping whole-brain disease factors. Each factor is modeled as a weighted combination of neocortical atrophy, hippocampal atrophy, FLAIR hyperintensity, T1w/FLAIR decrease, FA decrease and

MD increase across the gray and white matter (GM, WM), as well as hippocampus. Disease factors are expressed as posterior probabilities (P [Vertex | Factor]) across ipsi-/contra-lateral MRI vertices; higher probability (brighter color) signifies greater contribution of a given feature to the factor or disease load (p_{FDR}<0.05). For each feature, inset bar graphs indicate mean and standard deviation of the disease load in ipsi-/contra-lateral cortical GM, WM and hippocampus.

Patients co-expressed all factors to varying degrees, as indicated by the high density of individuals widely distributed across the central region of the tetrahedron, reflecting a continuum of individual variability (**Figure 15A**). Moreover, disease factors were not expressed in healthy controls and only negligibly in FLE, supporting specificity (**Figure 15B**).

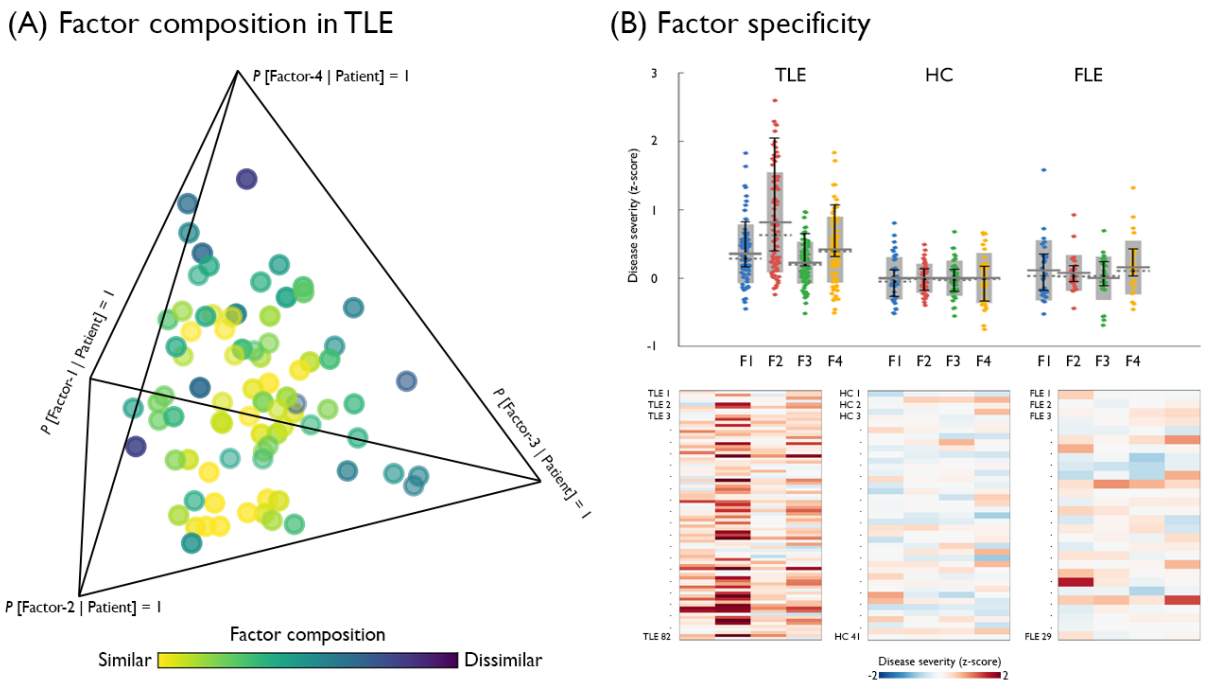

Figure 15. Factor composition and specificity. A. Factor composition in TLE. In the tetrahedron, each patient is a dot and its barycentric coordinate the factor composition expressed as posterior probability (P [Factor | Patient]). Patients located close to the corners predominantly express a given factor (F), whereas those located towards the centroid express various combinations of all factors. The scale represents the kernel density, with yellow/blue indicating similar/dissimilar composition among patients. **B. Specificity**

of factors. The bar graphs compare the severity of factor expression (z-score weighted by factor maps P [Vertex | Factor]) in TLE, healthy controls (HC) and disease controls composed of patients with frontal lobe epilepsy (FLE). The error bars indicate standard deviation. The matrices show subject-wise severity of each factor.

In relation to clinical parameters, a predominant Factor-1 expression was associated with history of febrile convulsion ($p_{FDR} \leq 0.05$, Cohen's d effect size=3.95), focal-to-bilateral tonic-clonic seizures ($p_{FDR} \leq 0.001$, d=1.1), MRI-positive ($p_{FDR} \leq 0.001$, d=13.9), no use of scalp EEG ($p_{FDR} \leq 0.001$, d=-3.5), HS histopathology ($p_{FDR} \leq 0.001$, d=24.5), drug-resistance ($p_{FDR} \leq 0.001$, d=9.7), Engel-I outcome ($p \leq 0.05$, d=4.5) and longer disease duration ($p_{FDR} \leq 0.001$, d=4.24). Factor-2 was associated with seizure frequency ($p \leq 0.05$, d=12.6). Factor-3 was associated with MRI-negative ($p_{FDR} \leq 0.001$, d=5.37), isolated gliosis ($p_{FDR} \leq 0.001$, d=12.8) and non-Engel-I outcome ($p \leq 0.05$, d=3.1). Factor-4 was associated with seizure frequency ($p \leq 0.05$, d=11.3), MRI-negative ($p_{FDR} \leq 0.05$, d=3.4) and Engel-I outcome ($p \leq 0.05$, d=3.7).

Individual-based predictions of clinical outcomes and cognitive scores

Predictions and their directionality are shown in **Figure 16**. Classifiers trained on latent disease factors out-performed those operating on group-level findings of individual MRI features. For drug response, factors yielded a balanced accuracy of 76±2.6% (*vs.* 60-68% across features, $p_{FDR} < 0.001$). Factor-1 expression showed high predictability for drug-resistance with 88±1.6%, while Factors 3 and 2 contributed moderately to a weaker prediction of drug-control (63±6.2%). For postsurgical outcome, disease factors yielded a balanced accuracy of 88±1.5% (*vs.* 57-80%, $p_{FDR} < 0.001$). Specifically, Factors 1 and 4 drove the model predictions towards Engel I outcome with 99±2.6% accuracy, while Factor-3

predicted Engel II-IV in 76±1.8% of cases. Correlations between predicted and true cognitive scores were also consistently higher for factor-based regressions (verbal IQ: r=0.40±0.03 *vs.* 0.08-0.32, memory: r=0.35±0.03 *vs.* 0.02-0.10, sequential motor tapping: r=0.36±0.04 *vs.* 0.02-0.28; p_{FDR}<0.001). Factor-1 expression drove predictions for decline in verbal IQ, Factors 1 and 3 for decline in memory, and Factor-4 predicted decline in sequential motor tapping.

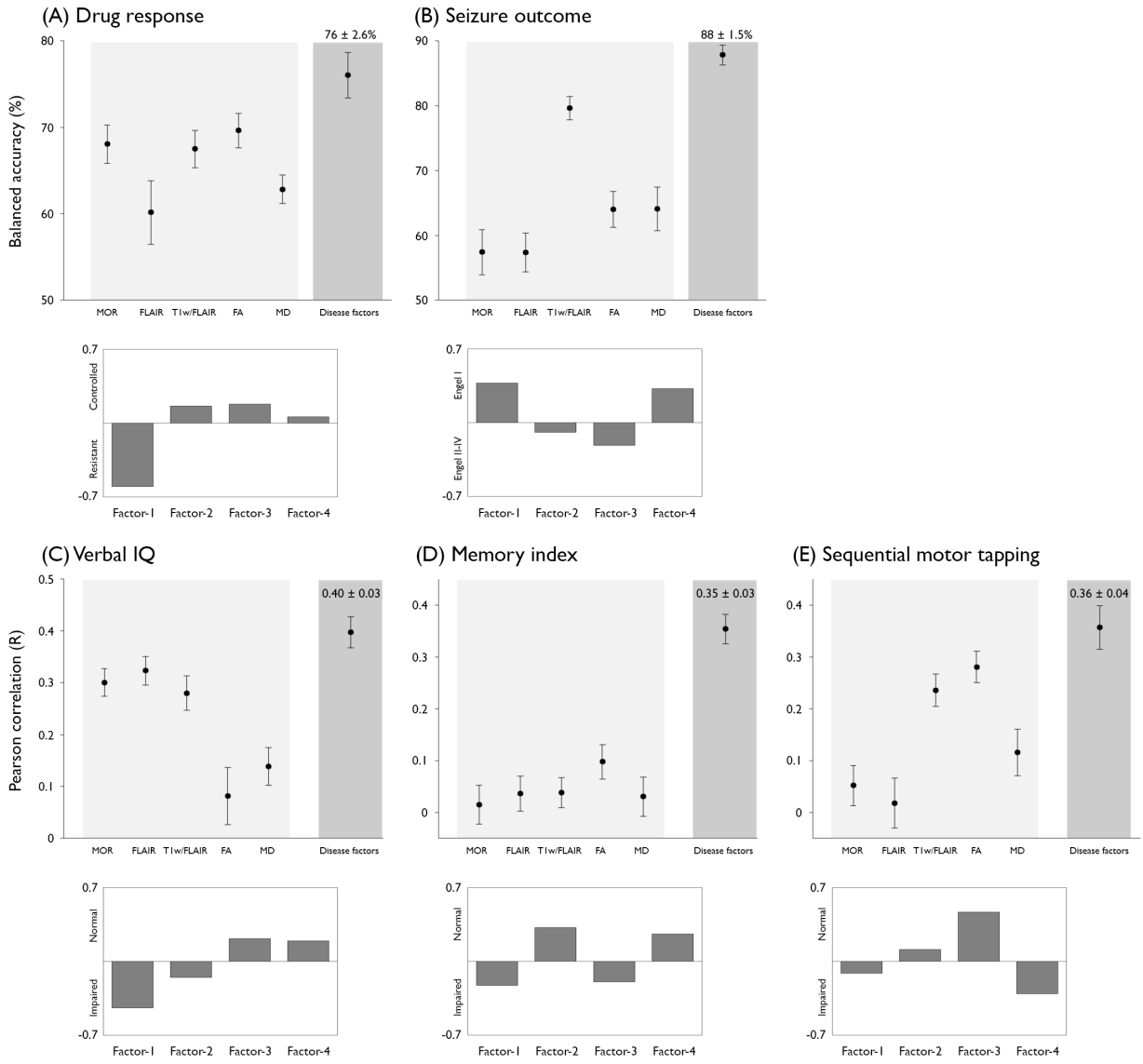

Figure 16. Individualized predictions. Drug response (**A**), seizure outcome (**B**), verbal IQ (**C**), memory index (**D**) and motoIndex (**E**) are more accurately predicted when using latent disease factors than when

relying on conventional group-level features (p_{FDR}<0.001). Data points indicate mean balanced accuracy for categorical data (drug-response, seizure outcome) and Pearson correlation coefficients for numerical data (cognitive scores) evaluated based on 100 repetitions of 10-fold cross-validation. Inset bar graphs represent the magnitude and direction of contribution from each selected feature. Note that the magnitude of bars adds to one and thus reflects relative feature importance. Upward bars indicate contribution toward drug-control, Engel I outcome or normal cognition, whereas downward bars indicate contribution toward drug-resistance, Engel II-IV and impaired cognition.

5.4 Discussion

To date, most studies in TLE have addressed overall between-group differences between patients and controls. However, there is a growing recognition that such case-control designs may not be adequately addressing biologically and clinically important variations between patients. In this context, data-driven discovery at an individual level offers novel avenues [312, 313]. This study addressed the continuum of interindividual variability in TLE in an attempt to predict patient specific clinical and cognitive outcomes. Specifically, we quantified multivariate latent relations from MRI features representing distinct patterns of gray and white matter structural pathology across the hippocampus and the whole brain and quantified their degrees of co-expression within each patient. By unveiling unique relationships between the main structural biomarkers of TLE, which were disease-specific, this integrative analysis extends our understanding of the complex landscape of this condition. Importantly, latent factors differentially contributed to predicting outcomes, with superior performance compared to conventional group-based analyses, further stressing the ability of dimensional modeling to mine salient but clinically relevant disease characteristics that would otherwise be missed.

We identified four latent disease factors variably expressed across patients. Factor-1 was related to strictly unilateral hippocampal, with marked effects across multiple imaging

modalities. Factor-2 involved both the hippocampus and the neocortex, while Factor-3 (bilateral neocortical thinning) and Factor-4 (bilateral WM microstructural damage) related only minimally to hippocampal damage, suggesting independence from the disease epicenter [180, 314]. Notably, the predominance of Factor-1 in patients with HS histopathology, history of febrile convulsion and long disease duration epitomizes core disease features [4, 110, 126, 131]. Factor-2, typified by bilateral hippocampal and neocortical paralimbic FLAIR hyperintensity, may represent an intermediate disease trait related to cytoarchitectural features of paralimbic cortices sensitive to gliotic processes [110, 132, 139]. Notably, this factor was more predominant in patients with a histology of isolated hippocampal gliosis. Commonly considered as a pathological marker of diseased tissue, gliosis is defined as a spectrum of molecular, cellular and functional changes that occur in response to injury [315]. In epilepsy, it has been shown to alter synaptic and neuronal activity, leading to hyperexcitability and spontaneous seizures [140]. Importantly, glial alterations may accompany neurogenic changes and even precede neuronal loss [316]. In addition, previous literature has shown seizure promoting effects of glia-mediated inflammation [141]. In concordance with reported patterns [130, 131]. Factor-3 was mainly marked by bilateral neocortical thinning, which may represent regions of neuronal loss [109] as well as synaptic reorganization [138], possibly due to seizure-related damage. This view is supported by its co-occurrence with isolated bilateral fiber architectural derangements of the hippocampus [125, 317]. Furthermore, cortical thinning has been shown to progress in drug resistant TLE, supported by cross-sectional correlations with duration and initial longitudinal evidence [4, 125, 150, 152]. In contrast to Factors 1-3 affecting the GM, Factor-4 was mainly characterized by widespread alteration of the subcortical WM indexed by increased MD and decreased FA, likely reflecting combined effects of decreased fiber density, altered myelin sheath and reactive astrogliosis [142-144]. Notably, this factor mainly affected the paralimbic cortices, in accordance with previous observation [318] and may underpin atypical

reorganization of long-range functional connections [180]. Previous reports of WM abnormalities include deep fiber tracks [143, 319], which may be coupled to superficial WM alterations captured by Factor-4. Bootstrap procedure showed within-sample robustness of the disease factors, supporting their generalizability. Moreover, they were not expressed in healthy controls and only marginally in patients with FLE, supporting specificity. Altogether our analysis allowed decomposing the complex disease signature of TLE by revealing co-existing, yet not mutually exclusive axes of pathology.

With respect to the predictive value of latent factors, our findings warrant several considerations. Compared to predictions based on conventional group-based analysis, capturing the heterogenous patterns of whole-brain alterations by latent factors led to a superior performance. Factor-1 expression drove the prediction towards drug-resistance, confirming the central role of multimodal MRI mapping of hippocampal pathology to streamline presurgical evaluation. On the other hand, we could not establish accurate predictors of drug-response, likely due to the small number of responders in our cohort. Regarding postsurgical outcome, previous studies have shown that mesiotemporal atrophy is a predictive biomarker for seizure freedom, achieving 80-90% accuracy, but modest predictor for seizure relapse, with <60% accuracy [162]. Using latent factors, we achieved 99% accuracy for Engel I patients and 76% accuracy for Engel II-IV patients. Our near-perfect prediction for favorable outcome reflects the combination of mesiotemporal lobe damage together with subcortical WM pathology, suggesting a role for neuroplasticity of possibly reversible WM anomalies [320]. On the other hand, Factor-3 prediction for unfavorable seizure outcome supports a role for bilateral neocortical atrophy as a marker of disease severity and possibly a widespread epileptogenic process. Factor-3 was also more prevalent in patients with isolated hippocampal gliosis; notably, these patients have been shown to express higher and more diffuse epileptogenicity in the neocortex compared to those with classical HS [321].

Previous studies have identified neural correlates of cognitive deficits, including hippocampal and neocortical atrophy [322] as well as WM abnormalities [323]. Indeed, the multifaceted nature of TLE is thought to underlie impairments in multiple cognitive domains [324]. Disease factors yielded substantial gain in the prediction accuracy compared to the conventional group-based approach, adequately capturing the complexity of multi-system structural pathology underpinning the impairments in multiple cognitive domains. Notably, Factor-1 drove the prediction towards decline in memory, in keeping with the central role of the hippocampus in spatial and episodic memory in health [325] and impairment in TLE [326, 327]. Factor-3, associating hippocampal features and neocortical atrophy, including the cingulate cortex, was also a predictor of memory decline. Given the importance of system-level pathology in cognitive impairment, an altered cingulate cortex may prevent memory consolidation and retrieval due to impaired top-down projections [328]. In addition to memory impairment, Factor-1 also drove the prediction towards decline in verbal IQ. In support of this finding, previous studies have shown decreased hippocampal neuronal density associated with verbal IQ decline [329, 330] and the role of hippocampus in the default mode network [223, 331-333], which is also associated with verbal intelligence [334]. Finally, the link between Factor-4 and decline in sequential motor tapping is likely driven by the pervasive bilateral WM microstructural damage. Indeed, visuo-motor function, which requires cross-modal integration, has shown to be related to white matter microstructural integrity and connections [335, 336].

Mounting evidence supports the diagnostic and prognostic values of data-driven MRI-based characterization of heterogeneity in several neurological conditions, including Alzheimer's disease [300], psychosis [337] and autism spectrum disorder [188, 338]. In epilepsy, patient stratification is mainly driven by seizure semiology and epileptiform activity. While this approach offers a well-defined clinical diagnostic framework, it does

not inform on the pathological processes, thus likely masking phenotypic heterogeneity [161, 162, 323]. In this context, data-driven disease factors provide a novel description of the continuum of interindividual variability in TLE. Our results also offer proof of principle that embracing inter-patient heterogeneity has utility in predicting clinically relevant outcomes.

BRIDGING TEXT

Previous project has established a continuum of inter-individual variability in TLE based on disease factors representing hippocampal and whole-brain MRI signatures. Yet, these factors do not explicitly capture the progression of disease expression, which has been suggested to be driven by seizure-induced damage and neurogenerative processes. The following project simultaneously characterized the patterns of temporal progressions and their inter-individual variability in TLE.

6. STAGING AND SUBTYPING THE EVOLUTION OF TEMPORAL LOBE EPILEPSY

PREFACE

To date, the pathological progression of brain structure and function in temporal lobe epilepsy (TLE) has been assumed to be steady across the entire temporal course of the disease and identical across patients. Meanwhile, increasing evidence suggests a multitude of mechanisms underlying TLE evolution, such as damage due to seizure spread and neurodegeneration due to amyloid-beta and tau accumulations, which likely manifest variably across time points and patients.

Here, we applied a computational technique called Subtype and Stage Inference for simultaneous subtyping and staging of TLE patients using 3T multimodal MRI. We assessed the evolution of disease trajectory in the uncovered subtypes. We then examined the clinical and cognitive profiles of the disease trajectory subtypes. Clinical utility was tested by comparing the performance of predictions of drug response and surgical outcome between a classifier trained on joint subtype and stage information against those trained on subtype- and stage-only models.

MANUSCRIPT IV- in preparation

Hyo Min Lee PhDc,[1] Fatemeh Fadaie PhDc,[1] Ravnoor Gill PhDc,[1] Benoit Caldairou PhD,[1] Viviane Sziklas PhD,[2] Joelle Crane PhD,[2] Seok-Jun Hong PhD,[1] Boris C. Bernhardt PhD,[3] Andrea Bernasconi MD,[1] Neda Bernasconi MD PhD,[1]

1) Neuroimaging of Epilepsy Laboratory, McConnell Brain Imaging Centre, Montreal Neurological Institute and Hospital, McGill University, Montreal, QC, Canada; 2) Department of Neurology and Neurosurgery, Montreal Neurological Institute and Hospital, McGill University, Montreal, QC, Canada; 3) Multimodal Imaging and Connectome Analysis Lab, McConnell Brain Imaging Centre, Montreal Neurological Institute and Hospital, McGill University, Montreal, QC, Canada

ABSTRACT

Evidence suggests that drug-resistant temporal lobe epilepsy (TLE) follows a progressive course impacting brain structure and cognitive function. However, previous studies have not considered phenotypic diversity across patients and stages. Event-based models capture patterns of evolution across disease stage from cross-sectional data, circumventing the logistical burden of longitudinal designs. Here, we applied **Su**btype and **Sta**ge **In**ference (SuStaIn), a technique that extends event-based models for simultaneous subtyping and staging. We studied 82 TLE patients and 41 healthy controls scanned at 3T multimodal MRI feature (cortical thickness, hippocampal volume, hippocampal MD and superficial white matter MD). SuStaIn estimated disease trajectory subtypes and stages by fitting a multi-component piece-wise linear z-score model of progression. Effects of normal aging in healthy controls were subtracted from patients. We identified three disease trajectory subtypes that suggested distinct regional vulnerabilities: S1 led by ipsilateral hippocampal atrophy and gliosis, S2 by bilateral neocortical atrophy and S3 by bilateral limbic white matter microstructural damage. Bootstrap analyses showed high within-sample stability of patients to their subtypes and stages. S1 had the highest proportions of patients with early disease onset, febrile convulsions, generalized tonic-clonic seizures, drug-resistance, a positive MRI, HS and Engel-I outcome, whereas S3 and S2 exhibited the lowest and intermediate proportions, respectively. Regarding cognition, S3 had higher verbal IQ and digit span and progressive decline with respect to stage in digit span and sequential motor tapping and at a faster rate than S2. S1 showed progressive decline in sequential motor tapping, declining faster than S2. Supervised classifiers trained on subtype and stage memberships could predict drug response in 73±1.0% of patients and Engel outcomes in 76±1.6%, outperforming subtype- and stage-only models. Disease evolution in TLE follows variable trajectories, each associated with distinct patterns of cortico-subcortical

and hippocampal structural alterations. Capturing the progression of subtype-specific MRI biomarkers enables an objective, fine-grained patient stratification, which may identify individuals at risk and help monitor the effectiveness of potential preventive therapies.

6.1 Introduction

In temporal lobe epilepsy (TLE), neuroimaging literature suggests a progressive course impacting brain structure and function. A large body of cross-sectional data has shown positive correlation between duration of epilepsy with gray matter (GM) atrophy and white matter (WM) microstructural alterations of the mesiotemporal structures and beyond [4, 125, 131, 135, 145]. Concordantly, there is progressive cognitive impairment across multiple domains with longer disease duration [146-149]. Although relatively scarce due to logistical constraints, longitudinal data that adequately control for effects of normal aging have confirmed these findings [125, 130, 150-152]. One key limitation of imaging studies analyzing disease progression has been the use of linear models that identify regions that undergo steady alterations, which do not account for the possibly variable temporal course of the disease that would inform on the sequence in which these regions become abnormal. In addition, by fitting a single population average, they did not account for possible phenotypic variability. Indeed, the increasingly recognized inter-individual heterogeneity of structural pathology and cognitive deficits [137, 161, 162, 339] is a strong incentive to adopt novel image-based models of disease evolution.

Event-based models [163] estimate distinct stages that capture dynamic patterns of disease evolution from cross-sectional data, circumventing logistical burdens of a longitudinal design. A recent ENIGMA-Epilepsy study identified progressive atrophy that begins in the hippocampus, subsequently extending to the neocortex [164]. However, in addition to limiting the analysis to GM only, the inherent assumption was that all patients follow the same disease trajectory. Inability to disentangle temporal heterogeneity from phenotypic diversity limits the biological insights into disease mechanisms and the utility for patient stratification. Conversely, a comprehensive framework that reconciles both sources of heterogeneity may inform on how TLE evolves for different subtypes, ultimately facilitating personalized diagnostics.

Our purpose was to parse phenotypic and temporal diversities of TLE evolution. To this end, we applied Subtype and Stage Inference (SuStaIn) [340], a computational technique that extends event-based models for simultaneous staging and subtyping. This approach offers several advantages. Firstly, the use of piecewise over frequently used conventional linear models allows inferring the sequence of biomarker progression [163]; in other words, while conventional models identify biomarkers that progress over time, they do not inform on their temporal sequence. Conversely, elucidating the temporal sequence sets a biologically plausible basis to stage patients [280]. Secondly, application to cross-sectional data permits a stratification of patients based on single evaluation. Thirdly, the ability to simultaneously subtype and stage patients in a data-driven manner precludes the need for *a priori* stratification. Owing to these advantages, SuStaIn has helped characterizing the phenotypic variability and temporal evolution of Alzheimer's disease [341, 342], frontotemporal dementia [340] and multiple sclerosis [343]. Applying SuStaIn to multimodal MRI markers of the GM and WM integrity, we identified disease trajectories to which individual patients were probabilistically assigned, the stability of which was assessed using Bootstrap analysis. We then examined associations with clinical and cognitive parameters and utility for individualized predictions.

6.2 Methods

Study design and participants

We studied 82 consecutive TLE patients (30 males, mean±SD age = 35±9 years, range=19-61 years) referred to our hospital who had a research-dedicated 3T MRI that included structural imaging and diffusion-weighted MRI. Seventy patients presented with drug-resistant seizures, 12 were responsive to anti-seizure medication.

Demographic and clinical data were obtained through interviews with patients and their relatives. In 65 patients, the focus was determined by video EEG monitoring with scalp electrodes showing unequivocal temporal lobe seizures onset (and >70% of spikes); in cases with non-localized seizure onset (17/82=21%), lateralization was established using stereoencephalography (SEEG). Accordingly, patients were dichotomized into LTLE (n=41; 28 females; age=35.0±8.9 years; range=19-53 years) and RTLE (n=41; 24 females; age= 35.3±10.5 years; range=19-61 years). As per neuroradiological reading, 40 (49%) patients had ipsilateral hippocampal atrophy together with T2 hypersignal, while the MRI was reported as unremarkable in 42 (51%). Notably, no patient had a mass lesion (*e.g.*, malformations of cortical development, tumor, vascular malformations) or a history of traumatic brain injury or encephalitis. In relation to clinical parameters, age at seizure onset was 17.8±11 years with a disease duration of 17.4±12 years, and 26 (32%) patients had a history of febrile convulsions.

Patients underwent a routine neuropsychological battery administered by clinical neuropsychologists (V.S. and J.C.); among tests, we chose those available for all. Verbal IQ and digit span were evaluated with the WAIS-III. Leonard tapping task measured sequential motor tapping [306], as a measure of motor coordination incorporating visuo-motor learning ability.

The comprehensive investigation recommended surgery for all 70 patients with drug-resistant epilepsy, 57 (81%) of whom underwent a selective amygdalo-hippocampectomy so far. Histological analysis of the resected specimens [105] revealed hippocampal sclerosis characterized by neuronal cell loss and gliosis (HS) in 37 patients and isolated hippocampal gliosis in 20. At a mean follow-up time of 72 ± 24 months (range: 14-120 months), 43 (75%) patients had Engel-I outcome, 7 (12%) Engel-II, and 7 (12%) Engel-III. Among the 13 non-operated patients, 8 are currently awaiting surgery and 5 delayed it for personal reasons. Patients responsive to anti-seizure medication remained seizure-

free. The control group consisted of age- and sex-matched healthy individuals (n=41, 18 males, mean±SD age=32±8years, range=20-53 years).

The Ethics Committee of the Montreal Neurological Institute and Hospital approved the study, and the written consent was obtained from all participants in accordance with the Declaration of Helsinki.

MRI acquisition and pre-processing

Images were acquired on a 3T Siemens Magnetom TimTrio scanner using a 32-channel head coil. In accordance with the HARNESS protocol [238], all patients and controls had 3D T1-weighted (T1w) MPRAGE (TR=2,300 ms, TE=2.98 ms, flip angle=9°, voxel size=1×1×1 mm^3) and 3D fluid-attenuated inversion recovery (FLAIR; TR=5000ms, TE=389ms, flip angle=120°, voxel size=0.9× 0.9 × 0.9 mm^3). In addition, we acquired twice-refocused diffusion-weighted images with axial slices (TR=8,400 ms, TE=90 ms, flip angle=90°, voxel size=2x2x2 mm^3, 64 directions, b=1,000 s/mm^2). T1-weighted and FLAIR images underwent field non-uniformity correction and intensity normalization, were linearly registered to stereotaxic space based on the hemisphere-symmetric MNI ICBM152 template [307] using MINC toolkit (https://bic-mni.github.io/). T1-weighted images were classified into white matter (WM), gray matter (GM) and cerebrospinal fluid (CSF) [196]. Using FSL 5.0 (http://fmrib.ox.ac.uk/fsl) [308], diffusion-weighted images underwent distortion correction, based on the gradient echo field map acquired within the same imaging session, and correction for motion and eddy currents. Mean diffusivity (MD) and fractional anisotropy (FA) maps were derived using a tensor model; these maps were registered to the native T1-weighted space using a boundary-based technique that maximizes alignment between intensity gradients of structural and echo-planar data [193, 196].

We applied Constrained Laplacian Anatomic Segmentation using Proximity algorithm (CLASP) to generate models of GM-WM and GM-CSF surfaces with 41,000 surface points (henceforth *vertices*) per hemisphere [191]. In short, CLASP iteratively expands a surface mesh to fit the GM-WM surface and subsequently estimates the GM-CSF surface by expanding the GM-WM surface along the Laplacian gradient between the two surfaces. Surface-based registration aligned individual participants based on cortical folding to enhance vertex-wise anatomical correspondence [195]. Surface extraction accuracy was visually verified, and inaccuracies were manually corrected.

Surface-based feature extraction

To model prevalent features of TLE pathology, namely atrophy, gliosis, demyelination and microstructural damage, we sampled at each vertex morphological (cortical thickness, hippocampal volume) and intensity features (FLAIR, T1w/FLAIR), as well as diffusion parameters (FA, MD). To minimize interpolation, we mapped the surfaces to the native space of each modality using the inverse transform of the initial co-registration. Cortical thickness was measured as the Euclidean distance between corresponding vertices on GM-WM and GM-CSF surfaces. To assess the WM immediately beneath the cortex, we generated a surface running 2 mm below the GM-WM surface guided by a Laplacian gradient between the GM-WM surface and ventricles [135]. Hippocampal subfields (CA1-4, dentate gyrus, subiculum) were segmented using a patched-based multi-template algorithm [309] trained on an open access dataset [344], followed by the automated generation of the medial surface sheet running along the central path of each subfield [310]. In brief, we extracted a 3D skeleton from a given subfield using Hamilton-Jacobi level-sets. To derive shape-inherent inter-subject correspondence, outer subfield surfaces were parametrized using spherical harmonics shape descriptors. The boundary

was deformed along a Laplacian field gradient towards the skeleton, propagating the vertex correspondence onto the medial sheet. We calculated hippocampal columnar volume by multiplying the distance between corresponding vertices on the outer and medial surfaces by the mean area of the triangles whose edges include both vertices.

Modeling phenotypic and temporal disease evolution

Prior to applying the Subtype and Stage Inference (SuStaIn) algorithm, to reduce data dimensionality [340], all features were averaged using a regional parcellation scheme (frontal, temporal, occipital and parietal lobes, cingulate and insular cortices and hippocampus) based on the automated anatomic labeling (AAL) atlas [240]. The features were then z-normalized with respect to the analogous parcels in healthy controls. An inherent assumption of SuStaIn is that the input features are progressive. Hence, we verified that features were correlated ($p<0.05$) with disease duration. Notably, cortical FLAIR, T1/FLAIR, and WM FA did not show such a relationship and hence they were excluded from the analysis. For the remaining features (cortical thickness, hippocampal columnar volume and WM MD), prior to input, the effects of aging in healthy controls were regressed from patients, a strategy that circumvents collinearity of aging and disease duration [340].

SuStaIn is based on event-based models [163] with two key modifications that allow continuous linear accumulation of a feature from one z-score to another and patient subgroups with distinct patterns of biomarker progression [340]. As it uses piecewise linear segments with z-score evolution as control points, and requires no information about the timescale of change, it can be conveniently applied to cross-sectional data. The model is based on a multicomponent z-score function, such that *stage* is established when a given biomarker progresses a decrement (for cortical thickness and hippocampal

columnar volume) or an increment (for MD) of 0.5 z-score; the piecewise linear trajectory allows for the biomarkers to progress (and plateau) at different stages, thereby capturing the sequence of progression.

The model fitting uses expectation-maximization to estimate the joint posterior distributions of subtype and stage for each patient [345]; in other words, it estimates a probability matrix (P[Subtype and Stage]) with rows indicating subtypes and columns indicating stages. First, subtype is determined by adding the probabilities across the columns (P[Subtype = S], S = S_1, S_2, …, S_n) and selecting the row that contains the maximum probability. Stage is then determined by choosing the column with the maximum probability (max(P[Stage = T | Subtype = $S_{selected}$]), T_1, T_2, …, T_m). SuStaIn assumes that all features begin at 0 z-score at stage 1 and progress one step at a time by delta z-score until the features reach their maximum z-score; delta was set at 0.5. For each feature, the maximum z-score was then selected based on the 95 percentiles in patients. Although stages ranged from 1 (corresponding to 0 z-score for all features) to 154 (when all features reached their maximum z-score), virtually all patients were staged on or before 80.

We evaluated a range of subtypes S from 1 to 4. Because the estimation of factors may vary depending on random initialization [301], for each S, we ran the algorithm 100 times and selected the solution closest to the remaining 99 runs [300] based on product-moment linear correlation (r) of the trajectories. We then chose the final S that offered stability across runs ($r > 0.8$). To assess within-sample robustness, we estimated bootstrap mean and standard deviation of disease trajectories and the consistency of patients' assignments to trajectory subtypes and stages based on 1,000 bootstrap samples.

Individual-based predictions of clinical outcomes

Phenotypic heterogeneity has been shown to provide added value for individual-based predictions [162, 339]. Yet, no study has assessed the combined predictive utility of phenotypic and temporal heterogeneity. To address this shortcoming, we assessed the performance of SuStaIn subtypes and stages to predict drug response (resistant *vs*. controlled) and seizure outcome (Engel I *vs*. Engel II-IV). We trained Extreme Gradient Boosting, an ensemble of decision trees that controls for overfitting [346], using patients' subtype membership and stages. To assess the added value of SuStaIn model, we applied the same classifier to the subtype memberships given by a subtype-only model and stage assigned by a stage-only model. For the subtype-only model, we combined spectral clustering [347] with 10,000 bootstraps to identify stable subgroups of patients [348]. For the stage-only model, we applied an event-based model to identify a continuous piecewise linear accumulation of z-scores, achieved using the SuStaIn model after setting S to 1. Classifiers were cross-validated using a 10-fold scheme repeated 100 times; this procedure, by which 10% of patients are predicted using the data of the other 90%, allows an unbiased assessment for previously unseen cases.

In relation to drug response, patients controlled with medication are rarely hospitalized at our center. To address the between-group size difference, we used balanced learning, a procedure that scaled the weights of the responder and non-responder groups so that both outcome groups contributed equally to the construction of the classifier. Secondly, our evaluation was based on balanced accuracy, defined as the arithmetic mean between sensitivity and specificity [349]. For a classifier that would blindly predict every patient as responder, if overall accuracy was used, it would achieve 85% (70 out of 82), a gross overestimation of performance. Conversely, using balanced accuracy (that computes the mean of accuracies calculated within the outcome groups), the same classifier would

achieve 50% accuracy (average of 100% for responders and 0% for non-responders), namely an unbiased estimation.

Statistical analysis

Student t-test assessed the relationship between subtypes and continuous clinical variables (age, age onset); Chi-squared test was used for binary clinical variables (sex, MRI positivity, surgery, history of febrile convulsion, generalized seizures, drug-resistance, postsurgical seizure outcome and histopathology). Linear regression assessed the relationship between cognitive scores in verbal IQ, digit span, learning, memory and motor domains with the subtypes, as well as the relationship between the stage and cognitive scores and its interactions with subtype membership. Age and sex were used as covariates. Findings were corrected at FDR of 0.05.

6.3 Results

Subtypes and stages

SuStaIn identified three subtypes characterized by distinct patterns of damage of hippocampal and whole-brain structural MRI anomalies and their evolution **(Figure 17)**. Subtype 1 (S1, n=35)) was led by early-stage, severe, rapidly evolving ipsilateral hippocampal atrophy and bilateral asymmetric gliosis (indexed by increased MD; ipsi > contra), followed by bilateral WM microstructural anomalies (indexed by increased MD) more marked in ipsilateral temporo-limbic areas. Very mild bilateral neocortical atrophy became apparent only at late stages. Subtype 2 (S2, n=27) was typified by early-stage, mild and slowly progressing bilateral neocortical atrophy, followed by bilateral asymmetric hippocampal gliosis and atrophy (most severe ipsilaterally). Mild bilateral

WM microstructural anomalies became apparent only at late stages. Subtype 3 (S3, n=20) was characterized by mild, slowly progressing, bilateral limbic WM microstructural alterations, followed by mild hippocampal gliosis and neocortical atrophy.

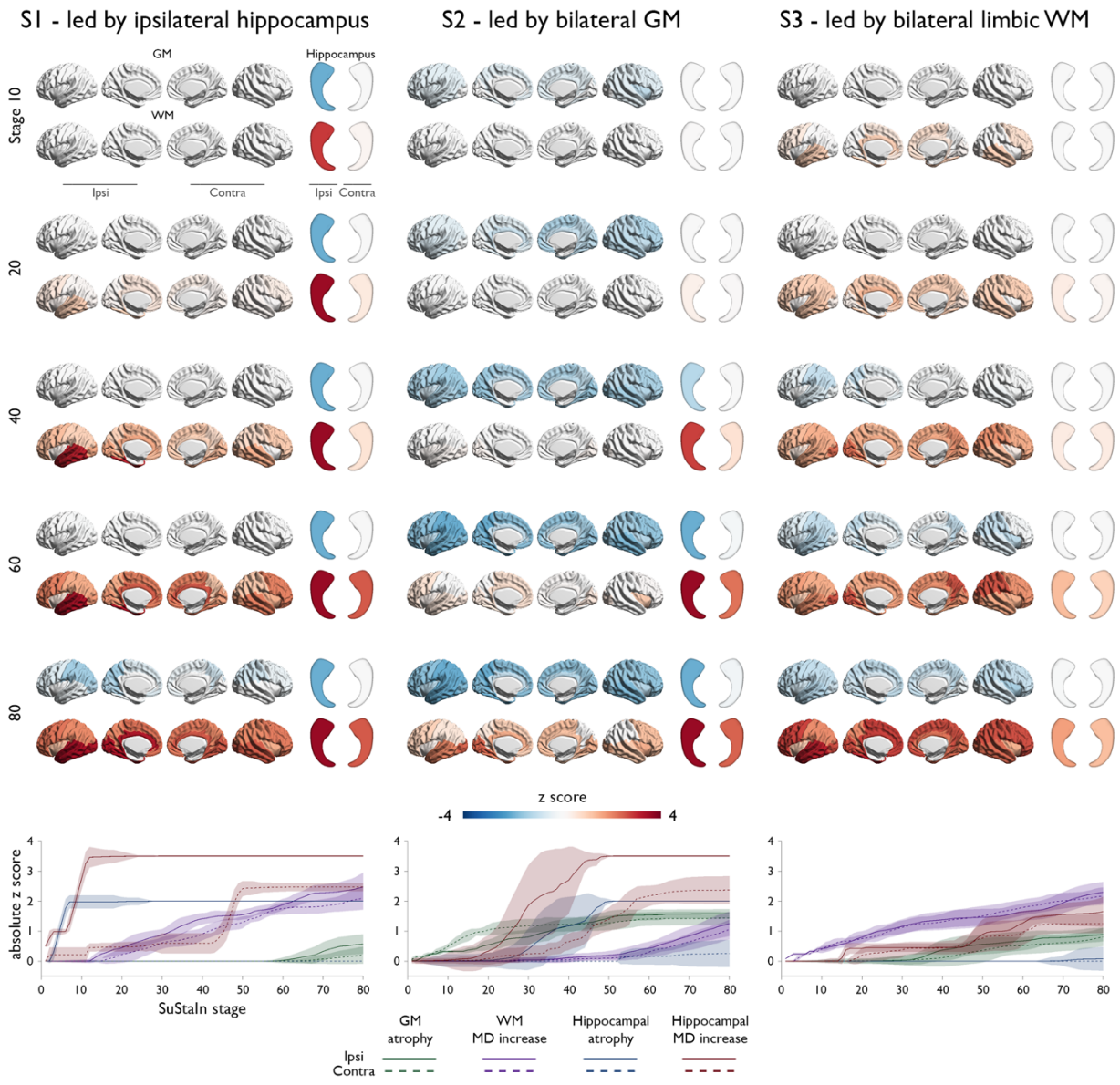

Figure 17. Staging and subtyping TLE evolution. Patterns of progression of MRI anomalies are shown. Each SuStaIn stage denotes a decrement (for cortical thickness and hippocampal columnar volume, indexing atrophy, in blue) or an increment (for MD, indexing hippocampal gliosis and white matter microstructural alterations, in red) by 0.5 z-score. SuStaIn stage ranges from 1 to 80, with all features starting at 0 z-score and reaching their maximum. MRI features are mapped on hippocampal and brain

surfaces. In the plots, lines and shades indicate bootstrap mean and SD of absolute z-scores depicting the within-sample stability of the sequence and severity of biomarkers' progression.

Patient distribution across stages and their probability of belonging to a given subtype are presented in **Figure 18**. Regardless of subtypes, most patients were assigned to stage 50 or earlier and showed high assignability to their given subtypes with 80/82 having a probability >50%. Within-sample stability of subtype and stage distributions were high with percent agreement across 1,000 bootstraps above 90%.

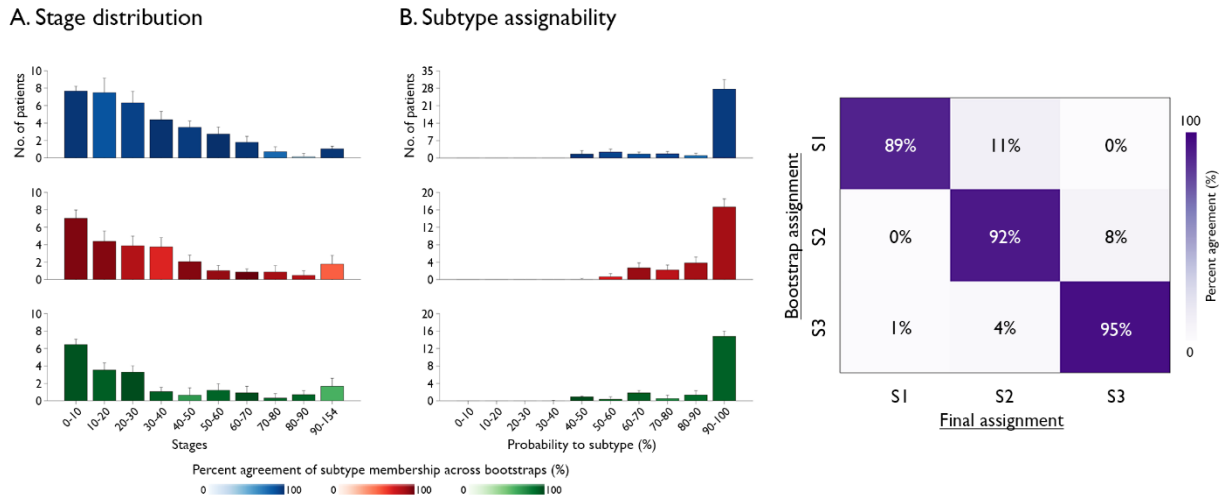

Figure 18. Patient stratification. A. Distribution of patients across SuStaIn stages. For all subtypes, most patients are stratified prior to stage 50. **B**. Distribution of patients with respect to the probability to their assigned subtypes. On histograms, error bars and color shades indicate bootstrap SD and percent agreement across bootstraps. Confusion matrix shows percent agreement of bootstrap-wise patient stratification with the final stratification. Overall, patients showed high assignability to their subtypes with high within-sample stability.

Relation to clinical parameters and cognitive scores

The TLE subtype S1, led by ipsilateral hippocampus, had the highest proportion of patients with early disease onset, febrile convulsions, GTCS, drug resistance, positive MRI, Engel I outcome and HS histopathology ($p_{FDR} < 0.05$ across all comparisons). Conversely, S3 led by bilateral limbic WM, and S2, led by bilateral neocortical atrophy, exhibited the lowest and intermediate proportions, respectively (**Table 4**). Bootstrap analysis confirmed robustness of findings.

	S1 - led by ipsilateral hippocampus	**S2 - led by bilateral GM**	**S3 - led by bilateral limbic WM**
Age ± SD (years)	34.4 ± 9.6	36.7 ± 9.9	34.7 ± 9.7
Sex (female/male)	21/14	16/11	15/5
Onset ± SD (years)	13.7 ± 10.1 †	19.3 ± 8.7	22.6 ± 13.0
Febrile convulsion	18 †	7	1
GTCS	24 *	14	7
Drug resistance	34 *	23	14
MRI (positive/negative)	28/7 †	12/15	1/19
Surgery/Engel I	28/24 •	17/12	12/7
Histopathology (HS/G)	25/3 †	9/8	3/9

Table 4. Relation to clinical parameters and outcomes. Student t-test compared the between subtypes comparisons for continuous variables (age, age onset), Chi-squared test was used for binary variables (sex,

MRI positivity, surgery, history of febrile convulsion, drug-resistance, postsurgical seizure outcome and histopathology). † indicates FDR<0.05 with respect to S2 and S3; * FDR<0.05 to S3; • p<0.05 to S3.

Regarding cognition (**Figure 19**), The three subtypes showed lower verbal IQ, digit span and sequential motor tapping with respect to the average performance of healthy individuals. However, directly contrasting subtypes, verbal IQ and digit span were lower in S1 and S2, as compared to S3 ($p_{FDR} < 0.05$). With respect to relations between stage and cognitive scores, S1 (R = -0.33, p_{FDR} = 0.027) and S3 (R = -0.46, p_{FDR} = 0.027) showed progressive decline in sequential motor tapping, faster than S2 (T = 2.03, p_{FDR} = 0.035; T = 2.14, p_{FDR} = 0.035). S3 also showed progressive decline in digit span (R = -0.53, p = 0.021).

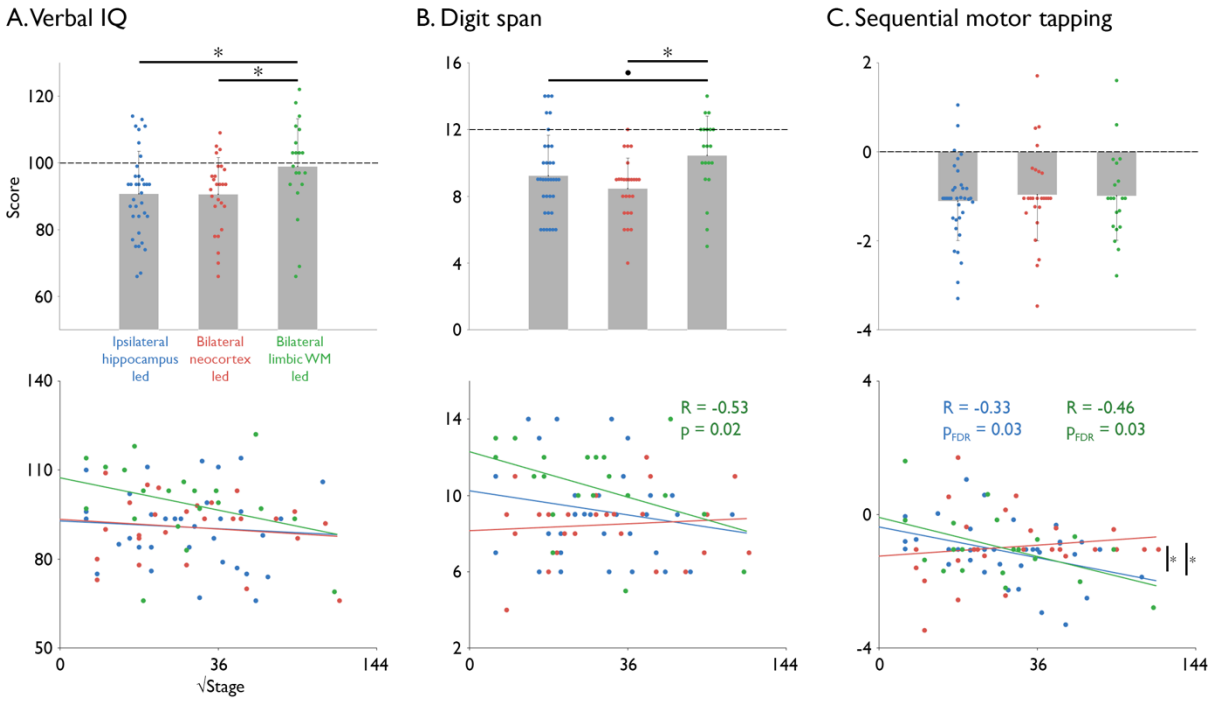

Figure 19. Relation to cognitive dysfunction. The graph bars show the mean score and standard deviation for each subtype for verbal IQ (A), digit span (B) and sequential motor tapping (C); dotted lines represent the average score in healthy controls. Individual patients are color-coded by their membership. The regression plots show the relationship between cognitive scores and stages; a vertical line indicate significant interactions. * $p_{FDR} < 0.05$. • $p < 0.05$.

Extreme Gradient Boosting classifiers trained on SuStaIn outperformed those trained on subtype- and stage-only models. Indeed, for drug response, SuStaIn yielded a balance accuracy of 73±1.0% (*vs.* 70±1.4% and 63±1.3%, $p_{FDR} < 0.05$) and 76±1.6% for Engel outcome (*vs.* 71±0.8% and 72±1.1%, $p_{FDR} < 0.05$).

6.4 Discussion

Using SuStaIn, a multicomponent piecewise linear accumulation model applied to cross-sectional MRI data, this study disentangled TLE disease trajectories characterized by distinct hippocampal and whole-brain signatures. Clinical utility was supported by differential relation to cognitive parameters; moreover, outcome predictions were more accurate when using classifiers trained on SuStaIn stratification, as compared to models trained separately on subtypes and stages.

Our analysis sheds light on the course of TLE progression, particularly in relation to the sequence in which these compartments become abnormal, as well as inter-individual phenotypical variability. The S1 subtype, led by early, rapidly evolving ipsilateral hippocampal atrophy and gliosis, exhibited the archetypal clinical features of TLE, including febrile convulsions, GTCS, drug resistance, MRI positivity and favorable post-surgical seizure outcome. Subsequent bilateral WM microstructural alterations are likely driven by large-scale effects of hippocampal pathology on connected temporo-limbic regions [135]. Besides such connectivity-based vulnerability and the longstanding hypothesis that TLE progression may be a direct effect of seizures, recent findings of amyloid-beta and tau pathology support a potential role of neurodegeneration akin to Alzheimer's disease [157, 158, 350]. Indeed, TLE shares similar pathology with Alzheimer's disease, namely myelin loss and axonal degeneration [112, 160], which are

widespread [318, 351] and preferentially located along subcortical WM tracts [352, 353], aberrant microvasculature [354-356] and astrogliosis [105, 113, 357]. Paralleling the observations that such anomalies are linked to amyloid-beta and tau accumulations in Alzheimer's disease, emerging data supports the notion that disease progression in TLE may be, at least partly, driven by these disordered proteins [157, 158], which may impart temporo-limbic WM damage by spreading through anatomical connections from the hippocampus [150, 353, 358, 359]. Moreover, amyloid-beta and tau may account for the bilateral neocortical atrophy, which emerge during the later SuStaIn stages of S1, suggesting temporal consistency with GM atrophy in late-adulthood Alzheimer's disease [360-362]. The S2 subtype was characterized early-stage, mild and slowly progressing bilateral GM atrophy, possibly embodying the damaging effects of seizure propagation [4, 125] along the highly interconnected cortical hubs [284, 363]. Contrary to S1, hippocampal pathology was apparent later in the course of the disease, which may explain the lesser degree of WM pathology in this subtype. The clinical parameters of S2 were similar to S1, yet to a lesser extent, likely reflecting the later involvement of the hippocampus. Contrary to S1 and S2 that presented with early GM damage, S3 was characterized by mild, slowly progressing, bilateral limbic WM microstructural alterations, with a greater overall load of pathology in both the neocortex and WM as compared to the hippocampus. In terms of clinical parameters, S3 was most dissimilar to the archetypal TLE features, especially with the highest rate of seizure relapse after surgery. Given that hippocampal sclerosis is among the strongest predictors of postsurgical seizure freedom [3, 364], sparing of hippocampus in S3 likely explains this dissimilarity. Regarding the underlying mechanisms that contribute to progression, the spatial and temporal similarities of bilateral limbic WM alterations between S3 and Alzheimer's disease [351, 352] suggest amyloid-beta and tau as potential contributors. With regards to pathophysiological link between TLE and AD progressions, there is evidence that amyloid and tau pathology may be induced by seizures [365]. Given the

observation that seizure freedom after resective surgery may prevent further progressive neocortical thinning [366], it is worthwhile to investigate whether successful surgery would prevent aberrant accumulation of these proteins and their downstream effects on WM microstructural compromise and late-adulthood neocortical atrophy as seen in AD.

With respect to cognition, while all subtypes showed impairments compared to healthy controls, S3 particularly exhibited the most subtle decline in verbal IQ and digit span. It has been established that hippocampus underpins verbal memory [330, 367] and their compromised contribution to the default mode network [223, 331, 333] may reduce verbal intelligence and memory [334]. Hence, the apparent sparing of hippocampus in S3 may explain why verbal IQ and digit span are least affected. On the other hand, S1 and S3 were associated with rapid decline in sequential motor tapping. Given that visuo-motor function requires cross-modal integration supported by WM integrity [335, 336], pervasive compromise of WM microstructure in these subtypes likely underpins this rapid progressive decline.

In neurological conditions, such as multiple sclerosis and Alzheimer's disease, simultaneous characterization of phenotypic variability and temporal progression has provided novel insights into pathophysiology and detailed patient stratification with added diagnostic and prognostic values [342, 343]. Conversely, in TLE, research has been directed mainly to the understanding of either phenotypic or temporal heterogeneity, thereby not informing on distinct trajectories. Our findings support the clinical relevance of both axes of variations by the improved performance of classifiers trained on SuStaIn subtype and stage information over learners relying separately on subtype- and stage-only models. Moreover, bootstrap resampling showed that patient stratification is robust for the three subtypes and the entire span of stages; in other words, at the time of diagnosis, irrespective of disease duration, patients can be reliably stratified into SuStaIn subtypes and stages based on cross-sectional MRI. Importantly, although longitudinal

designs offer greater statistical power and account for normal aging effects [150], SuStaIn circumvents the logistical and financial burdens of such designs [340]. Furthermore, the ability to model disease trajectories may shed light on distinct molecular and electrophysiological mechanisms, which may identify individuals at risk and help monitor the effectiveness of potential preventive therapies.

PART III

CONCLUSION

7. DISCUSSION OF KEY FINDINGS AND SIGNIFICANCE

This thesis includes a series of studies on inter-individual disease variability by combining multi-modal MRI and machine learning with clinical, cognitive and postsurgical follow-up data in the two most prevalent drug-resistant epilepsy syndromes, namely neocortical epilepsy related to focal cortical dysplasia (FCD) and temporal lobe epilepsy (TLE) related to mesiotemporal sclerosis. Two projects were aimed at capturing mesoscale structural variability of FCD lesions using multi-contrast MRI and at uncovering developmental processes that predispose cortical regions to harbor FCD using multi-scale approach combining whole-brain transcriptomics, histopathology and MRI. In two other studies, we investigated the inter-patient variability of static and progressive hippocampal and whole-brain structural pathology using multi-modal MRI and unsupervised machine learning and established the added clinical value of harnessing variability for predicting clinical outcomes and cognitive dysfunction. Overall, this dissertation provides evidence that the structural pathology in epilepsy is variably expressed between individual patients and such variability can be utilized to facilitate person-centered diagnosis and prognosis, which could ultimately improve care.

Project I (Chapter 3) combined multi-contrast MRI and unsupervised machine learning to identify "FCD classes" with distinct structural profiles that captured the mesoscopic structural variability within and across lesions, with the objective to address the pathological variability beyond current discrete histological subtypes. This work was motivated by the emerging evidence of substantial cellular variability across lesions and co-occurrence of multiple subtypes within the same lesion. Subsequent analyses showed that FCD classes are associated with differential impact on brain function and

histopathological embedding. Clinical utility was supported by the gain in the performance of class-informed lesion detection algorithm compared to class-naïve paradigms. The FCD classes offer a novel basis to establish genotype-phenotype associations and to improve automated lesion detection.

Project II (Chapter 4) implemented a multi-scale approach spanning from molecular processes to large-scale brain organization on a multi-centric dataset of 337 histologically verified FCDs to uncover the developmental processes that predispose certain cortices to harbor this malformation. This work demonstrated that FCD lesions preferentially occur in the prefrontal and fronto-limbic cortices, histologically marked by low neuron density, large soma and thick gray matter. FCD distribution showed a strong association with the anterior region of the antero-posterior axis, which is suggested to reflect the graded timetable of neurogenesis. The gene expression profiles of these cortices uncovered two components: prenatal neuroglial proliferation and differentiation and postnatal synaptogenesis and circuit organization. Both components were enriched for the risk genes of all epilepsies, with the prenatal component additionally enriched for FCD somatic variants. Taken together, multimodal associations with cytoarchitecture, gene expression and axes of cortical organization indicates that prenatal neurogenesis and postnatal synaptogenesis may be key points of developmental vulnerability of the frontal lobe to FCD. Concordant with a causal role of atypical neuroglial proliferation and growth, the results indicate that FCD-vulnerable cortices display properties indicative of earlier termination of neurogenesis and initiation of cell growth. They also suggest a potential contribution of aberrant postnatal synaptogenesis and circuit development to FCD epileptogenicity.

Project III (Chapter 5) applied an unsupervised dimensional approach to estimate latent relations (or disease factors) from 3T multi-modal MRI features of hippocampal and whole-brain structural pathology in histologically verified 82 TLE patients. We identified

four latent factors characterized by ipsilateral hippocampal microstructural alterations, loss of myelin and atrophy, bilateral paralimbic and hippocampal gliosis, bilateral neocortical atrophy and bilateral white matter microstructural alterations. Bootstrap analysis supported factors stability and robustness. While factors were variably co-expressed within each TLE patient, they were not expressed in healthy controls and only negligibly in disease controls, supporting specificity. Classifiers trained on latent disease factors accurately predicted patient-specific drug-response and postsurgical seizure outcome as well as inter-patient variability in verbal IQ, memory and sequential motor tapping outperforming baseline learners. Data-driven analysis of disease factors provides a novel appraisal of the continuum of interindividual variability, which is likely determined by multiple interacting pathological processes.

Project IV (Chapter 6) combined multimodal MRI with a computational technique that enables simultaneous staging and subtyping based on cross-sectional data, which circumvents logistical and financial burdens of longitudinal designs. This work identified three disease trajectory subtypes: Ipsilateral hippocampal atrophy and gliosis, followed by WM damage; Bilateral neocortical atrophy, followed by ipsilateral hippocampal atrophy and gliosis; bilateral limbic WM damage, followed by bilateral hippocampal gliosis. Patients showed high assignability to their subtypes and stages. The subtypes had differential proportions of patients with early disease onset, febrile convulsions, drug-resistance, a positive MRI, HS and Engel-I outcome and associated with distinct trajectories of verbal IQ, memory index and sequential motor tapping. Clinical utility is demonstrated by the higher performance of classifier trained on uncovered stages and subtypes for predicting antiepileptic drug response and postsurgical seizure outcome compared to classifiers trained on stage- and subtype-only models. Disease evolution in TLE follows variable trajectories, each associated with distinct patterns of cortico-subcortical and hippocampal structural alterations. Capturing the progression of

subtype-specific MRI biomarkers enables an objective, fine-grained patient stratification, which may identify individuals at risk and help monitoring the effectiveness of potential therapies preventive of further pathological progression.

Responses to questions on Project I

Question: How do FCD classes relate to seizure outcome after surgery?

Response: We did not find significant associations between the FCD class composition of lesions and seizure outcome after surgery. The lack of associations is consistent with the previous literature showing that the strongest predictor of seizure freedom is the complete resection of the structural lesion. The added value of FCD classes is in characterizing a wider spectrum of MRI phenotypes, which improves lesion detection.

Question: How do FCD classes translate to children?

Response: As the developing brains undergo dynamic changes in myelination and cytoarchitecture, the MRI profiles of the healthy tissues and their presentation of FCDs alter [368, 369]. However, the MRI profiles of FCD classes, which are defined relative to age-matched analogous healthy tissues, may not differ between children and adults, since the underlying histopathological features have not been shown to differ between the two age groups.

Question: How was T1w/T2w ratio normalized? Could you discuss cross-vendor replicability of this feature?

Response: T1w/FLAIR ratio was normalized relative to average T1w/FLAIR ratio across the cortical GM [370]. This normalization approach is robust across patients, as the alteration of T1w/FLAIR ratio is largely confined within the lesion, which generally make up a small areal proportion in the cortex. We also replicated the FCD classes across two independent datasets acquired using different MRI scanners and sequence parameters, which support wide applicability.

Responses to questions on Project II

Question: What topological and biological underpinnings are associated with drug controlled FCDs?

Response: While Project II examined the topological and biological underpinnings of drug-resistant FCD lesions, those of drug-controlled FCD lesions remain unknown. Our findings suggest that antero-posterior and superior-inferior axes of topology may underlie the formation of this malformation and the epileptogenesis of the precipitating lesion, respectively. On these bases, we hypothesize that drug-controlled FCD lesions would follow the antero-posterior axis but not the superior-inferior axis.

Question: Do FCDs with germline propensity towards seizures follow similar topological patterns?

Response: Germline mutations that constitutively activate mTOR pathway have shown to lead to a variety of brain malformations, including focal cortical dysplasia, hemimegaloencephaly and macrocephaly, affecting large cortical areas [63]. Although the topological patterns of FCDs due to germline mutations remain unknown, their larger sizes of malformation suggest that the precipitating molecular insult had occurred during

earlier stage of neurogenesis. Moreover, the pivotal role of mTOR pathway in germline FCDs further suggest pathogenic role of neurogenesis. Hence, FCDs with germline propensity may follow similar topological patterns as those with somatic propensity.

Question: How do the findings of this project relate to FCD type I?

Response: Given that type I FCDs present with cortical dyslamination without cytological abnormalities, their etiology may be driven more heavily by neuronal migration than by neurogenesis. Since the macroscale topological profile of neuronal migration is unclear, it is difficult to ascertain how the presented findings would relate to type I FCDs.

Responses to questions on Project III

Question: Would additional MRI sequences potentially improve the performance?

Response: Inclusion of advanced MRI sequences may potentially improve the discovery of the disease factors and their predictive power for individual clinical outcomes. Notably, multi-shelled, high-angular diffusion MRI techniques, such as neurite orientation distribution and density imaging [371] and diffusion kurtosis imaging [372], offer additional indices of tissue microstructure, which would likely offer richer insights into the disease processes. While such sequences are increasingly becoming a part of standard clinical protocols, other advanced sequences may add to the analysis with additional scan time. These include physiological MRI techniques that quantify the rate of metabolism [373-375], myelin water fraction [376, 377] and magnetic susceptibility [378] in tissues, which could further inform on the disease factors and enhance their predictive power.

Question: Does laterality of TLE factors relate to memory outcomes?

Response: The decline in memory was associated with Factors 1 (ipsilateral hippocampal damage) and 3 (bilateral neocortical thinning). This is consistent with previous functional MRI studies reporting asymmetry of memory activation in TLE patients, in contrast to symmetric memory activation in healthy controls [379, 380].

Question: How do subcortical volumes (i.e., thalamus) relate to factors?

Response: Thalamus has been suggested to drive seizure spread in TLE [156, 381, 382]. However, given that thalamic atrophy is tightly coupled with hippocampal atrophy [383], inclusion of thalamus is unlikely to alter the discovered factors.

Responses to questions on Project IV

Question: What are the added values of combining SuStaIn with factors?

Response: The main difference between the SuStaIn outputs and factors is that the former is based on progressive imaging phenotypes, while the latter includes both progressive and static phenotypes. For instance, Factor 2 defined by paralimbic FLAIR hyperintensity does not progressive with disease duration, which was why SuStaIn could not inform on the progression of FLAIR intensity. Hence, combining SuStaIn outputs with factors is expected to offer complementary insights into the disease processes and thereby enhance the prediction of individual clinical outcomes.

Question: Does early epilepsy surgery interrupt or modify disease trajectory?

Response: Our sample of 82 TLE patients, who were stratified into 3 subtypes and several stages, was insufficient to establish the modulatory effects of early epilepsy surgery. It will be worthwhile for future works with larger sample sizes to investigate how epilepsy surgery alters the disease trajectories in different SuStaIn subtypes.

Question: What are the assumptions or limitations in age regression in this cross-sectional study?

Response: To control for the effects of normal aging from the disease-related aging, we assumed that the effects of aging in health controls to be the effects of normal aging. The aging effects estimated in healthy controls were then regressed out from the patients to remove the assumed effects of normal aging from the patients [340]. It is worth noting that was an indirect approach to estimate the true effects of normal aging in patients. While longitudinal designs offer a direct approach, cross-sectional approach circumvents the logistical and financial burdens of repeated scanning, which are often prohibitive for patients.

Question: Why were cortical FLAIR and T1w/FLAIR not included?

Response: SuStaIn assumes that the inputs features are progressive [340]. We found that FLAIR and T1w/FLAIR ratio were not progressive and thereby not included them into the analysis.

Question: Is piece-wise linear accumulation (monotonic) a reasonable assumption for TLE?

Response: Monotonic progression of MRI profiles is a reasonable assumption. It is worth noting that a subset of TLE patients has shown to express hippocampal and amygdalal hypertrophy [162]. These patients are associated with isolated gliosis and poor seizure outcome. Although SuStaIn did not explicitly account for hypertrophy, this subset of patients should fall within Subtype 3 led by bilateral limbic white matter pathology, which show no signs of hippocampal atrophy and express highly similar clinical features.

Question: Three subtypes have different onset and severity. Do different groups have different stages?

Response: The clinical parameters differ between SuStaIn subtypes, with S1 (led by hippocampal atrophy) associated with severe features and favorable surgical outcome and with S2 and S3 associated with moderate and mild features with less and least favorable outcome, respectively. Notably, S1 is linked to earlier epilepsy onset compared to S2 and S3. Nevertheless, this difference in age onset does not translate to difference in SuStaIn stages, which are defined by the severity (i.e., z-score) of the MRI features [340].

Question: Does the pathology propagate in TLE?

Response: The associations between MRI profiles and histopathology have been established in previous studies [105, 110, 112]. Hence, the progression of MRI signatures, as depicted in SuStaIn-derived trajectories, should accompany corresponding progression of histopathology. The propagation of the pathology may be possible in two potential avenues. Increasing evidence of amyloid and tau accumulations in the limbic regions [157, 384] suggest that neurodegenerative processes may propagate in a manner similar to that seen in Alzheimer's disease [358]. In a similar vein, damage due to seizure

spread may facilitate a propagation of pathology via thalamocortical pathways [154] and with propensity towards topological hubs [363].

Question: Would the findings be replicable on 'typical' clinical scans?

Response: SuStaIn was applied to widely available and standard clinical MRI sequences, namely T1w MPRAGE and FLAIR. These protocols embody the consensus recommendation for epilepsy neuroimaging [238]. The findings in this project, as well as all other projects in this thesis, should render themselves replicable and relevant in typical clinical scans.

Significance

Characterizing focal epilepsy syndromes across multiple scales is a key to understanding how molecular perturbations and cellular pathology impart meso- and macro-scale alterations in brain structure, function and organization [385]. In clinical practice, such multi-scale framework may improve and enrich the diagnosis and prognosis of individual patients. To date, however, the characterization of focal epilepsy syndromes has been driven by the semiology and electrophysiology of seizures. Although these offer frameworks for patient stratification, such domains of patient profiles are neurobiologically remote phenomena that do not inform on the underlying etiology and pathological substrates. Aside from limited biological insights, these phenomena also do not offer a reliable biomarker for predicting the antiepileptic drug response and postsurgical seizure outcome. In this context, this thesis demonstrated that structural MRI, owing to its unmatched spatial resolution, whole-brain coverage and proximity to micro-scale phenomena, has unprecedented opportunities to transform the disease

characterization and clinical care. This thesis demonstrated that combining structural multi-modal MRI and inter-individual variability reconciles insights into multiple scales of neuropathology and biomarkers that reliably predict the responses to medication and surgery in the individual patients.

Although MRI offers a unique bridge between micro-scale neural phenomena and clinical and cognitive outcomes, incorporating genomic data acquired from the same individuals into the analysis may further inform on the etiology and clinical care. For example, measuring gene expression profiles from the plasma or CSF is logistically feasible and may identify germline variants that underpin the MRI phenotypes in the same individuals. However, gene expression profiles vary between peripheral sources and brain cells, which are hard to access from the patients. An alternative to circumventing this limitation is to use induced pluripotent stem cells (iPSC) derived from the patients [386, 387]. As patient-specific iPSCs can provide a large quantity of disease-relevant brain cells that are otherwise difficult to obtain, they can facilitate establishing direct links between brain-specific molecular mechanisms and MRI phenotypes within the same individuals [388]. Nevertheless, combining patient-specific iPSC-derived brain gene expression with MRI phenotypes may not address the region-specific somatic variants that occur in epileptogenic neocortical malformations. In these cases, whole-brain gene expression data of neurotypical individuals, such as those from Allen Human Brain Atlas and PsychENCODE, may serve as alternatives to investigate the molecular signatures associated with MRI phenotypes, as demonstrated in Project II. Taken together, a concerted efforts towards characterizing the multiscale neurobiology of focal epilepsy syndromes would be key step to establishing how developmental processes are altered to give rise to focal lesions and degenerative processes that underpin progressive alterations across the whole brain within individuals.

Although the presented models of inter-individual variability in FCD and TLE have been developed based on single-center datasets, the models are consistent with the known and widely established aspects of the pathology. Importantly, the novelty of these models is in the integration of multiple key disease features, as previous models of disease variability have been limited to one feature or features derived from unimodal MRI. Moreover, the presented models were validated using extensive resampling techniques to ensure that site-specific nuances in the data do not shape the final model, thereby supporting generalizability. Hence, the presented models should lend themselves useful for across centers.

In summary, this thesis combined multi-modal MRI with machine learning to model the inter-individual variability based on the key aspects of structural pathology in lesional tissues, cortical GM and superficial WM in common focal epilepsy syndromes. The presented approach informed on the phenotypic and temporal variability beyond histological and electro-clinical categories. It also offered novel basis to understand aberrant developmental and degenerative mechanisms that drive the lesional and whole-brain structural alterations across lifespan. The presented approach may offer biomarkers that may reduce ineffective drug trails and accelerate referrals for pre-surgical evaluation, improve the detection of subtle lesions for surgical removal and enable inference on the genotypes for individual patients.

PART IV

BIBLIOGRAPHY

1. S. Wiebe, N. Jette, Pharmacoresistance and the role of surgery in difficult to treat epilepsy. *Nature Reviews Neurology* **8**, 669 (2012).
2. J. de Tisi *et al.*, The long-term outcome of adult epilepsy surgery, patterns of seizure remission, and relapse: a cohort study. *The Lancet* **378**, 1388-1395 (2011).
3. A. M. McIntosh *et al.*, Temporal lobectomy: long-term seizure outcome, late recurrence and risks for seizure recurrence. *Brain* **127**, 2018-2030 (2004).
4. L. Caciagli *et al.*, A meta-analysis on progressive atrophy in intractable temporal lobe epilepsy. *Time is brain?* **89**, 506-516 (2017).
5. M. R. Keezer, S. M. Sisodiya, J. W. Sander, Comorbidities of epilepsy: current concepts and future perspectives. *The Lancet Neurology* **15**, 106-115 (2016).
6. B. C. Jobst, G. D. Cascino, Resective epilepsy surgery for drug-resistant focal epilepsy: A review. *JAMA* **313**, 285-293 (2015).
7. J. F. Téllez-Zenteno, L. H. Ronquillo, F. Moien-Afshari, S. Wiebe, Surgical outcomes in lesional and non-lesional epilepsy: A systematic review and meta-analysis. *Epilepsy Research* **89**, 310-318 (2010).
8. S. West *et al.*, Surgery for epilepsy. *Cochrane Database Syst Rev* **6**, CD010541-CD010541 (2019).
9. A. Bernasconi, N. Bernasconi, B. C. Bernhardt, D. Schrader, Advances in MRI for cryptogenic epilepsies. *Nature Reviews Neurology* **7**, 99 (2011).
10. R. Guerrini, W. B. Dobyns, Malformations of cortical development: clinical features and genetic causes. *The Lancet. Neurology* **13**, 710-726 (2014).
11. J. T. Lerner *et al.*, Assessment and surgical outcomes for mild type I and severe type II cortical dysplasia: a critical review and the UCLA experience. *Epilepsia* **50**, 1310-1335 (2009).
12. P. H. Iffland, P. B. Crino, Focal Cortical Dysplasia: Gene Mutations, Cell Signaling, and Therapeutic Implications. *Annual Review of Pathology: Mechanisms of Disease* **12**, 547-571 (2017).

13. J. N. Pulvers, N. Journiac, Y. Arai, J. Nardelli, MCPH1: a window into brain development and evolution. *Frontiers in Cellular Neuroscience* **9** (2015).
14. P. B. Crino, The mTOR signalling cascade: paving new roads to cure neurological disease. *Nature Reviews Neurology* **12**, 379 (2016).
15. I. Blumcke *et al.*, The clinicopathologic spectrum of focal cortical dysplasias: a consensus classification proposed by an ad hoc Task Force of the ILAE Diagnostic Methods Commission. *Epilepsia* **52**, 158-174 (2011).
16. L. Tassi *et al.*, Electroclinical, MRI and surgical outcomes in 100 epileptic patients with type II FCD. *Epileptic Disord* **14**, 257-266 (2012).
17. S. Budday, P. Steinmann, E. Kuhl, Physical biology of human brain development. *Frontiers in Cellular Neuroscience* **9** (2015).
18. Y. Zhu *et al.*, Spatiotemporal transcriptomic divergence across human and macaque brain development. *Science* **362**, eaat8077 (2018).
19. C. R. Cadwell, A. Bhaduri, M. A. Mostajo-Radji, M. G. Keefe, T. J. Nowakowski, Development and arealization of the cerebral cortex. *Neuron* **103**, 980-1004 (2019).
20. M. Götz, W. B. Huttner, The cell biology of neurogenesis. *Nature reviews Molecular cell biology* **6**, 777-788 (2005).
21. B. Nadarajah, J. G. Parnavelas, Modes of neuronal migration in the developing cerebral cortex. *Nature Reviews Neuroscience* **3**, 423-432 (2002).
22. I. Bystron, C. Blakemore, P. Rakic, Development of the human cerebral cortex: Boulder Committee revisited. *Nat Rev Neurosci* **9**, 110-122 (2008).
23. A. Pontious, T. Kowalczyk, C. Englund, R. F. Hevner, Role of intermediate progenitor cells in cerebral cortex development. *Developmental neuroscience* **30**, 24-32 (2008).
24. S. C. Noctor, V. Martínez-Cerdeño, L. Ivic, A. R. Kriegstein, Cortical neurons arise in symmetric and asymmetric division zones and migrate through specific phases. *Nature neuroscience* **7**, 136-144 (2004).

25. T. Sun, R. F. Hevner, Growth and folding of the mammalian cerebral cortex: from molecules to malformations. *Nat Rev Neurosci* **15**, 217-232 (2014).
26. T. Kowalczyk *et al.*, Intermediate neuronal progenitors (basal progenitors) produce pyramidal–projection Neurons for all layers of cerebral cortex. *Cerebral cortex* **19**, 2439-2450 (2009).
27. W. Haubensak, A. Attardo, W. Denk, W. B. Huttner, Neurons arise in the basal neuroepithelium of the early mammalian telencephalon: a major site of neurogenesis. *Proceedings of the National Academy of Sciences* **101**, 3196-3201 (2004).
28. A. R. Kriegstein, S. C. Noctor, Patterns of neuronal migration in the embryonic cortex. *Trends in neurosciences* **27**, 392-399 (2004).
29. J. H. Lui, D. V. Hansen, A. R. Kriegstein, Development and evolution of the human neocortex. *Cell* **146**, 18-36 (2011).
30. J. A. Del Río, A. Martínez, C. Auladell, E. Soriano, Developmental history of the subplate and developing white matter in the murine neocortex. Neuronal organization and relationship with the main afferent systems at embryonic and perinatal stages. *Cerebral Cortex* **10**, 784-801 (2000).
31. C. Raybaud, T. Ahmad, N. Rastegar, M. Shroff, M. Al Nassar, The premature brain: developmental and lesional anatomy. *Neuroradiology* **55**, 23-40 (2013).
32. I. Y. Buchsbaum, S. Cappello, Neuronal migration in the CNS during development and disease: insights from in vivo and in vitro models. *Development* **146**, dev163766 (2019).
33. S. Rakic, N. Zecevic, Emerging complexity of layer I in human cerebral cortex. *Cerebral Cortex* **13**, 1072-1083 (2003).
34. O. Marín, J. L. Rubenstein, Cell migration in the forebrain. *Annual review of neuroscience* **26**, 441-483 (2003).
35. B. J. Molyneaux, P. Arlotta, J. R. Menezes, J. D. Macklis, Neuronal subtype specification in the cerebral cortex. *Nature reviews neuroscience* **8**, 427-437 (2007).

36. E. Förster *et al.*, Recent progress in understanding the role of Reelin in radial neuronal migration, with specific emphasis on the dentate gyrus. *European Journal of Neuroscience* **23**, 901-909 (2006).
37. Y. Hirota, K. Nakajima, Control of neuronal migration and aggregation by reelin signaling in the developing cerebral cortex. *Frontiers in cell and developmental biology* **5**, 40 (2017).
38. M. A. Holland, K. E. Miller, E. Kuhl, Emerging brain morphologies from axonal elongation. *Annals of biomedical engineering* **43**, 1640-1653 (2015).
39. S. A. Bayer, J. Altman, *Neocortical development* (Raven Press New York, 1991), vol. 1.
40. G. N. Elston, Cortex, cognition and the cell: new insights into the pyramidal neuron and prefrontal function. *Cerebral cortex* **13**, 1124-1138 (2003).
41. A. R. Ypsilanti *et al.*, Transcriptional network orchestrating regional patterning of cortical progenitors. *Proceedings of the National Academy of Sciences* **118**, e2024795118 (2021).
42. K. M. Bishop, G. Goudreau, D. D. O'Leary, Regulation of area identity in the mammalian neocortex by Emx2 and Pax6. *Science* **288**, 344-349 (2000).
43. D. D. O'Leary, S.-J. Chou, S. Sahara, Area patterning of the mammalian cortex. *Neuron* **56**, 252-269 (2007).
44. P. Rakic, Specification of cerebral cortical areas. *Science* **241**, 170-176 (1988).
45. E. A. Grove, T. Fukuchi-Shimogori, Generating the cerebral cortical area map. *Annual review of neuroscience* **26**, 355-380 (2003).
46. R. V. Hoch, J. L. R. Rubenstein, S. Pleasure, Genes and signaling events that establish regional patterning of the mammalian forebrain. *Seminars in Cell & Developmental Biology* **20**, 378-386 (2009).

47. D. J. Cahalane, C. J. Charvet, B. L. Finlay, Systematic, balancing gradients in neuron density and number across the primate isocortex. *Front Neuroanat* **6**, 28-28 (2012).
48. C. J. Charvet, B. L. Finlay, Evo-devo and the primate isocortex: the central organizing role of intrinsic gradients of neurogenesis. *Brain, behavior and evolution* **84**, 81-92 (2014).
49. M. Barber *et al.*, Migration Speed of Cajal-Retzius Cells Modulated by Vesicular Trafficking Controls the Size of Higher-Order Cortical Areas. *Current Biology* **25**, 2466-2478 (2015).
50. E. M. Callaway, V. Borrell, Developmental Sculpting of Dendritic Morphology of Layer 4 Neurons in Visual Cortex: Influence of Retinal Input. *The Journal of Neuroscience* **31**, 7456-7470 (2011).
51. G. Pouchelon *et al.*, Modality-specific thalamocortical inputs instruct the identity of postsynaptic L4 neurons. *Nature* **511**, 471-474 (2014).
52. M. Z. Ozair *et al.*, hPSC Modeling Reveals that Fate Selection of Cortical Deep Projection Neurons Occurs in the Subplate. *Cell Stem Cell* **23**, 60-73.e66 (2018).
53. M. L. Kraushar *et al.*, Thalamic WNT3 secretion spatiotemporally regulates the neocortical ribosome signature and mRNA translation to specify neocortical cell subtypes. *Journal of Neuroscience* **35**, 10911-10926 (2015).
54. D. J. Price *et al.*, The development of cortical connections. *European Journal of Neuroscience* **23**, 910-920 (2006).
55. D. S. Margulies *et al.*, Situating the default-mode network along a principal gradient of macroscale cortical organization. *Proceedings of the National Academy of Sciences* **113**, 12574-12579 (2016).
56. C. Paquola *et al.*, Microstructural and functional gradients are increasingly dissociated in transmodal cortices. *PLOS Biology* **17**, e3000284 (2019).

57. I. Najm *et al.*, The ILAE consensus classification of focal cortical dysplasia: An update proposed by an ad hoc task force of the ILAE diagnostic methods commission. *Epilepsia* **63**, 1899-1919 (2022).

58. W. A. Chamberlain *et al.*, Interobserver and intraobserver reproducibility in focal cortical dysplasia (malformations of cortical development). *Epilepsia* **50**, 2593-2598 (2009).

59. J. S. Lim *et al.*, Brain somatic mutations in MTOR cause focal cortical dysplasia type II leading to intractable epilepsy. *Nature Medicine* **21**, 395 (2015).

60. J. S. Lim *et al.*, Somatic mutations in TSC1 and TSC2 cause focal cortical dysplasia. *The American Journal of Human Genetics* **100**, 454-472 (2017).

61. A. M. D'Gama *et al.*, Somatic mutations activating the mTOR pathway in dorsal telencephalic progenitors cause a continuum of cortical dysplasias. *Cell reports* **21**, 3754-3766 (2017).

62. S. H. Avansini *et al.*, Dysregulation of NEUROG2 plays a key role in focal cortical dysplasia. *Annals of Neurology* **83**, 623-635 (2018).

63. R. S. Møller *et al.*, Germline and somatic mutations in the MTOR gene in focal cortical dysplasia and epilepsy. *Neurology. Genetics* **2**, e118-e118 (2016).

64. S. Zhao *et al.*, A brain somatic RHEB doublet mutation causes focal cortical dysplasia type II. *Experimental & Molecular Medicine* **51**, 1-11 (2019).

65. E. Marsan, S. Baulac, Review: Mechanistic target of rapamycin (mTOR) pathway, focal cortical dysplasia and epilepsy. *Neuropathology and Applied Neurobiology* **44**, 6-17 (2018).

66. M. Laplante, D. M. Sabatini, mTOR signaling at a glance. *Journal of Cell Science* **122**, 3589-3594 (2009).

67. S. M. Park *et al.*, Brain Somatic Mutations in MTOR Disrupt Neuronal Ciliogenesis, Leading to Focal Cortical Dyslamination. *Neuron* **99**, 83-97.e87 (2018).

68. P. B. Crino (2008) Focal brain malformations: a spectrum of disorders along the mTOR cascade. in *Novartis Found. Symp*, pp 260-272.

69. S. Baldassari *et al.*, Dissecting the genetic basis of focal cortical dysplasia: a large cohort study. *Acta neuropathologica* **138**, 885-900 (2019).

70. A. A. Cohen-Gadol, K. Özduman, R. A. Bronen, J. H. Kim, D. D. Spencer, Long-term outcome after epilepsy surgery for focal cortical dysplasia. *Journal of Neurosurgery* **101**, 55-65 (2004).

71. N. Colombo *et al.*, Focal cortical dysplasia type IIa and IIb: MRI aspects in 118 cases proven by histopathology. *Neuroradiology* **54**, 1065-1077 (2012).

72. P. Krsek *et al.*, Different features of histopathological subtypes of pediatric focal cortical dysplasia. *Annals of Neurology* **63**, 758-769 (2008).

73. P. Krsek *et al.*, Incomplete resection of focal cortical dysplasia is the main predictor of poor postsurgical outcome. *Neurology* **72**, 217-223 (2009).

74. P. Widdess-Walsh *et al.*, Subdural electrode analysis in focal cortical dysplasia: predictors of surgical outcome. *Neurology* **69**, 660-667 (2007).

75. E. Hedegärd *et al.*, Complications to invasive epilepsy surgery workup with subdural and depth electrodes: a prospective population-based observational study. *Journal of Neurology, Neurosurgery & Psychiatry* **85**, 716-720 (2014).

76. S. Fauser *et al.*, Focal cortical dysplasias: surgical outcome in 67 patients in relation to histological subtypes and dual pathology. *Brain* **127**, 2406-2418 (2004).

77. G. D. Cascino, Surgical treatment for epilepsy. *Epilepsy Research* **60**, 179-186 (2004).

78. A. Bernasconi *et al.*, Texture analysis and morphological processing of magnetic resonance imaging assist detection of focal cortical dysplasia in extra-temporal partial epilepsy. *Annals of Neurology* **49**, 770-775 (2001).

79. O. Colliot, S. B. Antel, V. B. Naessens, N. Bernasconi, A. Bernasconi, In Vivo Profiling of Focal Cortical Dysplasia on High-resolution MRI with Computational Models. *Epilepsia* **47**, 134-142 (2006).
80. S. Adler *et al.*, Novel surface features for automated detection of focal cortical dysplasias in paediatric epilepsy. *NeuroImage. Clinical* **14**, 18-27 (2016).
81. R. S. Gill *et al.*, Automated Detection of Epileptogenic Cortical Malformations Using Multimodal MRI. *Deep Learning in Medical Image Analysis and Multimodal Learning for Clinical Decision Support : Third International Workshop, DLMIA 2017, ML-CDS 2017. Lecture Notes in Computer Science* **10553**, 349-356 (2017).
82. S.-J. Hong *et al.*, Automated detection of cortical dysplasia type II in MRI-negative epilepsy. *Neurology* **83**, 48-55 (2014).
83. B. Jin *et al.*, Automated detection of focal cortical dysplasia type II with surface-based magnetic resonance imaging postprocessing and machine learning. *Epilepsia* **59**, 982-992 (2018).
84. Y.-L. Tan *et al.*, Quantitative surface analysis of combined MRI and PET enhances detection of focal cortical dysplasias. *Neuroimage* **166**, 10-18 (2018).
85. K. Snyder *et al.*, Distinguishing type II focal cortical dysplasias from normal cortex: A novel normative modeling approach. *NeuroImage: Clinical* **30**, 102565 (2021).
86. L. G. Kini, J. C. Gee, B. Litt, Computational analysis in epilepsy neuroimaging: a survey of features and methods. *NeuroImage: Clinical* **11**, 515-529 (2016).
87. R. S. Gill *et al.*, Multicenter validation of a deep learning detection algorithm for focal cortical dysplasia. *Neurology* **97**, e1571-e1582 (2021).
88. I. Goodfellow, Y. Bengio, A. Courville, *Deep learning* (MIT press, 2016).
89. R. E. Gross *et al.*, Stereotactic laser amygdalohippocampotomy for mesial temporal lobe epilepsy. *Annals of Neurology* 10.1002/ana.25180, n/a-n/a (2018).

90. I. M. Najm, H. B. Sarnat, I. Blümcke, Review: The international consensus classification of Focal Cortical Dysplasia – a critical update 2018. *Neuropathology and Applied Neurobiology* **44**, 18-31 (2018).
91. F. Semah *et al.*, Is the underlying cause of epilepsy a major prognostic factor for recurrence? *Neurology* **51**, 1256-1262 (1998).
92. S. Wiebe, Epidemiology of temporal lobe epilepsy. *Canadian Journal of Neurological Sciences* **27**, S6-S10 (2000).
93. J. Engel Jr, Introduction to temporal lobe epilepsy. *Epilepsy research* **26**, 141-150 (1996).
94. J. French *et al.*, Characteristics of medial temporal lobe epilepsy: I. Results of history and physical examination. *Annals of Neurology: Official Journal of the American Neurological Association and the Child Neurology Society* **34**, 774-780 (1993).
95. V. Rusu *et al.*, Dystonic posturing in seizures of mesial temporal origin: electroclinical and metabolic patterns. *Neurology* **65**, 1612-1619 (2005).
96. S. Dupont, F. Semah, M. Baulac, Y. Samson, The underlying pathophysiology of ictal dystonia in temporal lobe epilepsy: an FDG-PET study. *Neurology* **51**, 1289-1292 (1998).
97. I. Savic, L. Altshuler, L. Baxter, J. Engel, Pattern of interictal hypometabolism in PET scans with fludeoxyglucose F 18 reflects prior seizure types in patients with mesial temporal lobe seizures. *Archives of neurology* **54**, 129-136 (1997).
98. F. Leutmezer, S. Wöginger, E. Antoni, B. Seidl, C. Baumgartner, Asymmetric ending of secondarily generalized seizures A lateralizing sign in TLE. *Neurology* **59**, 1252-1254 (2002).
99. W. Theodore *et al.*, The secondarily generalized tonic-clonic seizure: a videotape analysis. *Neurology* **44**, 1403-1403 (1994).

100. B. C. Jobst *et al.*, Secondarily generalized seizures in mesial temporal epilepsy: clinical characteristics, lateralizing signs, and association with sleep–wake cycle. *Epilepsia* **42**, 1279-1287 (2001).

101. J. B. Cavanagh, A. Meyer, Aetiological aspects of Ammon's horn sclerosis associated with temporal lobe epilepsy. *Br Med J* **2**, 1403-1407 (1956).

102. C. J. Bruton, The neuropathology of temporal lobe epilepsy. *Maudsley monographs* **31** (1988).

103. N. C. De Lanerolle *et al.*, A retrospective analysis of hippocampal pathology in human temporal lobe epilepsy: evidence for distinctive patient subcategories. *Epilepsia* **44**, 677-687 (2003).

104. I. Blümcke, R. Coras, H. Miyata, C. Özkara, Defining clinico-neuropathological subtypes of mesial temporal lobe epilepsy with hippocampal sclerosis. *Brain pathology* **22**, 402-411 (2012).

105. I. Blümcke *et al.*, International consensus classification of hippocampal sclerosis in temporal lobe epilepsy: A Task Force report from the ILAE Commission on Diagnostic Methods. *Epilepsia* **54**, 1315-1329 (2013).

106. R. Coras *et al.*, Good interobserver and intraobserver agreement in the evaluation of the new ILAE classification of focal cortical dysplasias. *Epilepsia* **53**, 1341-1348 (2012).

107. I. Blümcke *et al.*, A new clinico-pathological classification system for mesial temporal sclerosis. *Acta neuropathologica* **113**, 235-244 (2007).

108. M. Thom, G. W. Mathern, J. H. Cross, E. H. Bertram, Mesial temporal lobe epilepsy: How do we improve surgical outcome? *Annals of Neurology* **68**, 424-434 (2010).

109. J. Margerison, J. Corsellis, Epilepsy and the temporal lobes: a clinical, electroencephalographic and neuropathologic study of the brain in epilepsy, with particular reference to the temporal lobes. *Brain* **89**, 499-530 (1966).

110. M. Goubran *et al.*, Magnetic resonance imaging and histology correlation in the neocortex in temporal lobe epilepsy. *Annals of Neurology* **77**, 237-250 (2015).
111. M. Thom *et al.*, Microdysgenesis with abnormal cortical myelinated fibres in temporal lobe epilepsy: a histopathological study with calbindin D-28-K immunohistochemistry. *Neuropathology and Applied Neurobiology* **26**, 251-257 (2000).
112. R. Garbelli *et al.*, Blurring in patients with temporal lobe epilepsy: clinical, high-field imaging and ultrastructural study. *Brain* **135**, 2337-2349 (2012).
113. F. Blanc *et al.*, Investigation of widespread neocortical pathology associated with hippocampal sclerosis in epilepsy: A postmortem study. *Epilepsia* **52**, 10-21 (2011).
114. G. D. Cascino *et al.*, Magnetic resonance imaging–based volume studies in temporal lobe epilepsy: pathological correlations. *Annals of Neurology: Official Journal of the American Neurological Association and the Child Neurology Society* **30**, 31-36 (1991).
115. F. Cendes *et al.*, MRI volumetric measurement of amygdala and hippocampus in temporal lobe epilepsy. *Neurology* **43**, 719-719 (1993).
116. C. Watson, C. R. Jack, F. Cendes, Volumetric magnetic resonance imaging: clinical applications and contributions to the understanding of temporal lobe epilepsy. *Archives of Neurology* **54**, 1521-1531 (1997).
117. N. Bernasconi *et al.*, Mesial temporal damage in temporal lobe epilepsy: a volumetric MRI study of the hippocampus, amygdala and parahippocampal region. *Brain* **126**, 462-469 (2003).
118. N. Bernasconi *et al.*, Entorhinal cortex in temporal lobe epilepsy. *A quantitative MRI study* **52**, 1870-1870 (1999).
119. N. Bernasconi *et al.*, Entorhinal cortex atrophy in epilepsy patients exhibiting normal hippocampal volumes. *Neurology* **56**, 1335-1339 (2001).

120. R. E. Hogan *et al.*, MRI-based high-dimensional hippocampal mapping in mesial temporal lobe epilepsy. *Brain* **127**, 1731-1740 (2004).

121. M. Styner *et al.*, Framework for the Statistical Shape Analysis of Brain Structures using SPHARM-PDM. *Insight J*, 242-250 (2006).

122. H. Kim, P. Besson, O. Colliot, A. Bernasconi, N. Bernasconi, Surface-Based Vector Analysis Using Heat Equation Interpolation: A New Approach to Quantify Local Hippocampal Volume Changes. *Medical Image Computing and Computer-Assisted Intervention - MICCAI 2008. Lecture Notes in Computer Science* **5241**, 1008-1015 (2008).

123. H. Kim *et al.*, Multivariate Hippocampal Subfield Analysis of Local MRI Intensity and Volume: Application to Temporal Lobe Epilepsy. *Medical Image Computing and Computer-Assisted Intervention – MICCAI 2014. Lecture Notes in Computer Science* **8674**, 170-178 (2014).

124. H. Kim, T. Mansi, N. Bernasconi, A. Bernasconi, Surface-based multi-template automated hippocampal segmentation: Application to temporal lobe epilepsy. *Medical Image Analysis* **16**, 1445-1455 (2012).

125. B. C. Bernhardt *et al.*, Longitudinal and cross-sectional analysis of atrophy in pharmacoresistant temporal lobe epilepsy. *Neurology* **72**, 1747-1754 (2009).

126. B. C. Bernhardt, H. Kim, N. Bernasconi, Patterns of subregional mesiotemporal disease progression in temporal lobe epilepsy. *Neurology* **81**, 1840-1847 (2013).

127. H. Kim, T. Mansi, N. Bernasconi, Disentangling Hippocampal Shape Anomalies in Epilepsy. *Frontiers in Neurology* **4** (2013).

128. B. C. Bernhardt *et al.*, The spectrum of structural and functional imaging abnormalities in temporal lobe epilepsy. *Annals of Neurology* **80**, 142-153 (2016).

129. B. Caldairou *et al.*, MRI-Based Machine Learning Prediction Framework to Lateralize Hippocampal Sclerosis in Patients With Temporal Lobe Epilepsy. *Neurology* **97**, e1583-e1593 (2021).

130. B. C. Bernhardt, N. Bernasconi, L. Concha, A. Bernasconi, Cortical thickness analysis in temporal lobe epilepsy. *Reproducibility and relation to outcome* **74**, 1776-1784 (2010).

131. C. D. Whelan *et al.*, Structural brain abnormalities in the common epilepsies assessed in a worldwide ENIGMA study. *Brain : a journal of neurology* **141**, 391-408 (2018).

132. S. Adler *et al.*, Topographic principles of cortical fluid-attenuated inversion recovery signal in temporal lobe epilepsy. *Epilepsia* **59**, 627-635 (2018).

133. G. Jackson, A. Connelly, J. Duncan, R. Grünewald, D. Gadian, Detection of hippocampal pathology in intractable partial epilepsy: increased sensitivity with quantitative magnetic resonance T2 relaxometry. *Neurology* **43**, 1793-1793 (1993).

134. B. C. Bernhardt *et al.*, Preferential susceptibility of limbic cortices to microstructural damage in temporal lobe epilepsy: A quantitative T1 mapping study. *NeuroImage* **182**, 294-303 (2018).

135. M. Liu *et al.*, The superficial white matter in temporal lobe epilepsy: a key link between structural and functional network disruptions. *Brain* **139**, 2431-2440 (2016).

136. L. Bonilha *et al.*, Altered Microstructure in Temporal Lobe Epilepsy: A Diffusional Kurtosis Imaging Study. *American Journal of Neuroradiology* **36**, 719-724 (2015).

137. A. Reyes *et al.*, Cognitive phenotypes in temporal lobe epilepsy are associated with distinct patterns of white matter network abnormalities. *Neurology* **92**, e1957-e1968 (2019).

138. J. E. Cavazos, D. J. Cross, The role of synaptic reorganization in mesial temporal lobe epilepsy. *Epilepsy & Behavior* **8**, 483-493 (2006).

139. R. S. Briellmann, S. F. Berkovic, A. Syngeniotis, M. A. King, G. D. Jackson, Seizure-associated hippocampal volume loss: a longitudinal magnetic resonance study of temporal lobe epilepsy. *Annals of neurology* **51**, 641-644 (2002).

140. D. K. Binder, C. Steinhäuser, Functional changes in astroglial cells in epilepsy. *Glia* **54**, 358-368 (2006).

141. O. Devinsky, A. Vezzani, S. Najjar, N. C. De Lanerolle, M. A. Rogawski, Glia and epilepsy: excitability and inflammation. *Trends in neurosciences* **36**, 174-184 (2013).

142. C. Beaulieu, The basis of anisotropic water diffusion in the nervous system–a technical review. *NMR in Biomedicine* **15**, 435-455 (2002).

143. L. Concha, D. J. Livy, C. Beaulieu, B. M. Wheatley, D. W. Gross, Diffusion Tensor Imaging and Histopathology of the Fimbria-Fornix in Temporal Lobe Epilepsy. *The Journal of Neuroscience* **30**, 996-1002 (2010).

144. P. van Eijsden *et al.*, In vivo diffusion tensor imaging and ex vivo histologic characterization of white matter pathology in a post–status epilepticus model of temporal lobe epilepsy. *Epilepsia* **52**, 841-845 (2011).

145. L. Bonilha, S. S. Keller, Quantitative MRI in refractory temporal lobe epilepsy: relationship with surgical outcomes. *Quantitative imaging in medicine and surgery* **5**, 204-224 (2015).

146. B. Hermann, Tracking the consequences of chronic epilepsy on cognition. *Epilepsy Currents* **4**, 118-119 (2004).

147. B. P. Hermann *et al.*, Cognitive prognosis in chronic temporal lobe epilepsy. *Annals of neurology* **60**, 80-87 (2006).

148. P. J. Thompson, J. S. Duncan, Cognitive decline in severe intractable epilepsy. *Epilepsia* **46**, 1780-1787 (2005).

149. C. M. Marques *et al.*, Cognitive decline in temporal lobe epilepsy due to unilateral hippocampal sclerosis. *Epilepsy & Behavior* **10**, 477-485 (2007).

150. M. Galovic *et al.*, Progressive Cortical Thinning in Patients With Focal Epilepsy. *JAMA Neurology* 10.1001/jamaneurol.2019.1708 (2019).

151. M. K. Alvim *et al.*, Progression of gray matter atrophy in seizure-free patients with temporal lobe epilepsy. *Epilepsia* **57**, 621-629 (2016).

152. A. Coan, S. Appenzeller, L. Bonilha, L. Li, F. Cendes, Seizure frequency and lateralization affect progression of atrophy in temporal lobe epilepsy. *Neurology* **73**, 834-842 (2009).

153. W. R. Gowers, *Epilepsy and other chronic convulsive diseases: their causes, symptoms, and treatment* (Old Hickory Bookshop, 1901).

154. B. C. Bernhardt, N. Bernasconi, H. Kim, A. Bernasconi, Mapping thalamocortical network pathology in temporal lobe epilepsy. *Neurology* **78**, 129-136 (2012).

155. D. S. Barron, N. Tandon, J. L. Lancaster, P. T. Fox, Thalamic structural connectivity in medial temporal lobe epilepsy. *Epilepsia* **55**, e50-e55 (2014).

156. M. Guye *et al.*, The role of corticothalamic coupling in human temporal lobe epilepsy. *Brain* **129**, 1917-1928 (2006).

157. S. Gourmaud *et al.*, Alzheimer-like amyloid and tau alterations associated with cognitive deficit in temporal lobe epilepsy. *Brain* **143**, 191-209 (2020).

158. X. Y. Tai *et al.*, Hyperphosphorylated tau in patients with refractory epilepsy correlates with cognitive decline: a study of temporal lobe resections. *Brain* **139**, 2441-2455 (2016).

159. L. Pini *et al.*, Brain atrophy in Alzheimer's disease and aging. *Ageing research reviews* **30**, 25-48 (2016).

160. C. F. Slattery *et al.*, ApoE influences regional white-matter axonal density loss in Alzheimer's disease. *Neurobiology of Aging* **57**, 8-17 (2017).

161. R. Rodríguez-Cruces, B. C. Bernhardt, L. Concha, Multidimensional associations between cognition and connectome organization in temporal lobe epilepsy. *NeuroImage* **213**, 116706 (2020).

162. B. C. Bernhardt, S.-J. Hong, A. Bernasconi, N. Bernasconi, Magnetic resonance imaging pattern learning in temporal lobe epilepsy: Classification and prognostics. *Annals of Neurology* **77**, 436-446 (2015).

163. H. M. Fonteijn *et al.*, An event-based model for disease progression and its application in familial Alzheimer's disease and Huntington's disease. *NeuroImage* **60**, 1880-1889 (2012).

164. S. M. Lopez *et al.*, Event-based modelling in temporal lobe epilepsy demonstrates progressive atrophy from cross-sectional data. *Epilepsia* **n/a** (2022).

165. E. D. Smolyansky, H. Hakeem, Z. Ge, Z. Chen, P. Kwan, Machine learning models for decision support in epilepsy management: A critical review. *Epilepsy & Behavior* **123**, 108273 (2021).

166. S. Petrovski *et al.*, Multi-SNP pharmacogenomic classifier is superior to single-SNP models for predicting drug outcome in complex diseases. *Pharmacogenetics and genomics* **19**, 147-152 (2009).

167. K. Shazadi *et al.*, Validation of a multigenic model to predict seizure control in newly treated epilepsy. *Epilepsy research* **108**, 1797-1805 (2014).

168. M. S. Silva-Alves *et al.*, A prediction algorithm for drug response in patients with mesial temporal lobe epilepsy based on clinical and genetic information. *PloS one* **12**, e0169214 (2017).

169. S. An *et al.*, Predicting drug-resistant epilepsy—a machine learning approach based on administrative claims data. *Epilepsy & Behavior* **89**, 118-125 (2018).

170. O. Devinsky *et al.*, Changing the approach to treatment choice in epilepsy using big data. *Epilepsy & Behavior* **56**, 32-37 (2016).

171. D. Delen, B. Davazdahemami, E. Eryarsoy, L. Tomak, A. Valluru, Using predictive analytics to identify drug-resistant epilepsy patients. *Health informatics journal* **26**, 449-460 (2020).

172. L. Yao *et al.*, Prediction of antiepileptic drug treatment outcomes of patients with newly diagnosed epilepsy by machine learning. *Epilepsy & Behavior* **96**, 92-97 (2019).

173. N. Memarian, S. Kim, S. Dewar, J. Engel Jr, R. J. Staba, Multimodal data and machine learning for surgery outcome prediction in complicated cases of mesial temporal lobe epilepsy. *Computers in biology and medicine* **64**, 67-78 (2015).

174. R. Armañanzas *et al.*, Machine learning approach for the outcome prediction of temporal lobe epilepsy surgery. *PLoS One* **8**, e62819 (2013).

175. B. Bernhardt, S.-J. Hong, A. Bernasconi, N. Bernasconi, Imaging structural and functional brain networks in temporal lobe epilepsy. *Frontiers in Human Neuroscience* **7** (2013).

176. L. Caciagli, B. C. Bernhardt, S.-J. Hong, A. Bernasconi, N. Bernasconi, Functional network alterations and their structural substrate in drug-resistant epilepsy. *Frontiers in neuroscience* **8**, 411 (2014).

177. B. C. Munsell *et al.*, Evaluation of machine learning algorithms for treatment outcome prediction in patients with epilepsy based on structural connectome data. *Neuroimage* **118**, 219-230 (2015).

178. P. N. Taylor *et al.*, The impact of epilepsy surgery on the structural connectome and its relation to outcome. *NeuroImage: Clinical* **18**, 202-214 (2018).

179. X. He *et al.*, Presurgical thalamic "hubness" predicts surgical outcome in temporal lobe epilepsy. *Neurology* **88**, 2285-2293 (2017).

180. S. Larivière *et al.*, Functional connectome contractions in temporal lobe epilepsy: Microstructural underpinnings and predictors of surgical outcome. *Epilepsia* **61**, 1221-1233 (2020).

181. E. Gleichgerrcht *et al.*, Temporal lobe epilepsy surgical outcomes can be inferred based on structural connectome hubs: A machine learning study. *Annals of neurology* **88**, 970-983 (2020).

182. N. Sinha *et al.*, Structural brain network abnormalities and the probability of seizure recurrence after epilepsy surgery. *Neurology* **96**, e758-e771 (2021).

183. A. Lo, H. Chernoff, T. Zheng, S.-H. Lo, Why significant variables aren't automatically good predictors. *Proceedings of the National Academy of Sciences of the United States of America* **112**, 13892-13897 (2015).

184. M. R. Arbabshirani, S. Plis, J. Sui, V. D. Calhoun, Single subject prediction of brain disorders in neuroimaging: Promises and pitfalls. *NeuroImage* **145**, 137-165 (2017).

185. B. Abbasi, D. M. Goldenholz, Machine learning applications in epilepsy. *Epilepsia* **60**, 2037-2047 (2019).

186. X. Zhang *et al.*, Bayesian model reveals latent atrophy factors with dissociable cognitive trajectories in Alzheimer's disease. *Proceedings of the National Academy of Sciences of the United States of America* **113**, E6535-E6544 (2016).

187. A. T. Drysdale *et al.*, Resting-state connectivity biomarkers define neurophysiological subtypes of depression. *Nature Medicine* **23**, 28 (2016).

188. S.-J. Hong, S. L. Valk, A. Di Martino, M. P. Milham, B. C. Bernhardt, Multidimensional Neuroanatomical Subtyping of Autism Spectrum Disorder. *Cerebral Cortex* **28**, 3578-3588 (2017).

189. P. Bellec, P. Rosa-Neto, O. C. Lyttelton, H. Benali, A. C. Evans, Multi-level bootstrap analysis of stable clusters in resting-state fMRI. *NeuroImage* **51**, 1126-1139 (2010).

190. J. Engel, Jr., A proposed diagnostic scheme for people with epileptic seizures and with epilepsy: report of the ILAE Task Force on Classification and Terminology. *Epilepsia* **42**, 796-803 (2001).

191. J. S. Kim *et al.*, Automated 3-D extraction and evaluation of the inner and outer cortical surfaces using a Laplacian map and partial volume effect classification. *NeuroImage* **27**, 210-221 (2005).

192. J. D. Power, K. A. Barnes, A. Z. Snyder, B. L. Schlaggar, S. E. Petersen, Spurious but systematic correlations in functional connectivity MRI networks arise from subject motion. *Neuroimage* **59**, 2142-2154 (2012).

193. D. N. Greve, B. Fischl, Accurate and robust brain image alignment using boundary-based registration. *NeuroImage* **48**, 63-72 (2009).

194. S.-J. Hong *et al.*, Multimodal MRI profiling of focal cortical dysplasia type II. *Neurology* **88**, 734-742 (2017).

195. O. Lyttelton, M. Boucher, S. Robbins, A. Evans, An unbiased iterative group registration template for cortical surface analysis. *NeuroImage* **34**, 1535-1544 (2007).

196. H. Kim *et al.*, Accurate cortical tissue classification on MRI by modeling cortical folding patterns. *Human Brain Mapping* **36**, 3563-3574 (2015).

197. T. Scholl *et al.*, Impaired oligodendroglial turnover is associated with myelin pathology in focal cortical dysplasia and tuberous sclerosis complex. *Brain pathology (Zurich, Switzerland)* **27**, 770-780 (2017).

198. M. F. Glasser, D. C. Van Essen, Mapping human cortical areas in vivo based on myelin content as revealed by T1- and T2-weighted MRI. *J Neurosci* **31**, 11597-11616 (2011).

199. Z. Zhang *et al.*, fMRI study of mesial temporal lobe epilepsy using amplitude of low-frequency fluctuation analysis. *Human Brain Mapping* **31**, 1851-1861 (2010).

200. E. Bullmore, O. Sporns, Complex brain networks: graph theoretical analysis of structural and functional systems. *Nat Rev Neurosci* **10**, 186-198 (2009).

201. A. L. Cohen *et al.*, Defining functional areas in individual human brains using resting functional connectivity MRI. *NeuroImage* **41**, 45-57 (2008).

202. Y. Benjamini, Y. Hochberg, Controlling the False Discovery Rate: A Practical and Powerful Approach to Multiple Testing. *Journal of the Royal Statistical Society. Series B (Methodological)* **57**, 289-300 (1995).

203. T. Chen, C. Guestrin (2016) XGBoost: A Scalable Tree Boosting System. in *Proceedings of the 22nd ACM SIGKDD International Conference on Knowledge Discovery and Data Mining* (ACM, San Francisco, California, USA), pp 785-794.

204. P. B. Crino, The enlarging spectrum of focal cortical dysplasias. *Brain* **138**, 1446-1448 (2015).

205. J. M. Nakagawa *et al.*, Characterization of focal cortical dysplasia with balloon cells by layer-specific markers: Evidence for differential vulnerability of interneurons. *Epilepsia* **58**, 635-645 (2017).

206. A. Muhlebner *et al.*, Neuropathologic measurements in focal cortical dysplasias: validation of the ILAE 2011 classification system and diagnostic implications for MRI. *Acta Neuropathol* **123**, 259-272 (2012).

207. C. O. Oluigbo *et al.*, The influence of lesion volume, perilesion resection volume, and completeness of resection on seizure outcome after resective epilepsy surgery for cortical dysplasia in children. **15**, 644 (2015).

208. I. Blümcke *et al.*, International recommendation for a comprehensive neuropathologic workup of epilepsy surgery brain tissue: A consensus Task Force report from the ILAE Commission on Diagnostic Methods. *Epilepsia* **57**, 348-358 (2016).

209. R. A. Prayson, Classification and pathological characteristics of the cortical dysplasias. *Child's Nervous System* **30**, 1805-1812 (2014).

210. R. Citraro, A. Leo, A. Constanti, E. Russo, G. De Sarro, mTOR pathway inhibition as a new therapeutic strategy in epilepsy and epileptogenesis. *Pharmacological Research* **107**, 333-343 (2016).

211. A. M. D'Gama, C. A. Walsh, Somatic mosaicism and neurodevelopmental disease. *Nature Neuroscience* **21**, 1504-1514 (2018).

212. I. Blumcke *et al.*, Histopathological Findings in Brain Tissue Obtained during Epilepsy Surgery. *New England Journal of Medicine* **377**, 1648-1656 (2017).

213. S. S. Jamuar *et al.*, Somatic Mutations in Cerebral Cortical Malformations. *New England Journal of Medicine* **371**, 733-743 (2014).

214. A. M. D'Gama *et al.*, Mammalian target of rapamycin pathway mutations cause hemimegalencephaly and focal cortical dysplasia. *Annals of neurology* **77**, 720-725 (2015).

215. C. Chung *et al.*, Comprehensive multiomic profiling of somatic mutations in malformations of cortical development. *bioRxiv* 10.1101/2022.04.07.487401, 2022.2004.2007.487401 (2022).

216. H. J. Lamberink *et al.*, Seizure outcome and use of antiepileptic drugs after epilepsy surgery according to histopathological diagnosis: a retrospective multicentre cohort study. *The Lancet Neurology* **19**, 748-757 (2020).

217. K. Wagstyl *et al.*, Atlas of lesion locations and postsurgical seizure freedom in focal cortical dysplasia: A MELD study. *Epilepsia* (2021).

218. S. L. Valk *et al.*, Shaping brain structure: Genetic and phylogenetic axes of macroscale organization of cortical thickness. *Science advances* **6**, eabb3417 (2020).

219. E. Klingler, F. Francis, D. Jabaudon, S. Cappello, Mapping the molecular and cellular complexity of cortical malformations. *Science* **371** (2021).

220. M. Hawrylycz *et al.*, Canonical genetic signatures of the adult human brain. *Nature Neuroscience* **18**, 1832-1844 (2015).

221. J. C. Silbereis, S. Pochareddy, Y. Zhu, M. Li, N. Sestan, The cellular and molecular landscapes of the developing human central nervous system. *Neuron* **89**, 248-268 (2016).

222. J. B. Burt *et al.*, Hierarchy of transcriptomic specialization across human cortex captured by structural neuroimaging topography. *Nature neuroscience* **21**, 1251-1259 (2018).

223. C. Paquola *et al.*, Convergence of cortical types and functional motifs in the human mesiotemporal lobe. *Elife* **9**, e60673 (2020).

224. M. Demirtaş *et al.*, Hierarchical heterogeneity across human cortex shapes large-scale neural dynamics. *Neuron* **101**, 1181-1194. e1113 (2019).
225. K. Wagstyl, L. Ronan, I. M. Goodyer, P. C. Fletcher, Cortical thickness gradients in structural hierarchies. *Neuroimage* **111**, 241-250 (2015).
226. J. M. Huntenburg, P.-L. Bazin, D. S. Margulies, Large-Scale Gradients in Human Cortical Organization. *Trends in Cognitive Sciences* **22**, 21-31 (2018).
227. B.-y. Park *et al.*, Signal diffusion along connectome gradients and inter-hub routing differentially contribute to dynamic human brain function. *NeuroImage* **224**, 117429 (2021).
228. C.-H. Chen *et al.*, Genetic influences on cortical regionalization in the human brain. *Neuron* **72**, 537-544 (2011).
229. C. Paquola *et al.*, The BigBrainWarp toolbox for integration of BigBrain 3D histology with multimodal neuroimaging. *eLife* **10**, e70119 (2021).
230. V. J. Sydnor *et al.*, Neurodevelopment of the association cortices: Patterns, mechanisms, and implications for psychopathology. *Neuron* (2021).
231. M. M. Mesulam, From sensation to cognition. *Brain* **121**, 1013-1052 (1998).
232. C. F. von Economo, G. N. Koskinas, *Die cytoarchitektonik der hirnrinde des erwachsenen menschen* (J. Springer, 1925).
233. L. H. Scholtens, M. A. de Reus, S. C. de Lange, R. Schmidt, M. P. van den Heuvel, An mri von economo–koskinas atlas. *Neuroimage* **170**, 249-256 (2018).
234. K. Amunts *et al.*, BigBrain: An Ultrahigh-Resolution 3D Human Brain Model. *Science* **340**, 1472-1475 (2013).
235. M. J. Hawrylycz *et al.*, An anatomically comprehensive atlas of the adult human brain transcriptome. *Nature* **489**, 391-399 (2012).
236. M. Li *et al.*, Integrative functional genomic analysis of human brain development and neuropsychiatric risks. *Science* **362**, eaat7615 (2018).

237. T. I. L. A. E. Consortium, Genome-wide mega-analysis identifies 16 loci and highlights diverse biological mechanisms in the common epilepsies. *Nature communications* **9** (2018).

238. A. Bernasconi *et al.*, Recommendations for the use of structural magnetic resonance imaging in the care of patients with epilepsy: a consensus report from the International League Against Epilepsy Neuroimaging Task Force. *Epilepsia* **60**, 1054-1068 (2019).

239. O. Lyttelton, M. Boucher, S. Robbins, A. Evans, An unbiased iterative group registration template for cortical surface analysis. *Neuroimage* **34**, 1535-1544 (2007).

240. N. Tzourio-Mazoyer *et al.*, Automated Anatomical Labeling of Activations in SPM Using a Macroscopic Anatomical Parcellation of the MNI MRI Single-Subject Brain. *NeuroImage* **15**, 273-289 (2002).

241. A. Schaefer *et al.*, Local-Global Parcellation of the Human Cerebral Cortex from Intrinsic Functional Connectivity MRI. *Cereb Cortex* **28**, 3095-3114 (2018).

242. R. S. Desikan *et al.*, An automated labeling system for subdividing the human cerebral cortex on MRI scans into gyral based regions of interest. *Neuroimage* **31**, 968-980 (2006).

243. K. J. Whitaker *et al.*, Adolescence is associated with genomically patterned consolidation of the hubs of the human brain connectome. *Proceedings of the National Academy of Sciences* **113**, 9105 (2016).

244. R. V. de Wael *et al.*, BrainSpace: a toolbox for the analysis of macroscale gradients in neuroimaging and connectomics datasets. *Communications biology* **3**, 1-10 (2020).

245. A. F. Alexander-Bloch *et al.*, On testing for spatial correspondence between maps of human brain structure and function. *NeuroImage* **178**, 540-551 (2018).

246. Y. Liao, J. Wang, E. J. Jaehnig, Z. Shi, B. Zhang, WebGestalt 2019: gene set analysis toolkit with revamped UIs and APIs. *Nucleic Acids Research* **47**, W199-W205 (2019).

247. H. J. Kang *et al.*, Spatio-temporal transcriptome of the human brain. *Nature* **478**, 483-489 (2011).

248. L. A. Jansen *et al.*, PI3K/AKT pathway mutations cause a spectrum of brain malformations from megalencephaly to focal cortical dysplasia. *Brain* **138**, 1613-1628 (2015).

249. G. Terrone *et al.*, De novo PIK3R2 variant causes polymicrogyria, corpus callosum hyperplasia and focal cortical dysplasia. *European Journal of Human Genetics* **24**, 1359-1362 (2016).

250. K. Kobow *et al.*, Genomic DNA methylation distinguishes subtypes of human focal cortical dysplasia. *Epilepsia* **60**, 1091-1103 (2019).

251. V. Schick *et al.*, Activation of Akt independent of PTEN and CTMP tumor-suppressor gene mutations in epilepsy-associated Taylor-type focal cortical dysplasias. *Acta neuropathologica* **112**, 715-725 (2006).

252. J. C. Sim *et al.*, Familial cortical dysplasia caused by mutation in the mammalian target of rapamycin regulator NPRL3. *Annals of neurology* **79**, 132-137 (2016).

253. Z. Zhang *et al.*, Somatic variants in new candidate genes identified in focal cortical dysplasia type II. *Epilepsia* **61**, 667-678 (2020).

254. S. Baulac *et al.*, Familial focal epilepsy with focal cortical dysplasia due to DEPDC 5 mutations. *Annals of neurology* **77**, 675-683 (2015).

255. G. L. Carvill *et al.*, Epileptic spasms are a feature of DEPDC5 mTORopathy. *Neurology Genetics* **1** (2015).

256. T. Scerri *et al.*, Familial cortical dysplasia type IIA caused by a germline mutation in DEPDC 5. *Annals of clinical and translational neurology* **2**, 575-580 (2015).

257. Z. Ying *et al.*, A comprehensive clinico-pathological and genetic evaluation of bottom-of-sulcus focal cortical dysplasia in patients with difficult-to-localize focal epilepsy. *Epileptic Disorders* **21**, 65-77 (2019).

258. J. Grove *et al.*, Identification of common genetic risk variants for autism spectrum disorder. *Nat Genet* **51**, 431-444 (2019).

259. E. A. Stahl *et al.*, Genome-wide association study identifies 30 loci associated with bipolar disorder. *Nat Genet* **51**, 793-803 (2019).

260. R. Ferrari *et al.*, Frontotemporal dementia and its subtypes: a genome-wide association study. *The Lancet. Neurology* **13**, 686-699 (2014).

261. L. C. Katz, C. J. Shatz, Synaptic activity and the construction of cortical circuits. *Science* **274**, 1133-1138 (1996).

262. M. Thom *et al.*, Cortical neuronal densities and lamination in focal cortical dysplasia. *Acta Neuropathologica* **110**, 383-392 (2005).

263. S. M. Kolk, P. Rakic, Development of prefrontal cortex. *Neuropsychopharmacology* **47**, 41-57 (2022).

264. Y. Wang *et al.*, Comprehensive identification of somatic nucleotide variants in human brain tissue. *Genome Biology* **22**, 92 (2021).

265. T. Kroon, E. van Hugte, L. van Linge, H. D. Mansvelder, R. M. Meredith, Early postnatal development of pyramidal neurons across layers of the mouse medial prefrontal cortex. *Scientific Reports* **9**, 5037 (2019).

266. P. R. Huttenlocher, A. S. Dabholkar, Regional differences in synaptogenesis in human cerebral cortex. *Journal of comparative Neurology* **387**, 167-178 (1997).

267. R. K. Lenroot, J. N. Giedd, Brain development in children and adolescents: insights from anatomical magnetic resonance imaging. *Neuroscience & biobehavioral reviews* **30**, 718-729 (2006).

268. Z. Petanjek *et al.*, Extraordinary neoteny of synaptic spines in the human prefrontal cortex. *Proceedings of the National Academy of Sciences* **108**, 13281-13286 (2011).

269. L. Mrzljak, H. B. Uylings, I. Kostovic, C. G. van Eden, Prenatal development of neurons in the human prefrontal cortex: I. A qualitative Golgi study. *Journal of comparative neurology* **271**, 355-386 (1988).

270. M. Á. García-Cabezas, B. Zikopoulos, H. Barbas, The Structural Model: a theory linking connections, plasticity, pathology, development and evolution of the cerebral cortex. *Brain Structure and Function* **224**, 985-1008 (2019).

271. H. Barbas, General Cortical and Special Prefrontal Connections: Principles from Structure to Function. *Annual Review of Neuroscience* **38**, 269-289 (2015).

272. F. M. Benes, S. L. Vincent, M. Todtenkopf, The density of pyramidal and nonpyramidal neurons in anterior cingulate cortex of schizophrenic and bipolar subjects. *Biological psychiatry* **50**, 395-406 (2001).

273. B.-y. Park *et al.*, Multilevel neural gradients reflect transdiagnostic effects of major psychiatric conditions on cortical morphology. *bioRxiv* 10.1101/2021.10.29.466434, 2021.2010.2029.466434 (2021).

274. B. Zikopoulos, H. Barbas, Changes in prefrontal axons may disrupt the network in autism. *Journal of Neuroscience* **30**, 14595-14609 (2010).

275. J. Wegiel *et al.*, The neuropathology of autism: defects of neurogenesis and neuronal migration, and dysplastic changes. *Acta neuropathologica* **119**, 755-770 (2010).

276. M. F. Casanova *et al.*, Focal cortical dysplasias in autism spectrum disorders. *Acta neuropathologica communications* **1**, 1-11 (2013).

277. S. L. Valk, A. Di Martino, M. P. Milham, B. C. Bernhardt, Multicenter mapping of structural network alterations in autism. *Human Brain Mapping* **36**, 2364-2373 (2015).

278. S. E. Arnold, B. T. Hyman, J. Flory, A. R. Damasio, G. W. Van Hoesen, The topographical and neuroanatomical distribution of neurofibrillary tangles and neuritic plaques in the cerebral cortex of patients with Alzheimer's disease. *Cerebral cortex* **1**, 103-116 (1991).

279. C. Duyckaerts, M.-A. CoLLE, F. Dessi, F. Piette, J. Hauw, Progression of Alzheimer histopathological changes. *Acta neurologica belgica* **98**, 180-185 (1998).

280. H. Braak, K. Del Tredici, Spreading of tau pathology in sporadic Alzheimer's disease along cortico-cortical top-down connections. *Cerebral Cortex* **28**, 3372-3384 (2018).

281. J. Brettschneider, K. D. Tredici, V. M.-Y. Lee, J. Q. Trojanowski, Spreading of pathology in neurodegenerative diseases: a focus on human studies. *Nature Reviews Neuroscience* **16**, 109-120 (2015).

282. A. Sen *et al.*, Pathological Tau Tangles Localize to Focal Cortical Dysplasia in Older Patients. *Epilepsia* **48**, 1447-1454 (2007).

283. A. Iyer *et al.*, Cell injury and Premature Neurodegeneration in Focal Malformations of Cortical Development. *Brain Pathology* **24**, 1-17 (2014).

284. N. A. Crossley *et al.*, The hubs of the human connectome are generally implicated in the anatomy of brain disorders. *Brain* **137**, 2382-2395 (2014).

285. O. Sporns, Towards network substrates of brain disorders. *Brain* **137**, 2117-2118 (2014).

286. A. Raznahan *et al.*, Patterns of Coordinated Anatomical Change in Human Cortical Development: A Longitudinal Neuroimaging Study of Maturational Coupling. *Neuron* **72**, 873-884 (2011).

287. A. Alexander-Bloch, A. Raznahan, E. Bullmore, J. Giedd, The Convergence of Maturational Change and Structural Covariance in Human Cortical Networks. *The Journal of Neuroscience* **33**, 2889-2899 (2013).

288. Y. Ma, K. Kanakousaki, L. Buttitta, How the cell cycle impacts chromatin architecture and influences cell fate. *Frontiers in Genetics* **6** (2015).

289. B. E. Bernstein *et al.*, A Bivalent Chromatin Structure Marks Key Developmental Genes in Embryonic Stem Cells. *Cell* **125**, 315-326 (2006).

290. P. Batty, D. W. Gerlich, Mitotic Chromosome Mechanics: How Cells Segregate Their Genome. *Trends in Cell Biology* **29**, 717-726 (2019).

291. E. M. Goldberg, D. A. Coulter, Mechanisms of epileptogenesis: a convergence on neural circuit dysfunction. *Nature Reviews Neuroscience* **14**, 337-349 (2013).

292. N. T. Cohen *et al.*, Networks Underlie Temporal Onset of Dysplasia-Related Epilepsy: A MELD Study. *Annals of Neurology* **92**, 503-511 (2022).

293. S. Fauser *et al.*, Clinical characteristics in focal cortical dysplasia: a retrospective evaluation in a series of 120 patients. *Brain* **129**, 1907-1916 (2006).

294. M. Nakashima *et al.*, Somatic Mutations in the MTOR gene cause focal cortical dysplasia type IIb. *Annals of Neurology* **78**, 375-386 (2015).

295. M. D. D'Agostino *et al.*, Posterior quadrantic dysplasia or hemi-hemimegalencephaly. *A characteristic brain malformation* **62**, 2214-2220 (2004).

296. B. S. Kasper, B. S. Chang, E. M. Kasper, Microdysgenesis: Historical roots of an important concept in epilepsy. *Epilepsy & Behavior* **15**, 146-153 (2009).

297. A. Palmini *et al.*, Terminology and classification of the cortical dysplasias. *Neurology* **62**, S2-S8 (2004).

298. K. Opeskin, R. M. Kalnins, G. Halliday, H. Cartwright, S. F. Berkovic, Idiopathic generalized epilepsy. *Lack of significant microdysgenesis* **55**, 1101-1106 (2000).

299. M. Thom *et al.*, Temporal lobe sclerosis associated with hippocampal sclerosis in temporal lobe epilepsy: neuropathological features. *Journal of neuropathology and experimental neurology* **68**, 928-938 (2009).

300. S. Tang *et al.*, Reconciling Dimensional and Categorical Models of Autism Heterogeneity: a Brain Connectomics and Behavioral Study. *Biological Psychiatry* 10.1016/j.biopsych.2019.11.009 (2019).

301. D. M. Blei, A. Y. Ng, M. I. Jordan, Latent dirichlet allocation. *J. Mach. Learn. Res.* **3**, 993-1022 (2003).

302. J. J. Ryan, S. J. Lopez, "Wechsler Adult Intelligence Scale-III" in Understanding Psychological Assessment, W. I. Dorfman, M. Hersen, Eds. (Springer US, Boston, MA, 2001), 10.1007/978-1-4615-1185-4_2, pp. 19-42.

303. M. Jones-Gotman, J. Djordjevic, "Neuropsychological testing in presurgical evaluation" in The treatment of epilepsy. (Wiley Online Library, 2009), pp. 851-863.

304. A. Majdan, V. Sziklas, M. Jones-Gotman, Performance of healthy subjects and patients with resection from the anterior temporal lobe on matched tests of verbal and visuoperceptual learning. *Journal of Clinical and Experimental Neuropsychology* **18**, 416-430 (1996).

305. L. L. Thurstone, T. G. Thurstone, *Primary mental abilities* (University of Chicago Press Chicago, 1938), vol. 119.

306. G. Leonard, B. Milner, L. Jones, Performance on unimanual and bimanual tapping tasks by patients with lesions of the frontal or temporal lobe. *Neuropsychologia* **26**, 79-91 (1988).

307. V. S. Fonov, A. C. Evans, R. C. McKinstry, C. Almli, D. Collins, Unbiased nonlinear average age-appropriate brain templates from birth to adulthood. *NeuroImage*, S102 (2009).

308. S. M. Smith *et al.*, Advances in functional and structural MR image analysis and implementation as FSL. *Neuroimage* **23**, S208-S219 (2004).

309. B. Caldairou *et al.*, A surface patch-based segmentation method for hippocampal subfields. *International Conference on Medical Image Computing and Computer-*

Assisted Intervention - MICCAI 2016. Lecture Notes in Computer Science **9901**, 379-387 (2016).

310. H. Kim, T. Mansi, N. Bernasconi, A. Bernasconi, Robust Surface-Based Multi-template Automated Algorithm to Segment Healthy and Pathological Hippocampi. *Medical Image Computing and Computer-Assisted Intervention – MICCAI 2011. Lecture Notes in Computer Science* **6893**, 445-453 (2011).
311. S. M. Lundberg *et al.*, From local explanations to global understanding with explainable AI for trees. *Nature machine intelligence* **2**, 2522-5839 (2020).
312. C. H. Xia *et al.*, Linked dimensions of psychopathology and connectivity in functional brain networks. *Nature Communications* **9**, 3003 (2018).
313. Anonymous, Embracing patient heterogeneity. *Nature Medicine* **20**, 689-689 (2014).
314. B. C. Bernhardt *et al.*, Temporal lobe epilepsy: Hippocampal pathology modulates connectome topology and controllability. *Neurology* **92**, e2209-e2220 (2019).
315. M. V. Sofroniew, Molecular dissection of reactive astrogliosis and glial scar formation. *Trends in neurosciences* **32**, 638-647 (2009).
316. T. C. Kang *et al.*, Epileptogenic roles of astroglial death and regeneration in the dentate gyrus of experimental temporal lobe epilepsy. *Glia* **54**, 258-271 (2006).
317. W. A. Hauser, J. R. Lee, Do seizures beget seizures? *Progress in brain research* **135**, 215-219 (2002).
318. M. Liu, L. Concha, C. Lebel, C. Beaulieu, D. W. Gross, Mesial temporal sclerosis is linked with more widespread white matter changes in temporal lobe epilepsy. *NeuroImage: Clinical* **1**, 99-105 (2012).
319. L. Concha, C. Beaulieu, D. W. Gross, Bilateral limbic diffusion abnormalities in unilateral temporal lobe epilepsy. *Annals of Neurology* **57**, 188-196 (2005).

320. F. Cendes, F. Andermann, F. Dubeau, P. Matthews, D. Arnold, Normalization of neuronal metabolic dysfunction after surgery for temporal lobe epilepsy: evidence from proton MR spectroscopic imaging. *Neurology* **49**, 1525-1533 (1997).
321. F. Bartolomei, P. Chauvel, F. Wendling, Epileptogenicity of brain structures in human temporal lobe epilepsy: a quantified study from intracerebral EEG. *Brain* **131**, 1818-1830 (2008).
322. K. Dabbs, J. Jones, M. Seidenberg, B. Hermann, Neuroanatomical correlates of cognitive phenotypes in temporal lobe epilepsy. *Epilepsy & Behavior* **15**, 445-451 (2009).
323. A. Reyes *et al.*, Cognitive phenotypes in temporal lobe epilepsy utilizing data- and clinically driven approaches: Moving toward a new taxonomy. *Epilepsia* **61**, 1211-1220 (2020).
324. B. Hermann, M. Seidenberg, J. Jones, The neurobehavioural comorbidities of epilepsy: can a natural history be developed? *The Lancet Neurology* **7**, 151-160 (2008).
325. N. Burgess, E. A. Maguire, J. O'Keefe, The human hippocampus and spatial and episodic memory. *Neuron* **35**, 625-641 (2002).
326. Q. Li *et al.*, Atypical neural topographies underpin dysfunctional pattern separation in temporal lobe epilepsy. *Brain* (2021).
327. B. Bell, J. J. Lin, M. Seidenberg, B. Hermann, The neurobiology of cognitive disorders in temporal lobe epilepsy. *Nature Reviews Neurology* **7**, 154-164 (2011).
328. P. Rajasethupathy *et al.*, Projections from neocortex mediate top-down control of memory retrieval. *Nature* **526**, 653-659 (2015).
329. K. J. Sass *et al.*, Verbal memory impairment correlates with hippocampal pyramidal cell density. *Neurology* **40**, 1694-1694 (1990).

330. K. J. Sass *et al.*, Specificity in the correlation of verbal memory and hippocampal neuron loss: dissociation of memory, language, and verbal intellectual ability. *Journal of Clinical and Experimental Neuropsychology* **14**, 662-672 (1992).

331. P. N. Alves *et al.*, An improved neuroanatomical model of the default-mode network reconciles previous neuroimaging and neuropathological findings. *Communications Biology* **2**, 370 (2019).

332. R. V. de Wael *et al.*, Anatomical and microstructural determinants of hippocampal subfield functional connectome embedding. *Proceedings of the National Academy of Sciences* **115**, 10154-10159 (2018).

333. R. L. Buckner, J. R. Andrews-Hanna, D. L. Schacter, The brain's default network: anatomy, function, and relevance to disease. (2008).

334. M. Song *et al.*, Brain spontaneous functional connectivity and intelligence. *NeuroImage* **41**, 1168-1176 (2008).

335. M. R. Borich, K. E. Brown, L. A. Boyd, Motor skill learning is associated with diffusion characteristics of white matter in individuals with chronic stroke. *J Neurol Phys Ther* **38**, 151-160 (2014).

336. F. Zhai *et al.*, Disrupted white matter integrity and network connectivity are related to poor motor performance. *Scientific Reports* **10**, 18369 (2020).

337. B. A. Clementz *et al.*, Identification of Distinct Psychosis Biotypes Using Brain-Based Biomarkers. *American Journal of Psychiatry* **173**, 373-384 (2015).

338. S.-J. Hong *et al.*, Towards neurosubtypes in autism. *Biological Psychiatry* (2020).

339. H. M. Lee *et al.*, Decomposing MRI phenotypic heterogeneity in epilepsy: a step towards personalized classification. *Brain* 10.1093/brain/awab425, awab425 (2021).

340. A. L. Young *et al.*, Uncovering the heterogeneity and temporal complexity of neurodegenerative diseases with Subtype and Stage Inference. *Nature Communications* **9**, 4273 (2018).

341. A. L. Young *et al.*, Subtype and stage inference identifies distinct atrophy patterns in genetic frontotemporal dementia that MAP onto specific MAPT mutations: Imaging and non-AD neurodegeneration. *Alzheimer's & Dementia* **16**, e042996 (2020).

342. J. W. Vogel *et al.*, Four distinct trajectories of tau deposition identified in Alzheimer's disease. *Nature Medicine* **27**, 871-881 (2021).

343. A. Eshaghi *et al.*, Identifying multiple sclerosis subtypes using unsupervised machine learning and MRI data. *Nature communications* **12**, 1-12 (2021).

344. J. Kulaga-Yoskovitz *et al.*, Multi-contrast submillimetric 3 Tesla hippocampal subfield segmentation protocol and dataset. *Sci Data* **2**, 150059-150059 (2015).

345. B. E. Youngerman *et al.*, Laser ablation is effective for temporal lobe epilepsy with and without mesial temporal sclerosis if hippocampal seizure onsets are localized by stereoelectroencephalography. *Epilepsia* 10.1111/epi.14004, n/a-n/a (2018).

346. J. H. Friedman, Greedy function approximation: A gradient boosting machine. *Ann. Statist.* **29**, 1189-1232 (2001).

347. U. von Luxburg, A tutorial on spectral clustering. *Statistics and Computating* **17**, 1-32 (2007).

348. H. M. Lee *et al.*, Unsupervised machine learning reveals lesional variability in focal cortical dysplasia at mesoscopic scale. *NeuroImage: Clinical* **28**, 102438 (2020).

349. V. García, R. A. Mollineda, J. S. Sánchez (2009) Index of balanced accuracy: A performance measure for skewed class distributions. in *Iberian conference on pattern recognition and image analysis* (Springer), pp 441-448.

350. J. G. Sheng, F. A. Boop, R. E. Mrak, W. S. T. Griffin, Increased neuronal β-amyloid precursor protein expression in human temporal lobe epilepsy: association with interleukin-1α immunoreactivity. *Journal of neurochemistry* **63**, 1872-1879 (1994).

351. S. E. Nasrabady, B. Rizvi, J. E. Goldman, A. M. Brickman, White matter changes in Alzheimer's disease: a focus on myelin and oligodendrocytes. *Acta Neuropathologica Communications* **6**, 22 (2018).

352. B. T. Gold, N. F. Johnson, D. K. Powell, C. D. Smith, White matter integrity and vulnerability to Alzheimer's disease: Preliminary findings and future directions. *Biochimica et Biophysica Acta (BBA) - Molecular Basis of Disease* **1822**, 416-422 (2012).

353. L. Concha, H. Kim, A. Bernasconi, B. C. Bernhardt, N. Bernasconi, Spatial patterns of water diffusion along white matter tracts in temporal lobe epilepsy. *Neurology* **79**, 455-462 (2012).

354. M. Hildebrandt *et al.*, White matter angiopathy is common in pediatric patients with intractable focal epilepsies. *Epilepsia* **49**, 804-815 (2008).

355. L. Alonso-Nanclares, J. DeFelipe, Alterations of the microvascular network in the sclerotic hippocampus of patients with temporal lobe epilepsy. *Epilepsy & Behavior* **38**, 48-52 (2014).

356. J. C. de la Torre, Is Alzheimer's disease a neurodegenerative or a vascular disorder? Data, dogma, and dialectics. *The Lancet Neurology* **3**, 184-190 (2004).

357. A. Verkhratsky, M. Olabarria, H. N. Noristani, C.-Y. Yeh, J. J. Rodriguez, Astrocytes in Alzheimer's Disease. *Neurotherapeutics* **7**, 399-412 (2010).

358. J. W. Vogel *et al.*, Spread of pathological tau proteins through communicating neurons in human Alzheimer's disease. *Nature communications* **11**, 1-15 (2020).

359. A. Fornito, A. Zalesky, M. Breakspear, The connectomics of brain disorders. *Nature Reviews Neuroscience* **16**, 159-172 (2015).

360. E. Mak *et al.*, Progressive cortical thinning and subcortical atrophy in dementia with Lewy bodies and Alzheimer's disease. *Neurobiology of aging* **36**, 1743-1750 (2015).

361. R. J. Perrin, A. M. Fagan, D. M. Holtzman, Multimodal techniques for diagnosis and prognosis of Alzheimer's disease. *Nature* **461**, 916-922 (2009).

362. B. C. Dickerson *et al.*, The cortical signature of Alzheimer's disease: regionally specific cortical thinning relates to symptom severity in very mild to mild AD dementia and is detectable in asymptomatic amyloid-positive individuals. *Cerebral cortex* **19**, 497-510 (2009).

363. S. Larivière *et al.*, Network-based atrophy modeling in the common epilepsies: A worldwide ENIGMA study. *Science advances* **6**, eabc6457 (2020).

364. A. L. Jones, G. D. Cascino, Evidence on use of neuroimaging for surgical treatment of temporal lobe epilepsy: A systematic review. *JAMA Neurology* **73**, 464-470 (2016).

365. G. Canet *et al.*, Seizure activity triggers tau hyperphosphorylation and amyloidogenic pathways. *Epilepsia* **63**, 919-935 (2022).

366. M. Galovic *et al.*, Resective surgery prevents progressive cortical thinning in temporal lobe epilepsy. *Brain* **143**, 3262-3272 (2020).

367. K. J. Sass *et al.*, Verbal memory impairment correlates with hippocampal pyramidal cell density. *Neurology* **40**, 1694 (1990).

368. D. Vidal-Piñeiro *et al.*, Accelerated longitudinal gray/white matter contrast decline in aging in lightly myelinated cortical regions. *Human Brain Mapping* **37**, 3669-3684 (2016).

369. P. Shaw *et al.*, Neurodevelopmental Trajectories of the Human Cerebral Cortex. *The Journal of Neuroscience* **28**, 3586-3594 (2008).

370. M. F. Glasser, M. S. Goyal, T. M. Preuss, M. E. Raichle, D. C. Van Essen, Trends and properties of human cerebral cortex: correlations with cortical myelin content. *Neuroimage* **93 Pt 2**, 165-175 (2014).

371. H. Zhang, T. Schneider, C. A. Wheeler-Kingshott, D. C. Alexander, NODDI: practical in vivo neurite orientation dispersion and density imaging of the human brain. *Neuroimage* **61**, 1000-1016 (2012).

372. E. X. Wu, M. M. Cheung, MR diffusion kurtosis imaging for neural tissue characterization. *NMR in Biomedicine* **23**, 836-848 (2010).

373. J. A. Detre, J. S. Leigh, D. S. Williams, A. P. Koretsky, Perfusion imaging. *Magnetic resonance in medicine* **23**, 37-45 (1992).

374. D. C. Alsop *et al.*, Recommended Implementation of Arterial Spin Labeled Perfusion MRI for Clinical Applications: A consensus of the ISMRM Perfusion Study Group and the European Consortium for ASL in Dementia. *Magnetic resonance in medicine* **73**, 102-116 (2015).

375. F. Xu, Y. Ge, H. Lu, Noninvasive quantification of whole-brain cerebral metabolic rate of oxygen (CMRO2) by MRI. *Magnetic Resonance in Medicine: An Official Journal of the International Society for Magnetic Resonance in Medicine* **62**, 141-148 (2009).

376. S.-H. Oh *et al.*, Direct visualization of short transverse relaxation time component (ViSTa). *Neuroimage* **83**, 485-492 (2013).

377. A. Mackay *et al.*, In vivo visualization of myelin water in brain by magnetic resonance. *Magnetic resonance in medicine* **31**, 673-677 (1994).

378. Y. Wang, T. Liu, Quantitative susceptibility mapping (QSM): decoding MRI data for a tissue magnetic biomarker. *Magnetic resonance in medicine* **73**, 82-101 (2015).

379. J. Detre *et al.*, Functional MRI lateralization of memory in temporal lobe epilepsy. *Neurology* **50**, 926-932 (1998).

380. A. J. Golby *et al.*, Memory Lateralization in Medial Temporal Lobe Epilepsy Assessed by Functional MRI. *Epilepsia* **43**, 855-863 (2002).

381. E. H. Bertram, D. Zhang, J. M. Williamson, Multiple roles of midline dorsal thalamic nuclei in induction and spread of limbic seizures. *Epilepsia* **49**, 256-268 (2008).

382. D. Zhang, E. H. Bertram, Midline thalamic region: widespread excitatory input to the entorhinal cortex and amygdala. *Journal of Neuroscience* **22**, 3277-3284 (2002).

383. A. Labate, A. Cerasa, A. Gambardella, U. Aguglia, A. Quattrone, Hippocampal and thalamic atrophy in mild temporal lobe epilepsy: a VBM study. *Neurology* **71**, 1094-1101 (2008).

384. X. Y. Tai *et al.*, Review: Neurodegenerative processes in temporal lobe epilepsy with hippocampal sclerosis: Clinical, pathological and neuroimaging evidence. *Neuropathology and Applied Neurobiology* **44**, 70-90 (2018).

385. A. S. Mandal, M. Gandal, J. Seidlitz, A. Alexander-Bloch, A Critical Appraisal of Imaging Transcriptomics. *Biological Psychiatry: Global Open Science* **2**, 311-313 (2022).

386. C. Kim, iPSC technology-Powerful hand for disease modeling and therapeutic screen. *BMB reports* **48**, 256 (2015).

387. K. Sabitha, A. K. Shetty, D. Upadhya, Patient-derived iPSC modeling of rare neurodevelopmental disorders: Molecular pathophysiology and prospective therapies. *Neuroscience & Biobehavioral Reviews* **121**, 201-219 (2021).

388. G. L. Sequiera *et al.*, Development of iPSC-based clinical trial selection platform for patients with ultrarare diseases. *Science Advances* **8**, eabl4370 (2022).